Geometry and Visualization of Folds

Mattathias D. Needle

A dissertation

Submitted in partial fulfillment of the

Requirements for the degree of

Doctor of Philosophy

University of Washington

2023

Reading Committee:

Juliet G. Crider, Chair

Darrel S. Cowan

Gerard H. Roe

Program Authorized to Offer Degree:

Department of Earth and Space Sciences

University of Washington

Abstract

Geometry and Visualization of Folds

Mattathias D. Needle

Chair of the supervisory committee:

Juliet G. Crider

Department of Earth and Space Sciences

Reconstructing the geometry of geologic folds, and subsequently expressing this geometry visually, are necessary for understanding the kinematic and mechanical properties of folds. Novel technology for acquiring 3D geometric data, including drone-based photography and structure-from-motion photogrammetry, enables data collection at fold outcrops that were previously difficult to study in the field. This new technology introduces opportunities to enhance kinematic and mechanical models of folds from field data, but also requires the exploration of new methods for reconstructing and visualizing fold form from 3D point clouds. I present work involving point-cloud data collected from a drone-based photographic survey in the Bear Valley Strip Mine (Shamokin, Pennsylvania), where the 30-meter-high Whaleback Anticline and adjacent folds are exquisitely exposed in three dimensions. While the strip mine has been a popular field trip destination for half a century, it has not been previously possible to make detailed observations throughout the folded surface or making a detailed geometric

reconstruction. In Chapter 1, I provide the inspiration and roadmap of this work. In Chapter 2, I propose a new methodology of interpolating fold form with non-uniform rational basis splines to construct a smooth, continuous, mathematically operable fold surface from noisy and discontinuous point-cloud data of the fold train at the Bear Valley Strip Mine. In Chapters 3 and 4, I introduce the Structural Geology Query Toolkit – an open-source software package for building first-person-perspective field-geology simulations in which a student or researcher can visualize and interrogate geologic surfaces, like the folded sandstone surface at the Bear Valley Strip Mine, generated from 3D scans. Finally, in Chapter 5, I leverage 3D models of the Whaleback and the Structural Geology Query Toolkit to determine that mesoscale extensional faults accommodate <6% strain evenly distributed throughout the Whaleback's surface, which contributes to our understanding of the late-stage kinematics of buckle folding. Although the methods and new tools discussed in this dissertation revolve around data collected at the Bear Valley Strip Mine, they are intended to be applicable to other field sites where 3D scans of outcrops are possible.

Table of Contents

List of Figures

List of Tables

Acknowledgments

The guidance that my advisor, Juliet Crider, has offered throughout my experience at the University of Washington (UW) was key to my development as a scientific thinker, educator, communicator, and 2D/3D artist. Juliet's curiosity for the natural world is inspirational and contagious. Thank you, Juliet, for being a mentor, a role model, and a truly decent human being to me; you also gave me a so much support and a healthy amount of space to find and develop my own voice and tools to contribute to our field.

Darrel Cowan's perspectives as a field geologist and classical structural geologist were important contributions to tuning my research. Darrel also connected my work to the GSA Foundation which expanded my reach for sharing my work in virtual field geology. Darrel, you have been a role model, especially with regards to field-trip pedagogy and scientific writing.

Gerard Roe's input to this work was essential in helping frame neat and concise scientific questions, and subsequently, strategically developing research methods. Gerard, thank you for encouraging me to aim for scholar-level work, accelerating my math literacy, and engaging me in philosophical discussions.

The following organizations and institutions provided financial support for this work: National Science Foundation (EAR-1523909), Geological Society of America and GSA Foundation (Debbie Marcinkowski), UW Reality Lab Incubator (John Akers), UW Student Technology Fee, UW Dept. of Earth and Space Sciences and the donors to the department awards, and the UW Royalty Research Fund.

Keith Hodson photographed the Whaleback, and his photos are the basis for a lot of this work. Thank you, Keith, for being my "big brother" in research on the Whaleback. I am grateful for the Whaleback research collaboration with Arlo Weil (Bryn Mawr College) and Mary Beth

Gray (Bucknell University) who have shared their insight and expertise on the Bear Valley Strip Mine. Reading Anthracite provided access to the Bear Valley Strip Mine for this work.

The collaboration with Jacky Mooc on the toolkit featured in Chapters 3 and 4, as well as the methodology in Chapter 5, started as a side project that I pursued through the UW Reality Lab Incubator, directed by John Akers. Jacky and John, it has been a pleasure to work with you both. Your sustained interest in sharing our tools with the geoscience community warms my heart.

Thank you to my very supportive family: Jay and Bobbi Needle; Josh, Julia, Nathan, and Ari Needle; Aunt Myra; and Uncle David. Thank you to my family members who cheered for me through this academic journey, first in person, and later in spirit: Aunt Sara, Grandma Mildred, and Grandma Gerry. I love you all very much.

Chapter 1 Introduction

Geologic folds are alluring structures. I approached folds from a new perspective because new technology is available to capture fold geometry at an outcrop scale. The initial roadmap of this Ph.D. started with reconstructing the geometry of a uniquely exposed fold train and examining strain at this fold, motivated by a desire to inform mechanical models of buckle folding. The demand for remote education during the 2020 pandemic provided an additional opportunity to enhance access to and interactions with 3D digital outcrop and terrain models.

Drone-based photography can image both the accessible and inaccessible areas of geologic structures. Structure-from-motion photogrammetry and other tools to produce 3D point clouds have enabled geologists to capture the geometry structures exposed in outcrops at multiple scales for further analysis. Structure-from-motion photogrammetry has been widely adopted for geologic investigations and to produce educational resources, but how point-cloud data are processed, interpreted, and presented for advancing scientific knowledge and education is evolving.

Although applicable to other settings, the work I present in this dissertation is inspired by and rooted in observations from the Bear Valley Strip mine (Shamokin, Pennsylvania), where the Whaleback Anticline and adjacent folds are exquisitely exposed in three dimensions. Visitors to the strip mine can walk on the crests and adjacent to the limbs of the folds, which has allowed researchers to describe the fold geometry and observe the relationships among structures that record deformation during the progressive development of these folds. This unique exposure, and

the imagery collected to document it, are the foundations of the research that composes this dissertation.

For over a century, the methodology of reconstructing fold geometry has been evolving. A drone-based photographic survey of the Bear Valley Strip Mine produced a point-cloud data set of the exposed fold train, but the data also contain noise (e.g., vegetation) and the exposed fold train is discontinuous (e.g., the synformal components of the fold train are buried). In Chapter 2, I propose using non-uniform rational basis splines (NURBS), a common tool in computer-aided design for constructing smooth geometries, to reconstruct a smooth, continuous fold train from the point-cloud data. Applying the NURBS surface to the point cloud generated a fold-train geometry. Geometric data were collected from the NURBS surface and compared to in-situ field measurements at the strip mine, and a curvature analysis of the NURBS was used to investigate how well curvature can predict mesoscale fractures on folds. The work in this chapter intends to demonstrate that NURBS is a viable tool for reconstructing geologic folds from point-cloud data, and that the resulting models are mathematically operable and aid in fold visualization.

The 3D polygonal model of the Bear Valley Strip Mine derived from the point-cloud data can provide a means to simulate this popular field-trip location for geoscience students and enthusiasts around the globe. But how people meaningfully interact with 3D models produced from Structure-from-Motion photogrammetry is a relatively new topic. Chapters 3 and 4 explore how to provide remote access to outcrops and geologically significant terrains. While this work was initially inspired by just "sharing" the Whaleback, it evolved as the global pandemic of 2020 called for geoscience instruction, even field instruction, to be physically distanced and remote. Chapter 3 describes how I used video-game-building software to "gamify" 3D models, enabling

students to have simulated 1st-person-perspective field experiences during pandemic lockdowns. Chapter 4 details the Structural Geology Query Toolkit, an open-source software package that I created so that anyone with a 3D outcrop/terrain model can design an open-ended virtual field trip and share it for educational and/or research purposes.

While the pandemic made the application of virtual field simulations to geoscience education quite clear, using these simulations for research purposes is worth exploring. There has yet to emerge a popular user-friendly software in geoscience for interrogating 3D models that also simulates a field experience. In my Structural Geology Query Toolkit interface, geometric data can be collected from the terrain/outcrop models in a mode similar to field research. I use this approach specifically to address extension in the late stage of folding.

Buckle-fold theory suggests that in the late stage of folding, extension occurs on the folded surface as fold limbs tighten, (late-stage flattening). The distribution and amount of extension in this stage is not widely reported but is valuable when constraining initial conditions of buckle folding to gain insight to rheology. The Whaleback is a unique exposure: there may be no other outcrops of buckle folds at the scale of the Whaleback with such excellent exposure. The ability to observe and measure the mesoscale faults in the folded sandstone provides an opportunity to add to our understanding of extension in the late stage of folding. In Chapter 5, I measured strain accommodated by the late-stage extensional faults in high-resolution outcrop models of the Whaleback with the tools available in the Structural Geology Query Toolkit. I found that faults accommodated <6% extension in the late stage of folding and that the strain is evenly distributed both parallel and perpendicular to the fold axis. Furthermore, these findings are similar to in-situ field data from the Whaleback, confirming the utility of the Structural Geology Query Toolkit as a research tool.

Chapter 2 Nonlinear uniform basis spline surfaces for fold geometry: from point clouds to 3D interpolated structures

Abstract

Point-cloud datasets are becoming more prevalent in structural geology, accessible through scanning and photogrammetry techniques. These datasets enable 3D representation and analysis of geologic folds, but challenges arise due to noise and discontinuities in the data. To address this, we propose employing non-uniform rational basis splines (NURBS) for interpolating smooth, continuous fold surfaces from the point-cloud data. We demonstrate the application of this methodology in a case study on point-cloud data of a fold train at the Bear Valley Strip Mine (Shamokin, Pennsylvania, USA), comparing our NURBS-surface model to in-situ field measurements.

2.1 Introduction

In structural geology, point-cloud datasets are becoming increasingly common due to the accessibility of terrestrial laser scanning (e.g. Buckley et al. 2010; Pearce et al. 2011;), drone-based structure-from-motion photogrammetry (e.g. Pavlis and Mason 2017; and references therein), and hand held devices (e.g., Carr et al. 2019). At their roots, 3D point clouds consist of independent sets of x, y, and z coordinates that define a point in space and thus can be used to represent structures at any scale and in three dimensions. The ability to capture the geometry of folded surfaces at multiple scales as point clouds enables us to study folds and fold processes with a novel 3D perspective.

Points in space are not ideal models for structural analysis as they are not coherent surfaces, thus point clouds serve as the basis for the generation of other 3D-surface models for

analysis and interpretation. Furthermore, point cloud data may be "noisy." Apart from instrumental uncertainty, point-cloud noise in structural geology may include erosional surfaces, rubble, vegetation, and anthropogenic alterations which all can obscure the geometry of targeted features, such as bedding-surfaces. In addition, rock surfaces are not smooth, as they contain depositional or deformational structures at many different length-scales. The process of interpolating a 3D-surface geometry from point-cloud data can both filter and include surface variations of different length-scales, so decisions must be made regarding the most objective way to interpolate a surface. Objectively modeling geologic folds from point-cloud data poses several challenges: 1) modeling a smooth continuous folded surface, and 2) filtering undesired noise from the data, while 3) retaining geometric irregularities of the folded surface that can advance of understanding of the structure.

Here, we share our methodology for interpolating a smooth, continuous fold surface from point-cloud data of a bedding surface. We discuss why non-uniform rational basis splines (NURBS), which represent mathematically precise free-form curves and surfaces, are our choice for modeling folds from point clouds. We describe a case study in which we apply this methodology to point-cloud data of a series of folds at the Bear Valley Strip Mine in Shamokin, Pennsylvania and compare orientation data from our NURBS-surface model to field measurements.

2.1.1 Previous work: Interpolating fold geometry for mathematical operations

Discussions of the appropriate methodology to reconstruct fold form reach back more than a century. Geometric constructions were generally designed for cross-section construction from sparse data and assume plane strain with concentric arcs (e.g., Busk 1929, Fig. 2-1A) or

kink fold forms (e.g., Suppe 1983, Fig. 2-1B). While these geometries account for fundamental geometric fold models, much research has sought to represent fold surfaces as continuous wave forms.

Fourier analysis is a quantitative way to describe fold shape mathematically, as it relates a natural (but often irregular) fold form to sinusoidal functions of harmonic waveforms. Some researchers have described folds with two Fourier coefficients, yielding smooth 2D representations of folds (e.g. Stabler 1968; Hudleston 1973, Fig. 2-1C). Hudleston (1973) used a quarter-wavelength approach, where the shape of the fold is extrapolated from the fold limb's inflection point in the x-coordinate to the hinge of the fold in the y-coordinate. From these coordinates, a Fourier analysis produces a mathematical fold form in which the first term of the Fourier series relates to the amplitude/wavelength and the second term relates to the curvature at the hinge. This initial work is foundational in expressing fold form mathematically. This approach takes complex irregular forms and summarizes them in simple expressions. Stowe (1988) employed a more complex Fourier analysis for representing fold profile sections with computers. Stowe's (1988) approach increased the resolution of irregularities within the fold profile by the inclusion of ten Fourier coefficients and permitted asymmetrical profiles by including right and left quarter-wave forms.

Stowe demonstrated computers' abilities to generate fold geometry in the third dimension. He tested the ability for Fourier analysis to extrapolate fold geometry in 3D by taking four parallel fold profiles derived through his Fourier-based fold-construction methodology, generating intermediate synthetic profiles based on the four initial profiles, and compared the synthetic profiles to the observable fold geometry. Bergbauer and Pollard (2003) and Mynatt et al. (2007) apply Fourier analysis to filter and smooth gridded structure-contour data at Sheep

Mountain Anticline (Wyoming USA; Bellhansen et al., 2006). To extract additional information about the broader fold form (e.g., curvature), Mynatt et al. (2007) filtered wavelengths shorter than 500 m. For a dome with a wavelength of roughly ~2500 m, this degree of filtering could obscure interesting local variation. Additionally, the Fourier approach is not effective at interpolating fold form where data are sparse.

An alternative approach to a Fourier series is to approximate the form of a folded surface by a polynomial function. A single polynomial function facilitates the calculation of 2D curvature for the sake of locating a fold's hinge (highest curvature) and inflection points (curvature = 0). Srivastava and Ragstogi's (2009) Hingeflex Matlab code receives 2D fold geometry from an image and fits a polynomial to the fold, after which the hinge and inflection points can be located. This method objectively describes the fold form and identifies key features, but rotations of the fold image are necessary to address a fold with overturned or recumbent geometry.

Bezier curves have been employed to model geologic structures because they have a smooth geometry and variable form (De Paor 1996; Srivastava and Lisle 2004, Fig. 2-1D). Bezier curves consist of one or more polynomial segments linked together, and their shape is influenced by control points (e.g., De Paor, 1996). Because Bezier curves are linked polynomials, these parametric curves can appropriately model smooth overhanging surfaces, such as overturned/recumbent folds, that cannot be defined by a single-valued polynomial function. Bezier curves can also model folds with abrupt change in the surface orientation, such as cuspate-lobate geometries. Modeling folds in 2D with Bezier curves can be accomplished interactively as Bezier curves serve as the basis for vector-graphics software. Srivastava and Lisle (2004) introduced a methodology for fitting Bezier curves to folds, but locating the hinge

and inflection points of the fold was a subjective task (Srivastava and Rastogi 2009). After defining fold geometry with Bezier curves, the Fold Geometry Toolbox (Adamuszek, Schmid, and Dabrowski, 2011) can be used to analyze the fold geometry and interpret mechanical properties of the fold.

To model three-dimensional surfaces, meshes are commonly used. Three-dimensional polygonal meshes are comprised of vertices, linear edges, and faces. A mesh representation of a folded surface involves the subdivision of a continuous surface into discrete cells. Discrete modeling of natural objects has advantages over Bezier curves, because the approach respects complex data and generates models that are meshed and therefore prepared for finite-element analysis (Mallet 1992a, 1997). In finite element analysis, three-dimensional surfaces and solids are constructed with sets of interconnected nodes that hold both the geometry and physical properties of the geologic structures (Mallet 1997).

In GIS, triangulated irregular networks (TINs) are common, using points as vertices which are linked by lines to create interconnected triangular facets for surfaces. The TIN "2.5D" data structures in GIS software are limiting, however: they permit only a single elevation value for any horizontal position, and therefore cannot model overhanging features that require more than one elevation value for the surface in a single location (Caumon et al. 2009).

Other studies have used point cloud data to model fold geometry. Humair et al. (2015) modeled the 3D geometry of box fold, exposed in profile, from LiDAR- and SfM-acquired point-cloud data. First, Humair et al. (2015) fit planes to the point cloud in Coltop 3D software (Jaboyedoff et al. 2007) to construct a pi plot by which to measure the fold axis; then they used the orientation of the fold axis to extrude the 3D geometry of folded layers as a TIN, assuming a cylindrical fold. Although this box fold was primarily exposed in cross section at the outcrop, a

subsequent excavation at the outcrop permitted Humair et al. (2015) to repeat their survey and note changes in the fold-axis orientation by a few degrees at the crest.

Samson and Mallet (1997) combined smooth discrete interpolation with discretized triangular Bezier patches to facilitate mathematical operations (e.g., Gaussian curvature) on 3D geologic models. This discrete modeling serves as the basis for the software GoCAD which enables the user to integrate subsurface data to create geologic models for velocity and reservoir modeling (Mallet 1992a, 1992b). As an application of this tool to interpolating a folded surface from field observations, Pearce et al. (2006) surveyed spot elevations with GPS of a single folded bedding surface from which they interpolated functions in GoCAD. Pearce et al. (2006) resampled their interpolated surface with even spacing between points for export and subsequent analysis.

As point-cloud datasets become more common in structural geology, new approaches to surface modeling are required. In the case of modeling folded surfaces from point clouds, we need a flexible form, adaptable to variations at many length scales, and free from specific geometric constraints (e.g., sinusoidal, cylindrical). The tool should also be able to interpolate over large data gaps. Interpolating a surface from point-cloud data with Fourier series cannot honor overturned limbs and may filter fine scale features that can provide insight to fold form and its relationships to kinematics and mechanics. While discretization is a logical choice to model point-cloud data, as this process samples points as vertices during the interpolation of a connected 3D surface, meshing across large areas of missing points will introduce a rigid, polygonal, and flat interpolation. Surfaces of Bezier curves and patches avoid many of these pitfalls. For point clouds with sharp edges (e.g., where the bedding surface is obscured by noise)

and data gaps, Bureick et al. (2016) recommend B-spline and NURBS surfaces over Bezier surfaces.

2.1.2 What are NURBS?

NURBS are equations that define curves and surfaces. They are ubiquitous tools for computer-aided design (CAD) in manufacturing industries and engineering. Because NURBS are a computationally efficient way to represent a surface, they facilitate smooth graphical user interactions with the model and enable fast calculations (Hollister 2001; Jacquemyn et al. 2016).

The mathematical description of NURBS is well documented. Here, we briefly review some key differences between Bezier curves, B-splines, and NURBS to strengthen the case for using NURBS for modeling geologic surfaces from point cloud data. Bezier curves are calculated by linear combinations of polynomials that are influenced by control points (Fig. 2-1D). The first and last control point of a Bezier curve defines the starting and ending locations of the curves. The degree of the Bezier curve can be thought of as the polynomial expression for the Bezier curve. For many modeling applications, cubic Bezier curves (degree $n = 3$) are used. To generate a curve with 3-degrees, 4 control points are needed; and this relationship of control points to degrees, n + 1 + = degrees of polynomial, is maintained for higher-degree Bezier curves. A fundamental difference between Bezier and basis(B)-splines is that B-splines can have internal knots. Knot vectors influence the calculations of the basis functions and piece together basis functions to form a spline. B-splines can have uniform or non-uniform spacing for knots. With respect to point clouds, Bezier curves can model point clouds without leaps (Bureick et al. 2016).

NURBS are B-splines that can have non-uniform knot spacing as well as variable weights for control points (Fig. 2-1E). A NURBS surface, *S*, with splines in both the *u* and *v* directions is expressed as:

$$S(\bar{u}, \bar{v}) = \frac{\sum_{i=0}^{n} \sum_{j=0}^{m} \left(N_{i,p}(\bar{u})\, N_{j,q}(\bar{v})\, w_{i,j} \right) \mathbf{P}_{i,j}}{\sum_{i=0}^{n} \sum_{j=0}^{m} \left(N_{k,p}(\bar{u})\, N_{l,q}(\bar{v})\, w_{k,l} \right)}$$

in which $N_{i,p}(\bar{u})$ and $N_{j,q}(\bar{v})$ are basis functions that are parameterized by the knot vectors and degrees (p and q), $\mathbf{P}_{i,j}$ is the set of control points, and $w_{i,j}$ is the weight for every control point. "Rational," in the NURBS acronym, describes the possibility that an individual control point can be assigned greater influence on a basis function than other points with a rational number. The rational quality can be imagined as a single control point having more (or less) pull on a spline compared to the adjacent control points (represented by the magnets in Fig 2-1E). Rational basis functions permit changing the shape of a spline locally without changing the positions of the control points. Thus, non-uniform rational basis splines (NURBS) are comprised of control points, weights, knots that are not necessarily evenly spaced, and degrees which describe the highest exponent in the polynomials that are pieced together by the knots.

2.1.3 NURBS in Geoscience Research

A few researchers have reported using NURBS for interpolations of geologic structures. Fisher and Wales (1992) demonstrated for the application of NURBS to interpolate stratigraphic traps in aggradational stream deposits from well logs and topographic quadrangles containing the well locations. Using data from hard-rock drilling and geophysical inverse models, Sprague and de Kemp (2005) generated a NURBS surface as a visual guide for features within the

Musselwhite Gold Mine in Northern Ontario, Canada. Zhong et al. (2006) presented the integration of NURBS with triangulated irregular networks (TIN) for the visualization of the spatial distribution of structures associated with the Jinping first-level hydropower facility in China. Interestingly, Zhong et al. discuss the ability to take "digital" core samples from their integrated model. Similarly, Miao et al. (2012) constructed a NURBS model from geologic maps and borehole data of a alluvial floodplain that was dredged and filled; and they subsequently introduced a method for cross-sectional analysis of the model for engineers to visualize geology.

While the capability of NURBS for interpolating and modeling geologic structures has been previously established, the case presented in our study is novel in the following aspects: 1) We are using robust, yet incomplete, structure-from-motion-acquired point-cloud data to construct a NURBS surface; 2) we show that the interpolated surface accurately reproduces field measurements; and 3) we demonstrate the utility of the NURBS interpolation for subsequent quantitative analyses.

2.2 Case study: Whaleback Anticline (Pennsylvania, USA)

The Whaleback Anticline is a 30 m high central fold in an excavated fold train that also includes an anticline to the north and a steep limb the south. The exceptional three-dimensional exposure of the anticlines, non-periodic fold forms and unexposed synclines, makes this an ideal test case for modeling and interpolating the folds with NURBS.

2.2.1 Geologic Setting

In the 1950s, miners pursuing anthracite coal uncovered a sandstone fold train in the Bear Valley Mine. Within the center of the exposed fold train is an anticline resembling, and thus

named, “the Whaleback” (Fig. 2-2). This exposure provides a unique opportunity for direct observation of a large fold in three dimensions. Thorough characterization of structures and their distribution is permitted by the Whaleback’s accessibility and scale, as it is possible to walk along the crest of the fold and next to 200 m of exposed limbs. The anticline folds a ~4.5 m-thick sandstone layer, with coal stratigraphically above. The coal and sandstone are part of the Llewellyn Formation (Late Pennsylvanian, ~300 Ma), deformed during the Appalachian Orogeny (325 - 260 Ma). Six structural stages of the Appalachian Orogeny are observable in the Bear Valley Mine which (1) provides a framework for constraining the relative timing of the deformation related to progressive development of the fold (Nickelsen 1979), and (2) makes the Whaleback a popular spot for structural-geology field trips in the northeastern United States (and, recently, virtual field trips (Needle et al. 2022)).

Despite the excellent exposure of the Whaleback, the full fold form and its relationship to adjacent folds are not directly observable. The limbs of the Whaleback dip into troughs that are filled with mine tailings and sediments, thus, the synformal inflections that connect the Whaleback to the adjacent anticlines are buried (Fig. 2-3A). Furthermore, the steep southern limb of the fold train is partially disrupted by a rockslide (Fig. 2-3B). Similarly, a significant section of the crest of the northern anticline of the fold train is covered in debris (Fig. 2-3C). The inability to observe the syncline, limb, and crest geometries poses a problem in precisely defining hinges and inflection points for determining the fold’s amplitude, wavelength, and arclength (these measurement definitions are well illustrated in Adamuszek et al., 2011). Since the point-cloud data show only surficial features and not solely a continuous surface of sandstone, the data is not prepared for 2D measurements that are standard inputs to analytical solutions for bulk strain (e.g., Schmalholz 2006, Sherwin and Chapple 1968, Schmalholz and

Podladchikov 2001). Beyond the kinematics of folding, to advance our understanding of fold mechanics in 3D, the geometry of natural examples of folds are needed to constrain computational forward models that explore rheological parameters of folding.

2.2.2 Acquiring and preparing a robust point cloud for NURBS modeling

We used structure-from-motion (SfM) photogrammetry to produce a 3D point cloud of the Bear Valley Strip Mine, including the Whaleback and adjacent folds. SfM uses standard digital photographs from overlapping oblique views to estimate camera positions and orientations to reconstruct a digital model of a scene (Lowe 2004; James and Robson 2012). SfM does not require vertical imagery or special instruments, rather, arbitrary oblique images can be used for the construction of a 3D digital model (e.g. Pavlis and Mason, 2017; and references therein). Using SfM for the Whaleback has an advantage over other point-cloud-generating techniques, such as aerial lidar. Because the Whaleback anticline has a slightly overturned northern limb, oblique images are necessary to capture accurate limb geometry.

We photographed the strip mine with cameras on the ground and on unoccupied aerial vehicles (UAV) in 2015, including 25 ground-control points surveyed with GPS. We extracted 3D coordinates of surface points and generated a point cloud that represents the topographical surface of the mine with Agisoft Photoscan (AgiSoft PhotoScan Professional, 2018). The resulting georeferenced model (Figs. 2-2 (bottom) and 2-4A) is very detailed: structural details, from cm-scale faults to the broad geometry of the folds are apparent. However, vegetation, mine debris and erosion of the sandstone produce noise that obscures the complete form of the folded sandstone surface (Fig. 2-3).

We manually removed points that represented any feature other than in-situ sandstone (Fig. 2-4B and 2-4C), resulting in three disconnected surfaces that included the south fold, the Whaleback anticline, and the North Anticline. These surfaces have missing sections where the folded sandstone is covered by boulders and vegetation. For example, along the south limb of the Whaleback anticline, several meters of the exposed sandstone are slightly obscured by vegetation in the dense point cloud, making it difficult to distinguish rock and tree based on color (location of magenta points in Fig. 2-4D). We removed these ambiguous points. On the other hand, several post-drone-campaign visits to the field site enabled us to locate and add a few points of in-situ bedrock in the northeast section of the strip mine where vegetation significantly reduced sandstone exposure (Fig. 2-4C, points in in center-north of point cloud).

The remaining point cloud consists of about 10^7 points (Fig. 2-4C). While principally bedrock, it is impossible to remove all noise associated with smaller mine debris and small shrubs. Furthermore, faults, cracks, and concretions in the sandstone offset the surface and depart from a smoothed fold form. At this stage, it is customary to produce a standard TIN or DEM from the point cloud to represent the surface, but these techniques are inadequate, for reasons described above.

2.2.3 Generating the NURBS surface

We aimed to interpolate a smooth fold train, including the synclines, by applying a single NURBS surface to the point cloud. Before generating the final model, some additional steps include decimating the data, generating local patches over regions of missing points, and selecting the orientation and spacing for NURBS. Here, we evaluate several NURBS-surface-generation parameters: 1) point spacing, 2) directions of the applied NURBS relative to the fold

axes, 3) the spacing of the NURBS used to interpolate the surface, and 4) the "stiffness" of the NURBS surface.

In addition to the synclines, there were data gaps three regions of the point-cloud: 1) a rock slide on the South fold of the strip mine, 2) the crest of the North Anticline, and 3) the south limb of the Whaleback, close to a trough. Unlike the missing synclines or margins of the model, each of these gaps was enclosed by sandstone points on three or more sides (>75% enclosed). Individual NURBS patches were generated for these features using the closest points to guide the interpolation. Varying the NURBS density for these regions had little effect on their respective patch geometries, as only points around the perimeter of these patches were used. These NURBS patches were meshed, and points were placed at the mesh vertices. The point-cloud patches account for 3355 m^2 of surface area, less than 8% of the total area of the final surface (colored points in Fig. 2-4D)

To objectively decrease the overall remaining noise within the model and make the point cloud computationally more efficient for patching with NURBS, we decimated the point cloud by subsampling the 10^7-point model using a nearest-neighbor operation in CloudCompare, an opensource software package ("CloudCompare 2.10" 2019). We subsampled the dense point cloud in multiple trials, each with different point spacings (e.g., 0.5 m, 1 m, 5 m) to determine which spacing best preserved the geometric detail of the fold train while excluding noise and increasing computational efficiency. We also stripped the data of all information (e.g., color, normal direction, and other scalar information) other than (x, y, z) position, to reduce the overall file size and enhance computing speed for subsequent operations. The point clouds were imported to Rhinoceros 3D ("Rhino"), a computer-aided design program that constructs models with NURBS (McNeel and others 2010).

Subsampling the point cloud to 1-m spacing between points resulted in a model containing 2 x 10^4 points (Fig. 2-4D). The 1-m-spacing NURBS surface has less apparent irregularities in the fold; whereas a 0.5-m point spacing included noise and finer scale secondary structures (fault surfaces and cracks) that influenced subsequent curvature analyses. While point spacings of 2 m and greater yielded increasingly smoother NURBS surfaces, the 1-m spacing was sufficient in reducing noise and better honored the geometric integrity of the data.

The *u* and *v* parameters define the two principal directions of the NURBS curves that compose a NURBS surface. We explored the effect of varying the u and v directions of the NURBS surface relative to the trend of the Whaleback Anticline, the central fold in this exposure. Based on the classical technique of plotting the poles of field-measured surfaces in order to construct a stereographic pi-diagram (Ramsay and Huber 1987), Monfort (2016) determined the trend and plunge of the Whaleback fold axis to be 084/00. When the NURBS *u*-direction is aligned with the trend of the Whaleback, the *v*-parameterized NURBS interpolate synformal geometries between the folds that vary irregularly along the syncline axes. The variations are function of the variations in the edges of the point cloud at the troughs. As the *u* and *v* directions are rotated away from parallel and perpendicular to the trend of the Whaleback, the variations in the interpolated synclines decrease; thus, orienting *u* and *v* 45° from the trend of the Whaleback yields the smoothest interpolation of syncline geometries in the fold train.

When applying NURBS to interpolate a surface, the user chooses the number of NURBS in both the *u* and *v* directions. Having a NURBS density that is higher than the point spacing amplifies irregularities in the NURBS surface, while a NURBS spacing that is too broad can overly smooth the model. Despite the irregular shape of the point cloud, the application of an evenly spaced 100*u* x 100*v* NURBS grid (spacing of ~3-5 meters per spline in *u* or *v* directions)

oriented at 45° to the fold axis produced an interpolated surface that balanced representing irregularities in the general geometry while not introducing or compounding noise.

In Rhino3D, the NURBS surface starts as a best-fit *u* x *v* plane to the point cloud that is "pulled" to fit the point-cloud geometry. The "stiffness" of the NURBS surface controls how tightly the surface is stretched between control points: increasing the stiffness increases the surface's conformity to a plane. As we increased the stiffness, geometric details were lost, and the Whaleback increasingly resembled an idealized cylindrical fold. Stiffness values less than 1 cause the NURBS to vary in a geologically unrealistic manner between points. We found that a stiffness of 3 to 5 honored the data the best for most of the model while interpolating realistic, smooth synclines between the exposed folds.

2.2.4 Completed fold interpolation

In Fig. 2-5 we present a smooth, continuous NURBS surface with a stiffness of 3 and 100*u* x100*v* NURBS, for which the point cloud was rotated 45° off-trend for the application of the NURBS surface. The interpolated synclines are tighter than their adjacent anticlines, and the geometry of eastern half of the North Anticline is interpolated with geometric influences from the Whaleback and point-cloud data from the western half of the North Anticline. The overturned geometry of the Whaleback's north limb, as observed in the field, is reproduced by the application of the NURBS surface.

The NURBS surface permits sectioning the fold in any orientation. While arbitrarily cutting mesh objects poses problems and often involves an algorithm to reposition nodes, sectioning a NURBS surface produces clean edges. We sectioned the Whaleback anticline into four 50-m NURBS surfaces to observe variations in the fold's orientation along its axis using

classical structural geology data presentation. For each surface, we converted the NURBS into a polygonal mesh. The vertex normals of each mesh polygon were plotted as bedding normals to generate pi-diagrams on stereonets using a script adapted from Mookerjee and Nickleach (2011) (Fig. 2-6).

The pi-plots from the NURBS surface show that the axis of Whaleback trends linearly and is doubly plunging: the western half of the Whaleback's axis plunges sub-horizontally at a trend of ~260, while the eastern half of the Whaleback gradually plunges up to 10° at a trend of 082. Individual bedding poles capture the overturned geometry of the Whaleback's north limb, a geometry measured in the field and represented by the NURBS surface.

The NURBS surface enables a comparison of the fold axes of three exposed folds in the strip mine. We sectioned each fold from the NURBS surface and generated pi plots (Fig. 2-7). Based on their calculated axes, the three folds diverge from west to east, which provides fodder for future studies in exploring the kinematic and mechanical significance of this splay regarding fold development and regional tectonic history.

2.2.5 Comparison of NURBS model to field data

To evaluate the NURBS representation compared to traditional field techniques, we compared orientation data extracted from the model to bedding orientations measured in the field. Monfort (2016) acquired bedding-surface orientation data from the field by measuring along three scanlines approximately perpendicular the Whaleback fold axis. To mirror Monfort's (2016) survey, we isolated three 10-meter-wide segments of the Whaleback NURBS model in the same locations as Monfort's (2016) scanlines. We generated pi plots for our model segments for comparison to Monfort's (2016) field data (Fig. 2-8).

Between the NURBS-based pi-plots and field data, there are differing distributions of poles but similar axis orientations represented in the pi-plots. The orientations measured from the NURBS surface represent a mostly uniform distribution of data around the fold, whereas the field measurement data come from areas of the Whaleback that are easiest to access (Fig. 2-8). An exception on the NURBS stereonet is a gap of data between the 50 – 80° N small circles. This area corresponds to the south limb of the Whaleback where vegetation obscures the rock surface in UAV photographs. The field data (Monfort 2016) includes bedding normals that trend 060-075°, as the fold surface in this region is accessible on foot but not conducive to aerial photography. There is sparse point-cloud data in this region that we regard with high confidence, but nevertheless, their inclusion should yield bedding measurements that are similar to field observations. Comparing the subsampled point cloud to the NURBS surface shows that with greater stiffness, this region shows deviations of the NURBS from the point cloud.

2.2.6 Geometric Analyses with NURBS

By constructing the smooth folded surface with NURBS, the geometry of the folds can be analyzed with ease. One attribute is the curvature of the surface.

Curvature describes the spatial rate of change of gradient ,or slope (e.g., Lisle 1994; Bergbauer and Pollard 2003). In a 2D fold section, the highest and lowest values of curvature define the hinges and inflection points of a fold, respectively. Because buckle-fold form in nature deviates from the sinewave form with which we conceptualize folds, identifying the hinges and inflections is necessary for objective measurements of arclength, wavelength, and amplitude. In three dimensions, a surface has two principal curvatures, which can be defined at any given point in the directions of maximum and minimum curvatures. Mean curvature is the average of the

principal curvatures. Gaussian curvature is the product of the two principle curvatures measured along two orthogonal curves (e.g. Lisle 1994). To extract meaningful information from these measures, it is essential to start with a smoothed and interpolated surface (e.g. Mynatt et al.) otherwise results may be nonsensical (e.g. Welker et al. 2019).

Many researchers have considered the capabilities of curvature to predict the distribution of strain, although not all who have investigated this correlation have observed a meaningful correspondence of curvature to fracture density (Evans and Fischer 2012; and references therein). Considering the tangential-longitudinal-strain end-member model for buckle folds (J. G. Ramsay 1967), in which strain is concentrated at fold hinges, if TLS is the dominant mechanism for folding we would expect to see the greatest expression of strain within the hinges of the anticlines at the Bear Valley Strip Mine. By comparing curvature measurements on a smoothed continuous modeled surface of our fold train to field data of micro- and mesoscale strain on the natural folded surface, we can add weight to one side of the argument regarding the curvature-to-strain correspondence. Lack of correspondence might suggest that tangential-longitudinal strain is not the dominant fold mechanism for the Whaleback anticline (or that observed structures are not related to fold amplification).Calculated curvatures highlight the hinges of the NURBS-interpolated folds (Fig. 2-9). The absolute value of the mean curvature identified the hinges of the synclines (Fig. 2-9A and 2-9B). The trend of these curvature anomalies is consistent along the fold. Other highlighted features include the high mean curvature that trends parallel to the crest of the Whaleback, and another, sub-parallel curvature anomaly that intermittently corresponds to the edge of a meso-scale thrust fault. We could interpret this second curvature anomaly as a second hinge of the anticline, which would suggest that the Whaleback's geometry is less of a cylindrical fold and more of a box fold.

To predict the distribution of strain, three-dimensional curvature is of importance when modeling folds as developable surfaces. A developable surface can be "unrolled" into a flat planar surface without stretching or straining the surface in the process (Lisle and Martínez 2005). A perfectly cylindrical-fold surface produced through isometric bending could be unrolled into a flat sheet and is therefore "developable," whereas a fold with double curvature, such as a dome, would have to be internally deformed to be flattened. Gaussian curvature has a value of zero if one of the principal values of curvature is zero, as would be the case in a cylindrical fold. A non-zero value of Gaussian curvature points to a deviation from a developable surface and may describe to a variation in the distribution of strain within the fold. Despite applying a number of different filters for the range of measured Gaussian curvature on the NURBS surface (Fig. 2-9C and 2-9D), we do not find a meaningful correlation between Gaussian curvature and measures of internal strain, e.g., secondary faults.

2.3 Conclusion

Considering the growing availability of aerial surveying methods (e.g., LiDAR and Structure-from-Motion), there are new opportunities to capture fold geometry with robust point-cloud data sets; however, the robustness of these data poses a noise problem. We propose that NURBS surfaces are good modeling tools for cleanly representing fold form from incomplete and/or robust point cloud data. Because the NURBS are not confined to single-variable functions and can have multiple values in the height (z) axis, the NURBS represented the overturned geometry of a fold limb. While we found no meaningful first-order correspondence between curvature and brittle strain at the Whaleback, curvature can easily be calculated on a NURBS surface. Finally, a comparison of pi plots from field data and the NURBS surface shows that the

NURBS surface reproduces accurate spatial orientations but a more-even distribution of data points, as field measurements at the Whaleback have physical limitations.

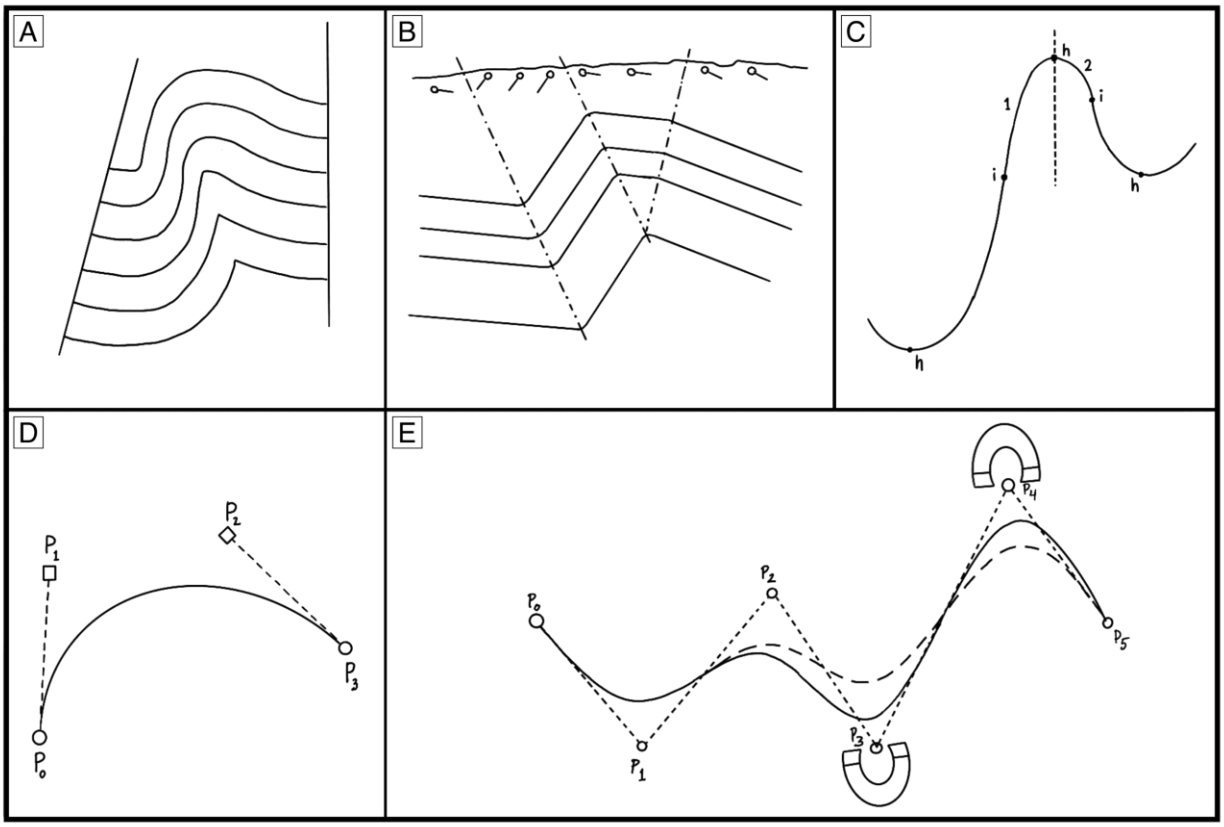

Fig. 2-1: Tools for modeling the geometry of folds.
A) Folds modeled as concentric arcs (modified from Busk, 1929). B) Kink fold forms (modified from Suppe, 1983). C) Sinusoidal functions modeling fold form (modified from Hudleston, 1973). D) Bezier curves with control points, P_n (modified from Srivastava and Lisle, 2004). E) NURB spline (solid line) with control points, P_n. Magnets pulling on the spline represent the ability to modify the influence of specific control points.

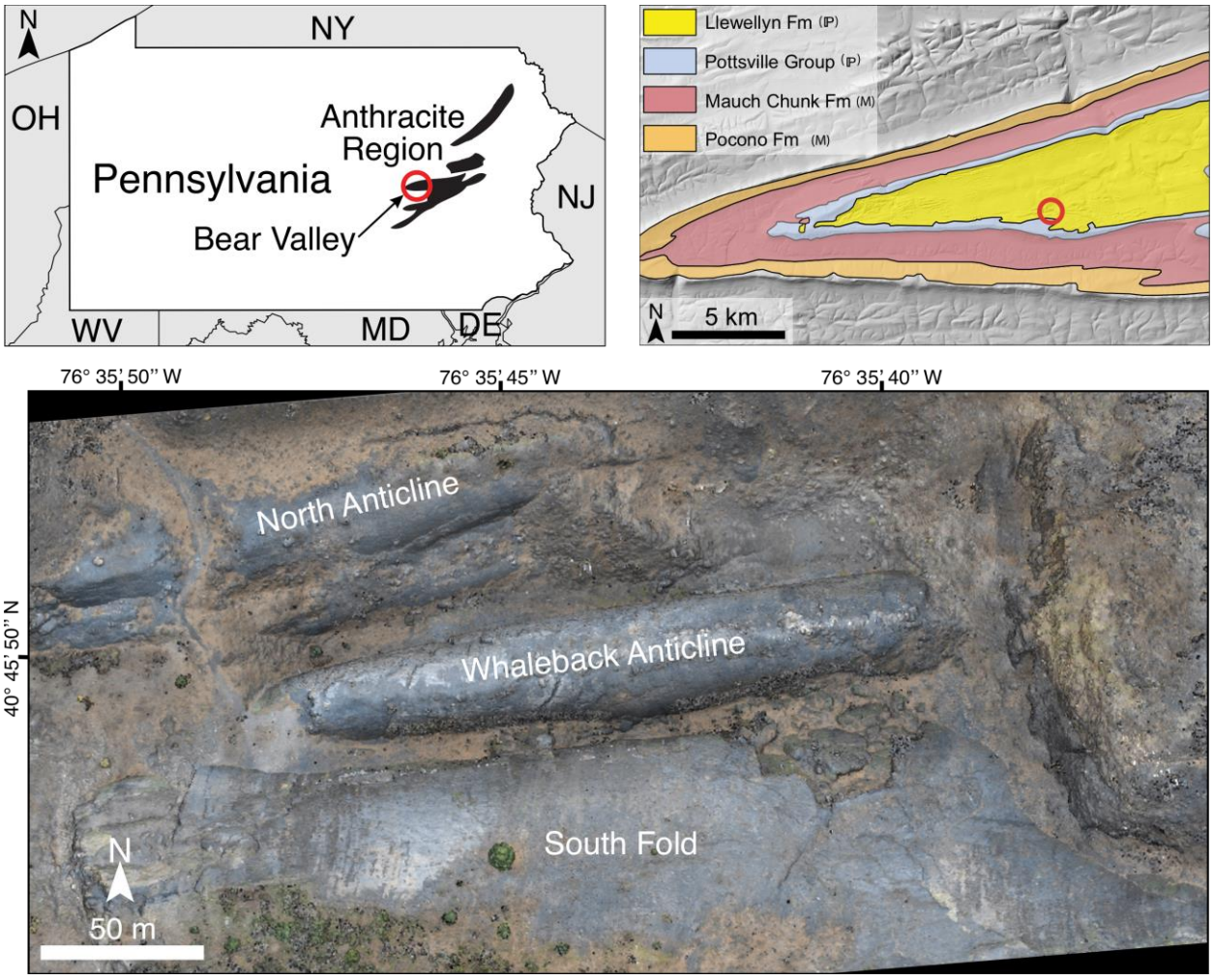

Fig. 2-2: Geography of Bear Valley Strip Mine (BVSM).
(Top Left) Map of Pennsylvania with location of BVSM in the Anthracite Region of the Valley and Ridge Province of the Appalachian Mountains. (Top Right) Geologic map of the Western Middle Synclinorium. Data from Pennsylvania Spatial Data Access (pasada.psu.edu). The location of BVSM is indicated by the red circle. (Bottom) The fold train in BVSM has exposures of the North Anticline, Whaleback Anticline, and South Fold. The image is an orthogonal view of a point cloud from which a lot of the vegetation has been removed.

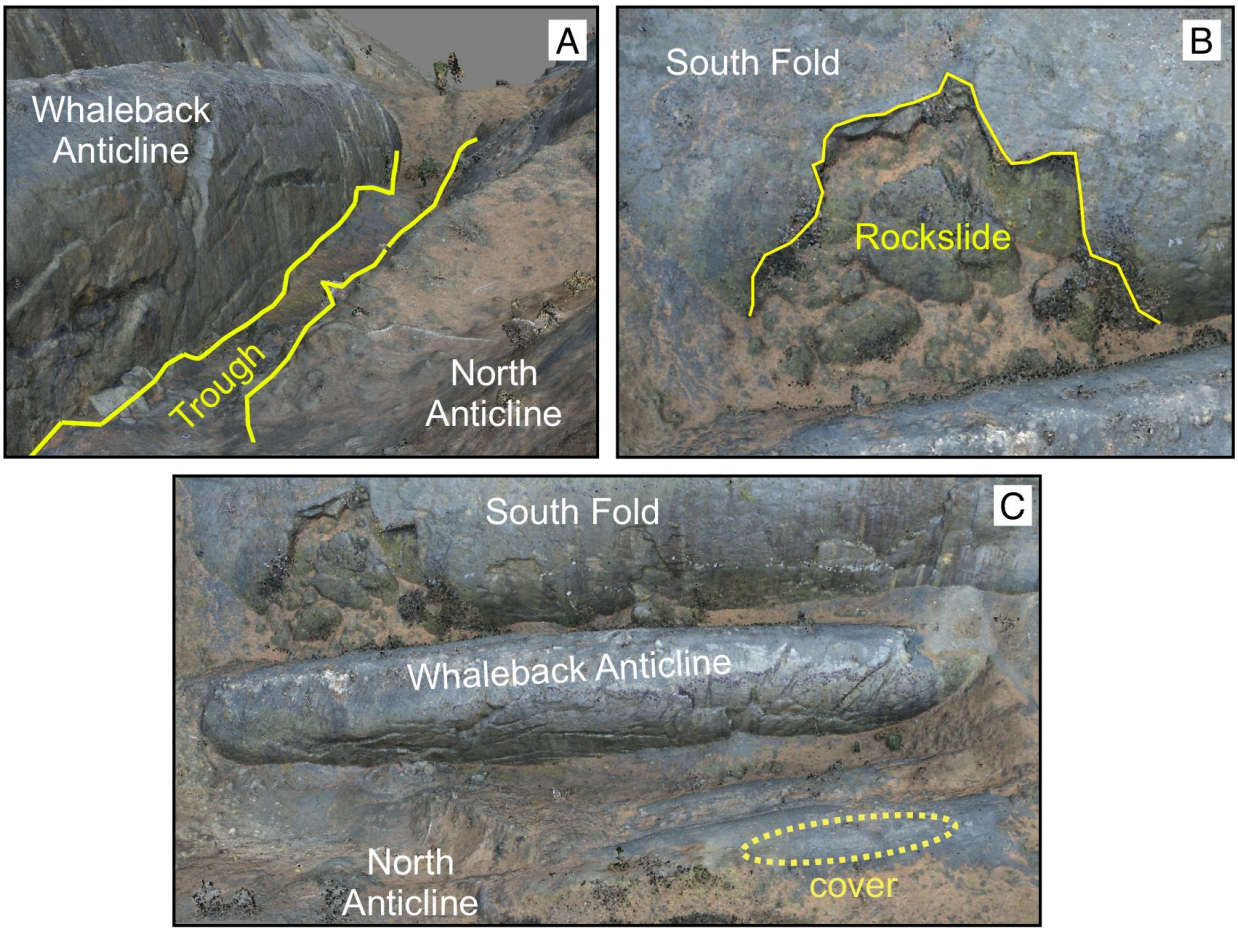

Fig. 2-3: Several features limit and/or obscure the geometry of the fold train.
A) Troughs hide synclines. B) A rockslide discontinues the South Fold. C) A sedimentary cover on/near the crest of the North Anticline.

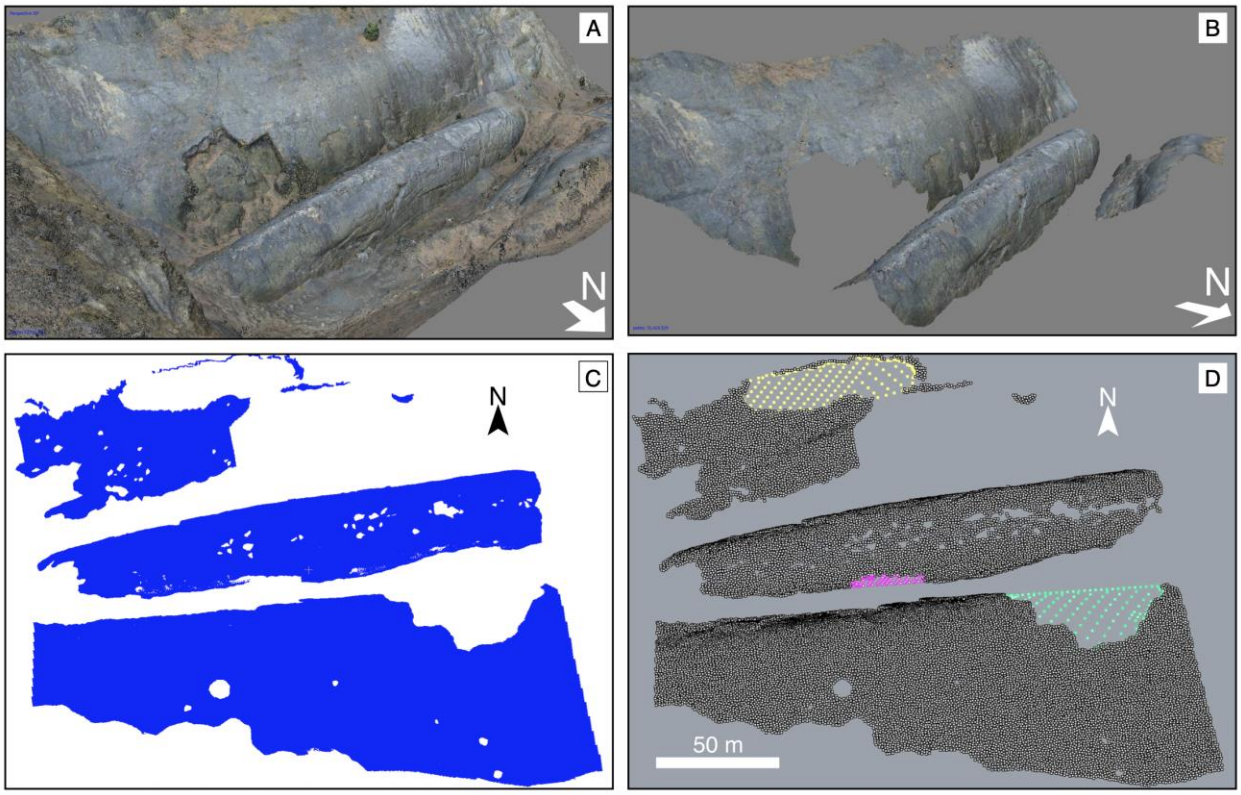

Fig. 2-4: Preparing the point-cloud model for further operations.
Renderings of point clouds in A and B are from Agisoft Photoscan and renderings in C and D are from Rhino3D. A) Oblique view of dense point cloud with vegetation removed. B) Oblique view of dense point cloud with in-situ sandstone. C) Aerial view of dense point cloud with added ground-truthed points to North Anticline. The point cloud appears primarily as a solid surface due to the density of the points in CloudCompare. D) Aerial view of the sub-sampled point cloud (1-m spacing) with patches for the crest of the North Anticline (yellow points), removed vegetation in the south limb of the Whaleback (magenta), and rockslide on the South Fold (green).

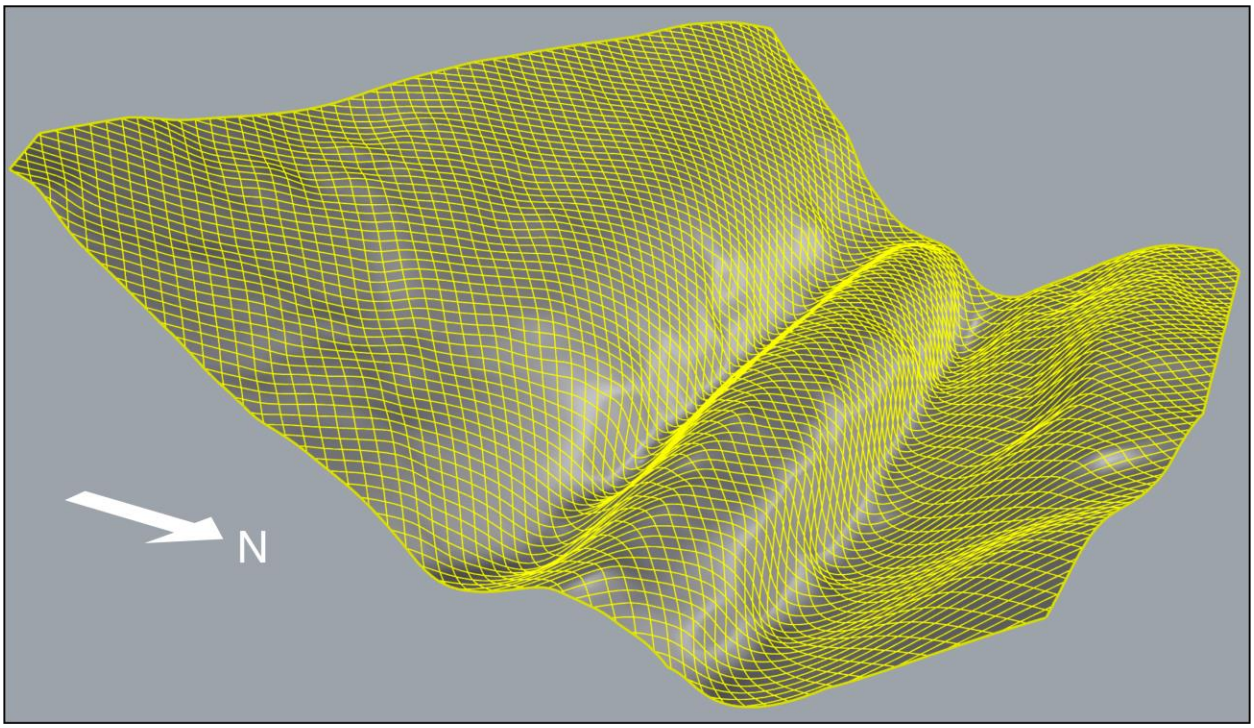

Fig. 2-5: NURBS surface.
This surface was generated from a 100x100 NURBS spacing with a stiffness of 3 (oblique view). The NURBS surface models a smooth, complete fold train with geometric variations. NURBS are highlighted in yellow while the interpolated NURBS surface is rendered with shading. The NURBS in this surface were generated 45° from the trend (Monfort, 2016) of the Whaleback. This surface has been trimmed to the exterior extent of point-cloud data. Within the point-cloud data, the rockslide is not apparent, the crest of the North Anticline has a smooth geometry, and the synclines connecting the anticlines of the fold train are smoothly interpolated.

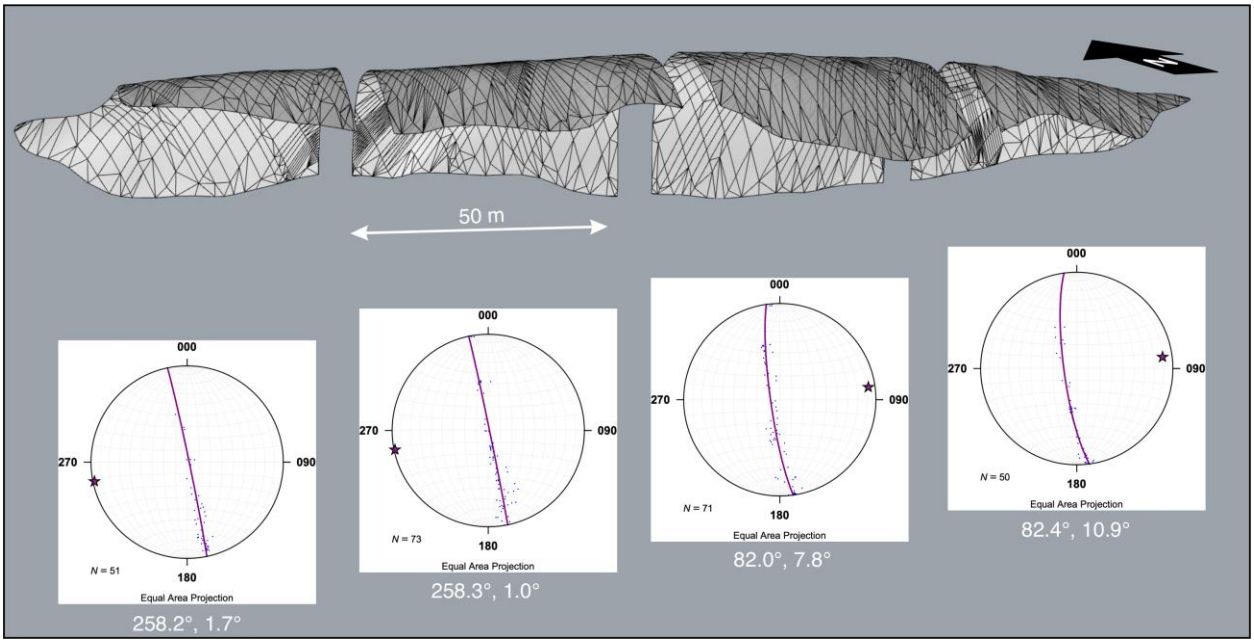

Fig. 2-6: Meshed NURBS surface sectioned into 50-m segments from west to east.
In equal area stereonet projections, plotted poles are vertex normals to polygons. Stars in stereonets represent the trend and plunge of the fold axis for a give segment. The stereonet pi-plots associated with each segment demonstrate that the Whaleback is doubly plunging – the western segments plunge to the west while the eastern segments increasingly plunge to the east. Pi-plots were produced using a Mathematica code by Mookerjie and Nickleach (2011).

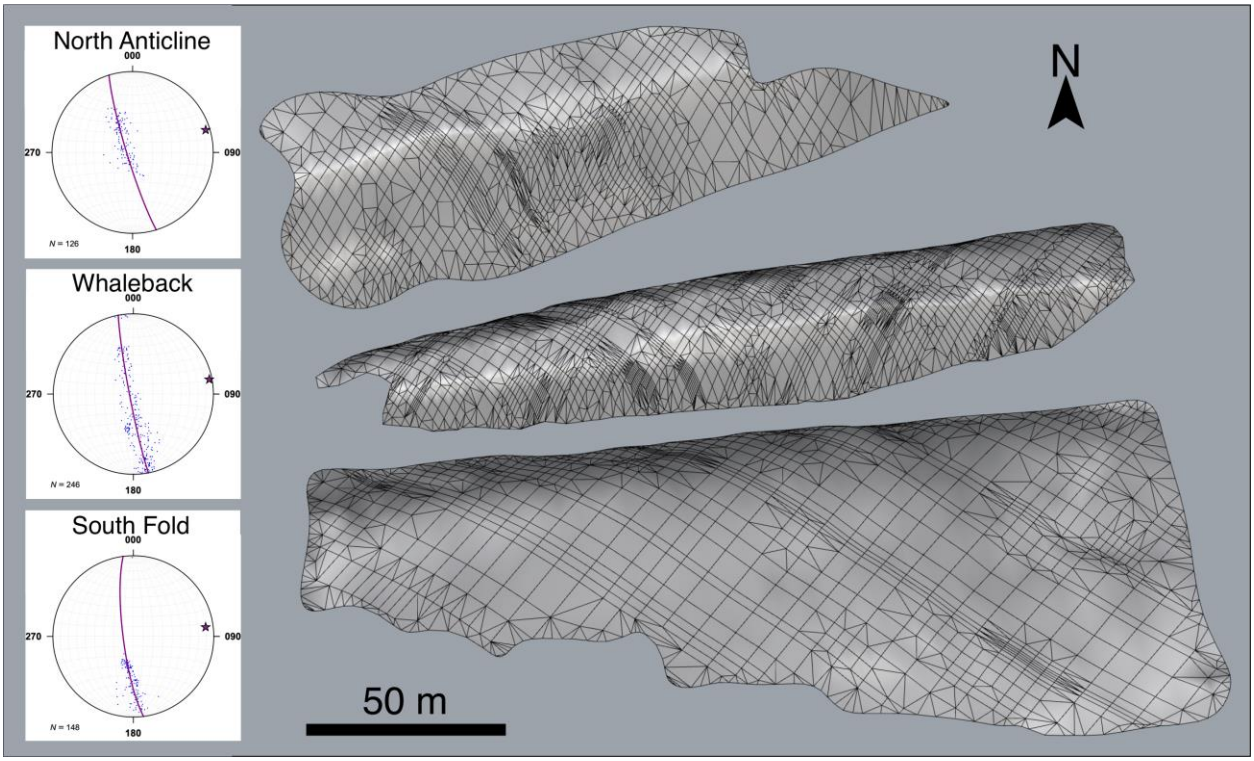

Fig. 2-7: Meshed NURBS surfaces of three folds in the strip mine.
These are aerial views of the North Anticline, Whaleback, and South Fold with their associated pi plots. Stars in the pi plots indicate the trend and plunge of the fold axes for each fold. The pi plots demonstrate that the axes of these folds are diverging to the east. Pi-plots were produced using a Mathematica code by Mookerjie and Nickleach (2011).

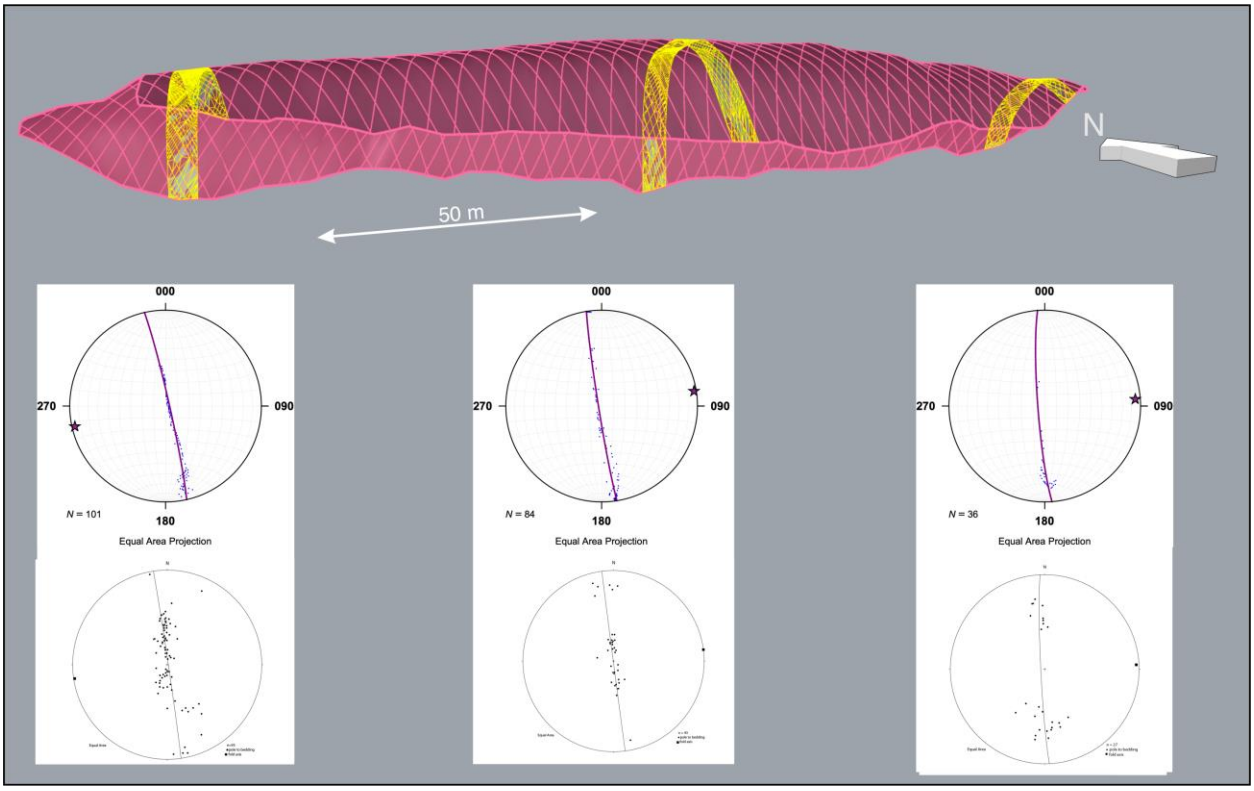

Fig. 2-8: Comparison of NURBS surface orientations to field data from Monfort (2016). Top: Meshed NURBS surface (magenta) with 10-m-wide sections in locations correlate to the scanlines investigated by Monfort (2016). Stereonets: (top) Pi-plots produced from NURBS surface sections in comparison to (bottom) section-correlated pi-plots from Monfort (2016). Although the distribution of measured data varies from our study to Monfort's, data from the NURBS surface reproduce the fold-axis approximations from Monfort's (2016) field data.

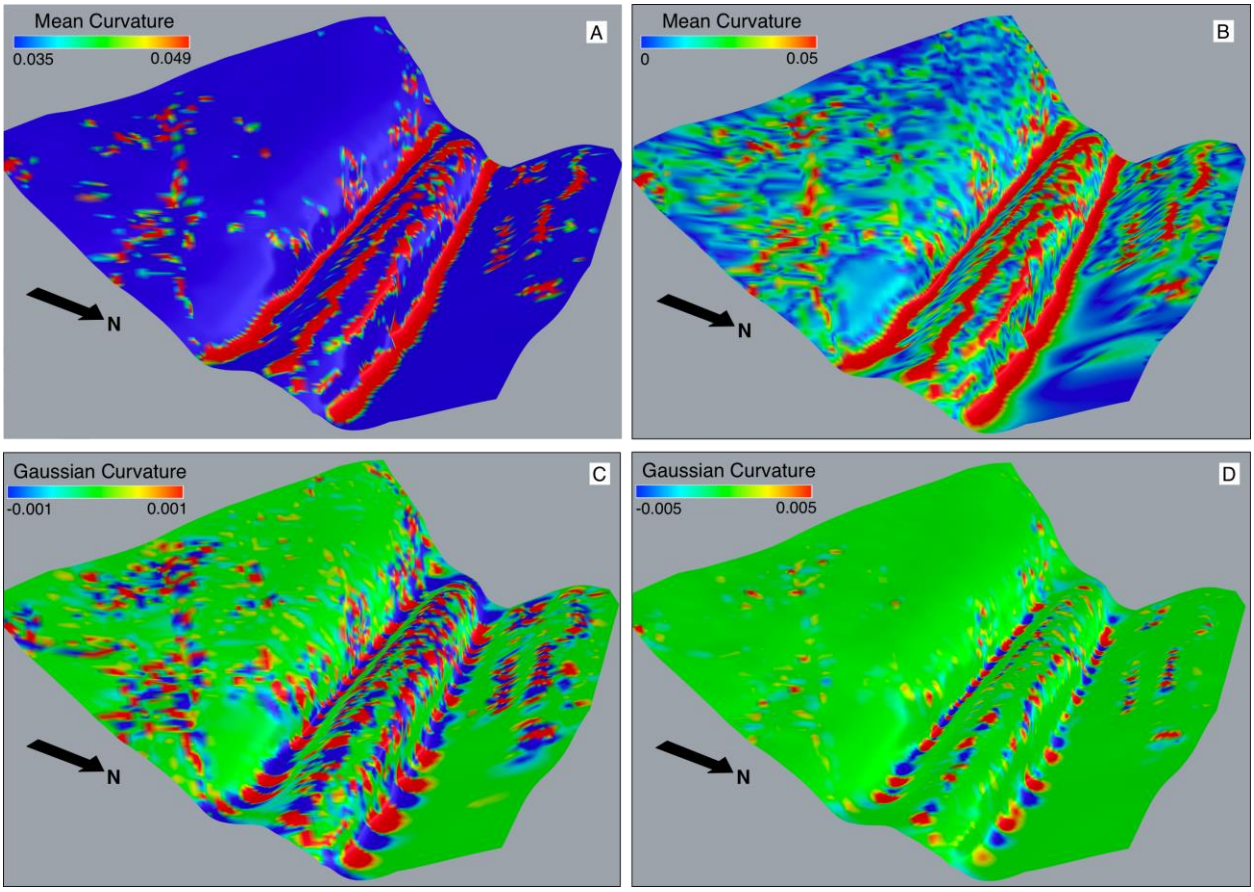

Fig. 2-9: Mean and Gaussian curvature analyses of the NURBS surface.
(A and B) Two ranges of mean curvature also highlight features on the crest and the interpolated synclines. (C and D) Two ranges for Gaussian curvature primarily highlight undulating features on the fold crests and interpolated synclines. Positive values of Gaussian curvature (red) indicate basin and dome geometries while negative values (blue) indicate synformal or antiformal saddles.

References in Chapter 2

Adamuszek, Marta, Daniel Walter Schmid, and Marcin Dabrowski. 2011. "Fold Geometry Toolbox -- Automated Determination of Fold Shape, Shortening, and Material Properties." *Journal of Structural Geology* 33: 1406–16. https://doi.org/10.1016/j.jsg.2011.06.003.

"AgiSoft PhotoScan Professional." 2018. http://www.agisoft.com/downloads/installer/.

Bergbauer, Stephan, and David D Pollard. 2003. "How to Calculate Normal Curvatures of Sampled Geological Surfaces." *Journal of Structural Geology* 25: 277–89. www.elsevier.com/locate/jsg.

Buckley, Simon J., Håvard D. Enge, Christian Carlsson, and John A. Howell. 2010. "Terrestrial Laser Scanning for Use in Virtual Outcrop Geology." *The Photogrammetric Record* 25 (131): 225–39. https://doi.org/10.1111/j.1477-9730.2010.00585.x.

Bureick, Johannes, Hans Neuner, Corinna Harmening, and Ingo Neumann. 2016. "Curve and Surface Approximation of 3D Point Clouds." *Allgemeine Vermessungs-Nachrichten (AVN)* 123 (11–12): 315–27.

Busk, Henry Gould. 1929. *Earth Flexures*. London: Cambridge University Press.

Carr, Brett B., Amanda B. Clarke, J. Ramón Arrowsmith, Loÿc Vanderkluysen, and Bima Eko Dhanu. 2019. "The Emplacement of the Active Lava Flow at Sinabung Volcano, Sumatra, Indonesia, Documented by Structure-from-Motion Photogrammetry." *Journal of Volcanology and Geothermal Research* 382 (September): 164–72. https://doi.org/10.1016/J.JVOLGEORES.2018.02.004.

Caumon, G, · P Collon-Drouaillet, · C Le Carlier De Veslud, · S Viseur, and · J Sausse. 2009. "Surface-Based 3D Modeling of Geological Structures." *Math Geosci* 41: 927–45. https://doi.org/10.1007/s11004-009-9244-2.

"CloudCompare 2.10." 2019. http://www.cloudcompare.org/.

Evans, Mark A, and Mark P Fischer. 2012. "On the Distribution of Fluids in Folds: A Review of Controlling Factors and Processes." *Journal of Structural Geology* 44: 2–24. https://doi.org/10.1016/j.jsg.2012.08.003.

Fisher, T. R., and R. Q. Wales. 1992. "Three Dimensional Solid Modeling of Geo-Objects Using Non-Uniform Rational B-Splines (NURBS)." In *Three-Dimensional Modeling with Geoscientific Information Systems*, edited by A. K. Turner, 85–105. Dordrecht: Springer Netherlands. https://doi.org/10.1007/978-94-011-2556-7_9.

Hollister, Stephen M. 2001. "The Dirty Little Secrets of NURBS." Www.Pilot3D.Com. 2001.

Hudleston, P. J. 1973. "Fold Morphology and Some Geometrical Implications of Theories of Fold Development." *Tectonophysics* 16 (1–2): 1–46. https://doi.org/10.1016/0040-1951(73)90129-7.

Humair, Florian, Antonio Abellan, Dario Carrea, Battista Matasci, Jean-Luc Epard, and Michel Jaboyedoff. 2015. "European Journal of Remote Sensing Geological Layers Detection and Characterisation Using High Resolution 3D Point Clouds: Example of a Box-Fold in the Swiss Jura Mountains) Geological Layers Detection and Characterisation Using High Resolution 3D Point C." *European Journal of Remote Sensing* 48 (1): 541–68.

https://doi.org/10.5721/EuJRS20154831.

Jaboyedoff, M., R. Metzger, T. Oppikofer, R. Couture, M.H. Derron, J. Locat, and D. Turmel. 2007. "New Insight Techniques to Analyze Rock-Slope Relief Using DEM And 3Dimaging Cloud Points: COLTOP-3D Software." In *Rock Mechanics: Meeting Society's Challenges and Demands. Proceedings of the 1st Canada-US Rock Mechanics Symposium*, 1:61–68. American Rock Mechanics Association.

Jacquemyn, C., Y. Melnikova, M.D. Jackson, G.J. Hampson, and C.M. John. 2016. "Geologic Modelling Using Parametric NURBS Surfaces," no. September. https://doi.org/10.3997/2214-4609.201601884.

James, Michael R., and Stuart Robson. 2012. "Straightforward Reconstruction of 3D Surfaces and Topography with a Camera: Accuracy and Geoscience Application." *Journal of Geophysical Research: Earth Surface* 117 (F3).

Lisle, Richard J. 1994. "Detection of Zones of Abnormal Strains in Structures Using Gaussian Curvature Analysis." *American Association of Petroleum Geologists Bulletin* 78 (12): 1811–19. https://doi.org/10.1177/0192513X12437708.

Lisle, Richard J., and Juan Luis Fernánde Martínez. 2005. "Structural Analysis of Seismically Mapped Horizons Using the Developable Surface Model." *AAPG Bulletin* 89 (7): 839–48. https://doi.org/10.1306/01300504072.

Lowe, David G. 2004. "Distinctive Image Features from Scale-Invariant Keypoints." *International Journal of Computer Vision*, no. 60: 91–110.

Mallet, J. L. 1992a. "Discrete Smooth Interpolation in Geometric Modelling." *Computer-Aided Design* 24 (4): 178–91. https://doi.org/10.1016/0010-4485(92)90054-E.

———. 1992b. *GOCAD: A Computer Aided Design Program for Geological Applications*. Edited by A. K. Turner. *Three-Dimensional Modeling with Geoscientific Information Systems*. Vol. 354. Springer, Dordrecht. https://doi.org/10.1007/978-94-011-2556-7_11.

Mallet, J L. 1997. "Discrete Modeling for Natural Objects." *Mathematical Geology*. Vol. 29. https://link.springer.com/content/pdf/10.1007%2FBF02769628.pdf.

McNeel, R, and others. 2010. "Rhinoceros 3D." Seattle, WA: Robert McNeel & Associates.

Miao, Zhengjian, Ming-Chao Li, and Deng-Hua Zhong. 2012. "Automatic Generation Method of Geological Cross-Sections in Dredging Engineering Based on 3D Solid NURBS Models." *Transactions of Tianjin University* 18: 393–400. https://doi.org/10.1007/s12209.

Monfort, Eric Michael. 2016. "A Study of Three-Dimensional Grain-Scale Strain on the Bear Valley Strip Mine Whaleback Anticline Using Normalized Fry Analysis, Shamokin, PA." Bucknell University. https://digitalcommons.bucknell.edu/honors_theses.

Mookerjee, Matty, and Scott Nickleach. 2011. "Three-Dimensional Strain Analysis Using Mathematica." *Journal of Structural Geology* 33 (10): 1467–76. https://doi.org/10.1016/j.jsg.2011.08.003.

Mynatt, Ian, Stephan Bergbauer, and David D Pollard. 2007. "Using Differential Geometry to Describe 3-D Folds." https://doi.org/10.1016/j.jsg.2007.02.006.

Needle, Mattathias D., Jacky Mooc, John F. Akers, and Juliet G. Crider. 2022. "Virtual Field

Experiences in a Web-Based Video Game Environment: Open-Ended Examples of Existing and Fictional Field Sites." *Geosci. Commun* 5 (3): 251–60. https://doi.org/https://doi.org/10.5194/gc-5-251-2022.

Nickelsen, Richard P. 1979. "Sequence of Structural Stages of the Alleghany Orogeny, At the Bear Valley Strip Mine, Shamokin, Pennsylvania." *Am J Sci* 279 (3): 225–71. https://doi.org/10.2475/ajs.279.3.225.

Paor, Declan G. De. 1996. "Bezier Curves and Geological Design." In *Structural Geology and Personal Computers*, edited by Declan G. (Harvard University) De Paor, 1st ed., 389–417. Pergamon.

Pavlis, Terry L., and Kelsey A. Mason. 2017. "The New World of 3D Geologic Mapping." *GSA Today* 271 (10). https://doi.org/10.1130/GSATG313A.1.

Pearce, Mark A., Richard R. Jones, Steven A. F. Smith, and Kenneth J. W. McCaffrey. 2011. "Quantification of Fold Curvature and Fracturing Using Terrestrial Laster Scanning." *AAPG Bulletin* 95 (5): 771–94. ftp://ftp.ingv.it/pub/steven.smith/Paper reprints/2011_Pearce_et_al_AAPG.PDF.

Pearce, Mark A., Richard R. Jones, Steven A.F. Smith, Kenneth J.W. McCaffrey, and Phill Clegg. 2006. "Numerical Analysis of Fold Curvature Using Data Acquired by High-Precision GPS." *Journal of Structural Geology* 28 (9): 1640–46. https://doi.org/10.1016/J.JSG.2006.05.010.

Ramsay, J. G. 1967. *Folding and Fracturing of Rocks*. New York: McGraw-Hill.

Ramsay, John G., and Martin I. Huber. 1987. *The Techniques of Modern Structural Geology, Vol 2: Folds and Fractures*. *Academic Press (Elsevier)*. 4th printi. Academic Press.

Samson, Philippe, and Jean-Laurent Mallet. 1997. "Curvature Analysis of Triangulated Surfaces in Structural Geology." *Mathematical Geology* 29 (3): 391–412. https://doi.org/10.1007/BF02769642.

Schmalholz, Stefan M., and Yuri Yu. Podladchikov. 2001. "Strain and Competence Contrast Estimation from Fold Shape." *Tectonophysics* 340 (3–4): 195–213. https://doi.org/10.1016/S0040-1951(01)00151-2.

Schmalholz, Stefan M. 2006. "Scaled Amplification Equation: A Key to the Folding History of Buckled Viscous Single-Layers." https://doi.org/10.1016/j.tecto.2006.03.008.

Schmalholz, Stefan M, and Yuri Yu Podladchikov. 2000. "Finite Amplitude Folding: Transition from Exponential to Layer Length Controlled Growth." *Earth and Planetary Science Letters* 179: 363–77. www.elsevier.com/locate/epsl.

Sprague, Kevin B., and Eric A. de Kemp. 2005. "Interpretive Tools for 3-D Structural Geological Modelling Part II: Surface Design from Sparse Spatial Data." *GeoInformatica* 9 (1): 5–32. https://doi.org/10.1007/s10707-004-5620-8.

Srivastava, Deepak C, and Richard J Lisle. 2004. "Rapid Analysis of Fold Shape Using Bézier Curves." *Journal of Structural Geology* 26: 1553–59. https://doi.org/10.1016/j.jsg.2004.02.004.

Srivastava, Deepak C, and Vipul Rastogi. 2009. "HingeInflex: A MATLAB-Based Method for

Precise Selection of the Hinge and the Inflection Points in Folds." *Geol. Mag* 147 (2): 233. https://doi.org/10.1017/S0016756809990641.

Stabler, C.L. 1968. "Simplified Fourier Analysis of Fold Shapes." *Tectonophysics* 6 (4): 343–50. https://doi.org/10.1016/0040-1951(68)90049-8.

Stowe, C.W. 1988. "Application of Fourier Analysis for Computer Representation of Fold Profiles." *Tectonophysics* 156 (3–4): 303–11. https://doi.org/10.1016/0040-1951(88)90067-4.

Suppe, John. 1983. "Geometrv and Kinematics of Fault-Bend Folding Dynamics of Fold Growth View Project Area Relief Analysis in Detachment Folds View Project." *American Journal of Science* 283 (September): 684–721. https://doi.org/10.2475/ajs.283.7.684.

Welker, Avery J., John P. Hogan, Andreas Eckert, Sarah Tindall, and Chao Liu. 2019. "Conical Folds – An Artefact of Using Simple Geometric Shapes to Describe a Complex Geologic Structure." *Journal of Structural Geology* 123 (June): 96–104. https://doi.org/10.1016/J.JSG.2019.04.005.

Zhong, Deng-Hua, Ming-Chao Li, Ling-Guang Song, and Gang Wang. 2006. "Enhanced NURBS Modeling and Visualization for Large 3D Geoengineering Applications: An Example from the Jinping First-Level Hydropower Engineering Project, China." *Computers & Geosciences* 32 (9): 1270–82. https://doi.org/10.1016/J.CAGEO.2005.11.007.

Chapter 3 Virtual field experiences in a web-based videogame environment: Open-ended examples of existing and fictional field sites

Abstract

We present two original, videogame-style field-geology experiences designed to allow flexible, open-ended exploration for geologic mapping and structural geology. One simulation features the Whaleback anticline, a site in central Pennsylvania (USA) with three-dimensional exposure of a 30-m-high fold, based on a terrain model that was acquired through structure-from-motion photogrammetry. The second example is a fictional location with simplified geology, built with digital modeling software and inspired by the geology of northwestern Washington. Users move through the terrain, as if in the field, selecting where to make observations of the geologic structure. Additionally, these virtual field experiences provide novel visualization opportunities through tools like a geodetic compass that instantly plots data to a stereonet, and a jetpack simulation which allows the user to interrogate geologic surfaces in hard-to-reach locations. We designed the virtual field experiences in a widely used videogame-creation software and published the field simulations for access via the internet and common web browsers, so that no special hardware or software is required to play. We implemented these field simulations to partially replace field and lab exercises in two different courses offered remotely through the University of Washington Department of Earth and Space Sciences, with assignments that address many of the learning goals of traditional in-person exercises. Because the virtual field experiences are open ended, other instructors can design different exercises to meet different learning goals. While this game environment currently serves as an enhancement

to remote education, this format can also augment traditional educational experiences, overcoming several challenges to accessing the field or particular outcrops and thereby broadening opportunities for participation and scientific collaboration.

3.1 Introduction

Starting in March 2020, safety measures to dampen the transmission of COVID-19 impacted field instruction related to geoscience education. While the COVID-19 pandemic forced geoscience educators to design alternatives to in-person field instruction, this demand for remote instruction also highlighted shortcomings of the traditional geoscience curriculum to include students who for a multitude of reasons have difficulties accessing traditional field-based coursework (e.g., Wolfe and Riggs 2017; Carabajal, Marshall, and Atchison 2017). The need for educational experiences that incorporate fundamentals traditionally taught in field-based courses will remain after the pandemic. Such educational experiences might be deployed for the purpose of inclusion or for skill development in data collection and analysis as an alternative or precursor to traditional field courses.

Historically, the emergence of geoscience in Europe and North America was closely tied to objective descriptions of outcrops and discussion of the observations in the field (e.g., Hallam 1990). The practice dates from at least the time of James Hutton in the late 1780's (e.g., Gould 1982), and the tradition continues in modern field conferences (e.g. Evenson et al. 2000) and field trips associated with professional geoscience assemblies (e.g. Lageson et al. 1999). Contemporary geology education recapitulates this process, with Bachelor degrees commonly culminating in a required capstone field course (Whitmeyer et al. 2009).

In the Department of Earth and Space Sciences at the University of Washington, capstone field instruction includes components of objective rock description at outcrops and measurement of bedding orientation and other structural data for the purpose of mapping, constructing cross-sectional interpretations from maps, and interpreting a geologic history from the observed data. A course typically taken in the first year of the major also includes these components in a staged, fictional scenario with hand samples in the classroom. Remote-learning mandates related to the COVID-19 pandemic precluded field or classroom instruction, and we sought alternative approaches that could address at least some of the original learning goals of these exercises.

We designed video-game-style exercises to provide a three-dimensional, first-person-perspective, virtual field experience accessible via standard internet browsers. Here, we present two examples of virtual field experiences that we implemented during the COVID-19 pandemic for remote instruction in: 1) the department's capstone field-course as part of a module on folding; and 2) an introductory geology course as a substitute for the usual in-classroom rock-identification and map-making final laboratory project. Each virtual field experience incorporates a terrain model that was generated through different means: a structure-from-motion (SfM) model made from drone-captured photographs for the capstone course; and a fictional terrain model designed in 3D-modeling software for the first-year geology course. Here, we report on pandemic-related "emergency" replacements for field exercises, with a prototype game to provide proof-of-concept for our approach.

3.2 Overview of Virtual Field Experiences

We aimed to make an experience in which students could explore outcrops and terrains in first-person-perspective without limitations on where they could collect data. We designed the

virtual field experiences in Unity (Unity Technologies 2020), a cross-platform game engine in which we imported our geologic terrain models into a 3D environment and wrote scripts to govern how the users (in this case, geoscience students) can interact with the outcrops and terrain. The cross-platform nature of Unity allowed us to choose how to package the virtual field experience for student access. We chose WebGL, a JavaScript application-programming interface (API) for rendering interactive 3D graphics within web browsers, as the ideal platform for sharing the virtual field experiences. By building the exercises for the web, anyone with a computer and internet connection can be granted access, no special equipment (e.g., headset, glasses, or joystick) is needed, and no extra steps in downloading an operating-system-specific application are required.

Here, we report on the some of the functions within our virtual field exercises, but we intend to publish a detailed report on how we developed our virtual-field-experience interface in Unity. Our workflow and Unity-based software package for generating a video-game-style virtual field experience is currently available at https://github.com/UWRealityLab/StructuralQueryToolkit so that anyone with a 3D model can design their own virtual field experience and leverage the tools we developed for education and/or research.

The user interface for our course-related virtual field experiences simulates some classic geology tools with novel visualization abilities: A distance-measuring tool permits linear measurements between multiple points in 3D space and prints distances along user-generated line segments. Toggling the map view grants an orthogonal aerial view of the terrain and shows the user's position. The video-game setting also permits tools that are not typically available to geologists: A jetpack allows users to fly over the terrain and enables interrogation of outcrops

that would typically be difficult or unsafe locations at which to collect data (Fig. 3-1a). The user can control movement in all directions with their computer-keyboard arrow keys and change perspective using their mouse or track pad. While in jetpack mode, the user can also change elevation.

Our Unity-based stereonet tool (written in C# programming language) is a novel way to collect data from surfaces and instantly have the data printed to a stereonet within the user's view. When the stereonet tool is activated, the user can click on surfaces within the virtual field experience and take three different types of measurements: 1) planes (Figs. 3-1b-c), for which the user generates polygons on the surface; 2) poles to planes (Fig. 3-1d), for which the user clicks once on the surface and generates a flag normal to the surface; and 3) lineations (Fig. 3-1e), for which the user clicks twice to generate a line on the surface. For each measurement, the data is not only plotted to the stereonet, but the numeric values (strike-and-dip, trend-and-plunge) are printed on the screen (e.g., Fig. 3-1a). The pole component has two extra features: pole-style measurements also print the elevation at the measured point; and once several poles are collected, the user can initiate a stereonet pi-plot (e.g., Marshak and Mitra 1988, p. 157) which indicates an approximate trend and plunge of a fold axis (Fig. 3-1a) and updates as more measurements are taken. Data acquired with these tools can be exported for use in Strabo (Walker et al. 2019), Stereonet (Cardozo and Allmendinger 2013) and other plotting and analysis software.

3.3 The Whaleback Anticline Virtual Field Experience

As part of the remote instruction for our department's capstone summer field-geology course, we devised a module on fold geometry that included a virtual field trip. Creation of the

virtual field experience leveraged an existing SfM-derived terrain model of folded sedimentary rocks. The assignment related to this virtual field experience revolved around the special opportunities to study folds at this site in the field, while also providing the opportunity to collect data from locations at the field site that are not accessible on foot.

The Bear Valley Strip Mine (Shamokin, Pennsylvania) is a popular destination for structural-geology field trips due to its excellent, three-dimensional exposure of an excavated sandstone fold train, of which the central anticline is named "The Whaleback" (Fig. 1a; Nickelsen 1979; Levine and Eggleston 1992). Visitors can walk along the crests of two anticlines, or next to the 200-m-long fold limbs, which feature fossils, concretions, joints, and decimeter-scale secondary faults. Because the Whaleback is 30 m high (from trough to crest) with steeply-dipping/overturned limbs, most of the sandstone surface is inaccessible to direct measurement in the field. To study the geometry of the Whaleback for a research project, drone-acquired photographs of the strip mine were used with SfM photogrammetry to make a 3D point cloud of the surface in AgiSoft PhotoScan Professional (2018). We edited the point cloud by removing as much vegetation as possible to preserve only the exposed sandstone surface and sediment cover. Within the PhotoScan workflow, a polygonal mesh was generated from the point cloud, along with an associated texture which contains the color information for the mesh. Because the photogrammetry utilized real-world coordinates, the polygonal mesh (subsequently referred to as a "model") is scaled to real coordinates (UTM and elevation) and dimensions (meters). This model forms the basis of the virtual field experience; our virtual geology tools (compass and stereonet, ruler, map, and jetpack) provide the mechanism for the students to explore the virtual field site and collect data. In addition to the 3D model, we also produced an orthorectified aerial image of the site to use as a base map (Fig. 3-2c).

We piloted this virtual field experience in July 2020 with 31 undergraduate geology students enrolled in University of Washington's remote field course, in a day-long workshop. Following a refresher on stereonets and fold geometry, the students received access to the Whaleback WebGL-based virtual field experience which was hosted on a department server. The assignment had four components: First, to familiarize them with the game controls, we asked the students to explore the strip mine by walking or flying(!), screen-capture an interesting geologic feature, and write an associated objective description. Many students noted the anticline and syncline on the mine's eastern wall (Fig. 3-2a; the syncline is apparent in the background of Fig. 3-1a); however, one student wrote an interesting geological description of some automobile tires that are remnants of trash within the mine. To help students understand the geologic compass function and practice the transition from 3D "field" perspective to 2D map, the students took strike-and-dip measurements of the surface of the Whaleback and plotted strike-and-dip symbols on the orthorectified aerial image. Once they were fully introduced to the game, we asked the students to investigate the along-trend variability of the Whaleback Anticline. Students used the pole tool to create transects across the fold in four different areas that they selected (e.g., orange flags plotted in Fig. 3-1a). They then produced annotated aerial images, with four stereonets to show how the trend-and-plunge of the fold axis varies longitudinally (Figs. 3-2b-c). From their data, students were able to observe that the Whaleback is doubly-plunging rather than purely cylindrical. The fourth exercise required constructing a profile of the fold train and interpolating the synclines that presumably connect the three exposed anticlines. In order to make this profile, students used the "pole" tool to measure elevation on the surface and the distance-measuring tool to constrain horizontal distance a long a transect perpendicular to the fold, and plotted the values, interpolating below the sedimentary cover.

Implementation of the exercise was straightforward. Regarding the WebGL-performance on students' machines, no computing or model-rendering problems were reported. Although students were not discouraged from working in groups, the students primarily worked alone for these exercises.

The virtual experience we created is open-ended, as there are no specific checkpoints or pieces of information that the user is required to collect; rather, the user chooses what data to collect and where to make those observations. Because of flexibility this virtual field experience, other instructors can design exercises appropriate to their courses and students. In addition to the exercises we piloted, students could: make a structure contour map of the top of the Whaleback sandstone using the elevation tool; compare arc-length to wavelength of the fold; examine meso-scale structures on the larger fold; compare pi-diagram (poles to bedding) to beta-diagram (intersecting great circles) to direct measurements of the fold hinge line for representation of the fold axis; compare axes and shapes of different folds (Whaleback vs. North anticline); compare folds in different stratigraphic horizons (Whaleback vs. syncline above); and there are undoubtably other possibilities. In short, the open structure of the virtual field experience gives instructors similar opportunities that they have in the field to adapt to the needs of their students.

At the time of the pilot exercise, we gave the students an optional, open-ended opportunity to provide feedback about the game: ("If you have any comments regarding improvements to the interface in the Whaleback part of the game, please let me know in the space below!") Although the prompt requested feedback regarding improvements to the game interface, we also received comments related to the student learning experience. Note that, although responses to this question were optional, it was included as part of a graded assignment, and this may have affected how students responded. Out of 31 students, fourteen students (48%)

noted that the virtual experience was aesthetically pleasing and/or fun. Examples of these statements are "I thought it was great! It's a really cool way to visualize an area we are not able to visit," and "This is a lovely game! I absolutely enjoyed it and it really helped with the immersion. It was super enjoyable!" On the other hand, one student reported getting "scared by the walking sounds because it's the same soundbite a lot of pixel horror games use." Positive remarks about the interface were made by eleven students (35%). Examples of these are "I really liked the interface; I thought it was very user-friendly and intuitive to use.", "I think that the games works very well and is pretty intuitive", and "I really liked the map mode button which created a standardized view of the map; it made it easy to orient myself and compare my map view to the instructions." An additional eight students (26%) offered only suggested improvements to the interface. Examples of these include, "I think an F1, instructions command that provides the full scope of the program would be helpful!", and "Add an ability to click/highlight a previous point so that we can see what the strike and dip values were. This way, we don't have to go back and redo it to find out what the values were." Finally, six students (19%) volunteered that their education was enhanced by the virtual field experience. Examples of these comments include, "The stereonet tool is really cool! Stereonets in mineralogy were so confusing –this illustrates how they work spatially so well.", "I am 100% a visual learner... So what you are doing is right up my alley, and genuinely allowed me to learn more about structural geology, on a conceptual level, than any of my other previous classes."

3.4 Cartoon-style Virtual Field Experience

Plate Tectonics and Materials of the Earth is a first-year geology course at University of Washington that introduces rock identification and geologic structures. The course traditionally

culminates with an in-classroom mapping exercise for which rock specimens are arranged around the lab room, and for which students produce a map, cross section, and geologic history. By creating a fictional (but realistic) mapping exercise, we can adjust the complexity appropriate to introductory students and create scenarios that draw on important concepts from the ten-week course. This type of classroom-based mapping exercise also has the advantage of being accessible to many students (e.g., Cooke et al. 1999). During remote instruction for Winter 2021, we aimed to simulate this exercise within a virtual field experience. We produced a fictional field site, generally inspired by the geology of northwestern Washington State (USA). We designed the map to include only a handful of different rock types, with elements that represent accreted oceanic crust, folded terrestrial sedimentary rocks, arc volcanism, and simple geologic structures with clear cross-cutting relationships.

The topography and lithology featured in the cartoon-style virtual field experience (Figs. 3-3a-b), were constructed in 3D from a simple map and associated cross section, including a topographic profile based on relative resistance to weathering of each rock type. The terrain model, outcrop surfaces, and various other game elements (e.g., trees, campfire, rock hammer, etc.) were designed in Blender (Blender Foundation and Community 2020), a free and open-source 3D computer graphics software. To make a hillshade-style base map of the terrain ("virtual lidar"), we rigged artificial lights in Blender to highlight the topography of the terrain and then exported a gray-scale image of the shaded aerial view (Fig. 3-3c). Model outcrops began as cubes in Blender and were subsequently beveled to have varying bedding geometries. The 35 outcrops were positioned throughout the terrain and geographically oriented; thus, if students identified the outcrop lithology and took the strike-and-dip of bedding, they would be able to make the desired geologic map for the final project.

Identifying rocks at outcrops in the remote environment poses obvious problems of not being able to perform the standard battery of tests on a physical specimen. To simulate examining rocks at outcrops, each outcrop had an adjacent rock-hammer icon (Figs 3-3a and 3-3b), which opened an on-screen canvas with information about an outcrop. These informational canvases included photographs (of real outcrops of the rock type, hand samples, and/or petrographic-microscope images), and brief descriptions of characteristics that could not be conveyed from the photos alone.

The cartoon-style virtual field experience was hosted on itch.io (itch.io 2021), a website for hosting, selling, and downloading videogames. Since the virtual field experience is WebGL-based, students could explore the terrain in their internet browsers without having to permanently download files. Itch.io allows for user paywalls and/or for password protection of games. We password-protected the virtual field experience and provided a link and password within the assignment instructions. Students connected to the game via their own computers (with various processor speeds and operating systems) and home internet connections (with various data rates). If student computers and/or internet connections could not support the game, the course instructors were prepared to share their screens while using the virtual field experience as students directed the game-play; however, no issues of access were reported. Therefore, we assume that student computer systems that could successfully run common videoconference software (a requirement to participate in the class) were also sufficient for accessing the virtual field exercise. It is important to note, that some remote-learning situations in primary and secondary schools limit the types of websites students can visit; therefore, it may be important to consider such conditions depending on the intended audience of a particular virtual field experience.

To complete the virtual field work of mapping, students worked in preassigned groups via videoconference, and much like in-person student field work, divided and alternated tasks. In video break-out rooms, one student shared their screen while moving through the terrain, measuring bedding orientations at outcrops, and activating the informational canvases. Other students used the shaded terrain map to guide the main player, similar to how students use terrain maps during field mapping exercises. Other participants updated the group's shared spreadsheet to record bedding measurements and include objective descriptions, based on the informational canvases, for future discussions on rock identifications. With the orientation and lithologic data collected from the virtual field experience, students successfully generated geologic maps, and subsequently drafted cross sections and interpreted a geologic history for the fictional field site. Furthermore, students reported this assignment to be a highlight of the online course, and several students mentioned showing the game to friends or family outside of class. These anecdotal reports of increased student engagement are corroborated by analytics that record the number of browser-plays between the time the assignment start date and due date: that number was 3-to-5 times greater than the minimum number required for student groups to complete the assignments. In other words, students visited the virtual field experience, on their own, for fun.

3.5 Final Remarks

The implementation of interactive virtual field experiences in the two courses successfully addressed the immediate need by substituting engaging online lessons for field and classroom exercises that were precluded by pandemic-related restrictions. Considering the stress and exhaustion that many students experienced as a result of the global pandemic, the students submitted work that conveyed comprehension of the intended educational goals. We also

demonstrated that our structural-geology-query interface in Unity is successful for both structure-from-motion-generated models of actual field sites and custom-designed 3D models of fictional geology. For the college courses, students did not report access issues with regards to where the virtual field experiences were hosted or how their personal computers and internet connections performed. That is, the games functioned well for more than 130 individual users across the globe, with an array of hardware, connection speeds, and browsers. With this contribution, we establish that these virtual field experiences are functional and accessible to many students and that students understand how to operate the tools and can make interpretations from the information they collect.

In response to the 2020 pandemic, the National Association of Geoscience Teachers and the International Association for Geoscience Diversity led a collaboration of more than 300 geoscience educators in developing a framework for designing remote/virtual field experiences to meet the same learning outcomes as in-person exercises (Atchison et al. 2020). The exercises that we implemented within each virtual field experience address many of the highlighted learning outcomes (Table 3-1). Importantly, however, the open-ended nature of these simulations, and especially the Whaleback, enables other geoscience educators to design assignments tailored to different educational goals. We have made the Whaleback virtual field experience available to anyone (virtualfieldgeology.com 2021); at the time of this writing, hundreds of individuals have played the game, including temporal clusters that suggest many instructors have designed their own field trips to this virtual site.

These virtual field experiences have a utility beyond the emergency transition to remote learning. Such simulations can continue to enable students to investigate 3D outcrops without the physical, geographic, and financial limitations often associated with field-based instruction. For

example, the Whaleback Anticline is more than 4300 km from Seattle (an impractical field trip), but we will continue to visit virtually, post-pandemic, via the game interface. We also see a role for these games in blended learning (c.f. Bond and Cawood 2021; this issue) and scientific visualization more broadly. In the virtual field experience, it is possible to observe and collect data from areas of the Bear Valley mine that are inaccessible on-foot; thus, the Whaleback game can augment in-person educational field trips to the site. Because the game is built on a high resolution, georeferenced terrain model, it could be used for research collaboration. Furthermore, the Whaleback is on private land, and public/educational access is evolving. The immersive virtual field experience we have created can help to preserve a record of this geoheritage site (Geyer and Bolles 1979), should access be further restricted.

Benefits also persist for the virtual field experiences in fictional sites even after a full return to the classroom. While there are obvious advantages to the laboratory-based version of a fictional mapping exercise with real hand specimens for petrologic description, the videogame-based exercise offers independent collection of structural data, and more information in the terrain. Our success in building a fictional mapping exercise suggests that geoscience educators need only imagination and bit of 3D modeling skills to design unlimited virtual geologic settings and structural histories for their students to map. It is thus possible to create idealized geology to permit students to discover foundational concepts. For example, imagine a unit on fold geometry in which students visit and measure bedding orientations on folds in the full range of shapes and attitudes, and can instantly compare stereonets from each one. In these open-ended, fictional settings it is also possible to deliberately manipulate how much uncertainty the students encounter (c.f. Wilson et al. 2021, this issue).

The modular nature of the Unity game engine and our structural-geology-query tools means that it is relatively simple to build new virtual field experiences on other outcrop models. We intend to share the template and modules to enable others in the geoscience community to generate virtual field experiences using our interface and their own terrain models. Future work includes creating instructions and workshop for this process, so that anyone with a 3D model can produce a field simulation without significant programming effort or experience. We see field simulations, like the two we describe here, as an emerging opportunity to provide the exploration of geologically interesting features without the typical limitations of field-based geology. Upon re-establishing many of our traditional practices as geologists (post-pandemic), we envision broader adoption of videogame-based field experiences as one way to include more people in our geologic conversations.

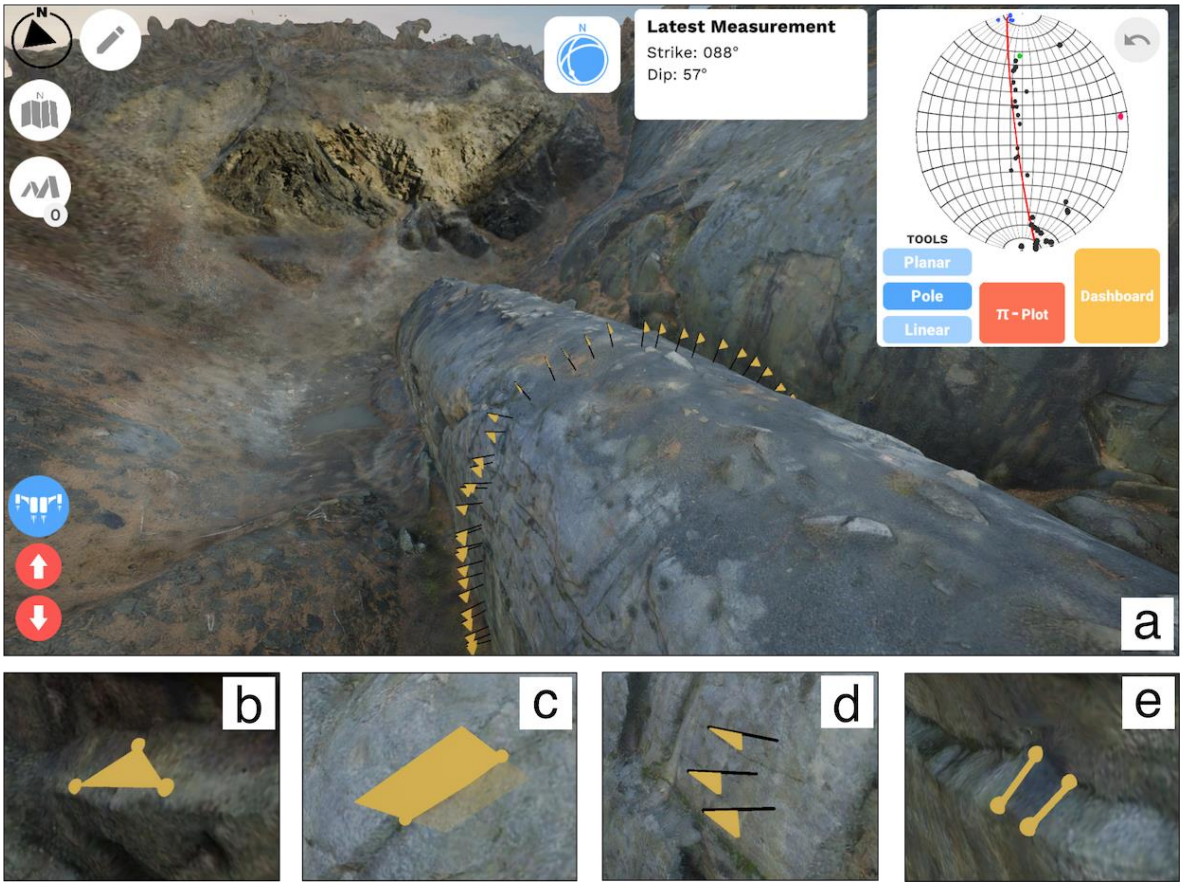

Fig. 3-1: The interface and custom geology tools within our virtual field experiences.
(a) View of the Whaleback Anticline while the user is in jetpack mode. From the top right and continuing counter-clockwise, icons on the perimeter enable the user to toggle the stereonet measurement tools, drawing tools, a compass, map (orthographic aerial) view, linear-distance measurement tool, and jetpack mode. Poles to bedding, represented by orange flags, are plotted as a scanline roughly perpendicular to the trend of the fold crest. The stereonet pi-plot, shows the measured poles and automatically updates as more data is collected. A best-fit great circle and corresponding pole (red line and point on stereonet) calculate the approximate trend and plunge of the fold axis. (b-e) User-constructed representations of measurements include 3-point planes, 2-point-and-rotate planes, poles to planes (flags), and lineations.

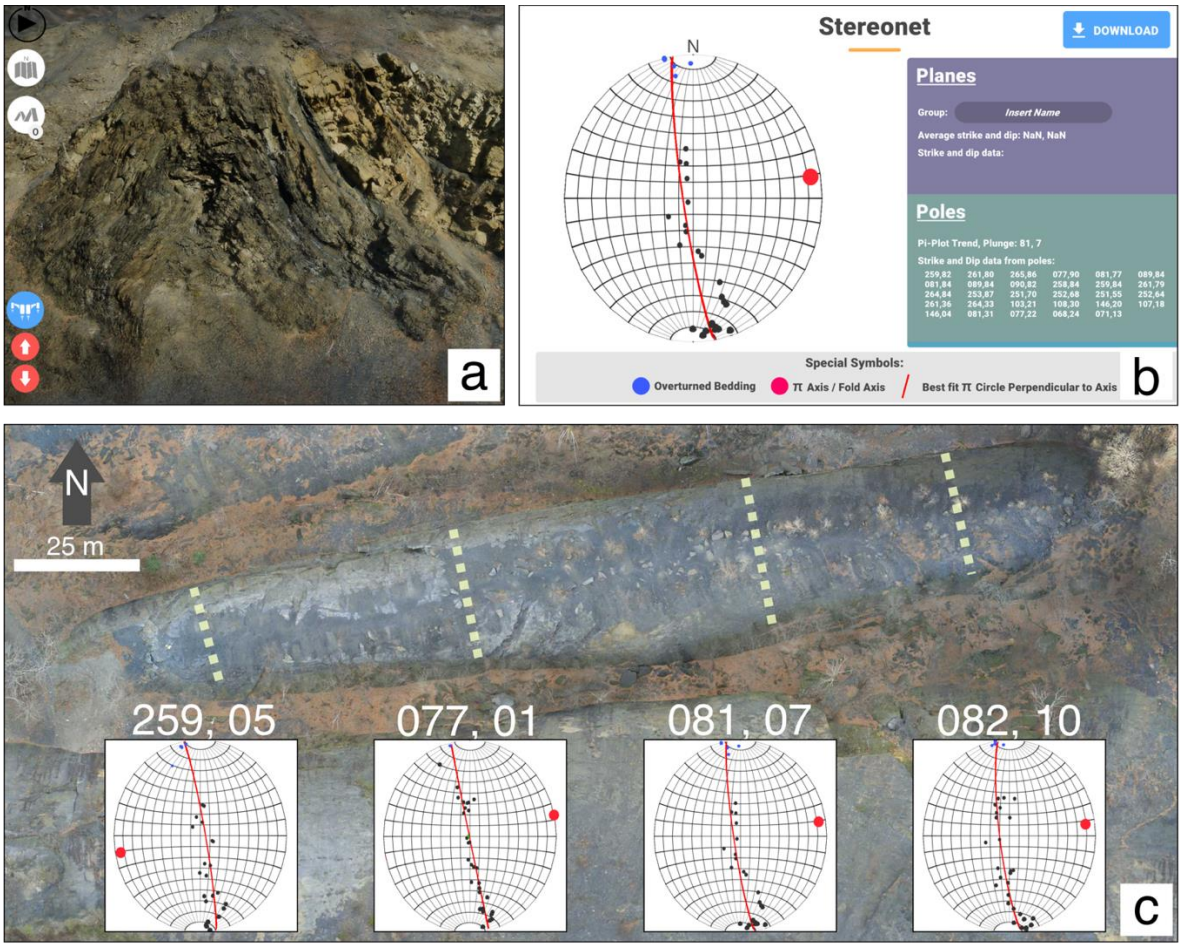

Fig. 3-2: Examples of exercises and data. (a) An anticline (and often, the adjacent syncline) exposed in profile in the east wall of the strip mine was a common feature that the students selected for description. The field of view is 55 meters wide. (b) Screenshot of data from a scanline used to determine the trend and plunge of the fold axis of the Whaleback in the central eastern quarter. The fold axis orientation, generated from an automatic pi-plot feature, is exaggerated as a red circle; the data for each measurement is printed on the right. (c) Students annotated an orthophoto of the Whaleback with stereonet data to investigate variations in the fold axis and best characterize the fold geometry. Each stereonet is associated with a student-made scanline (shown as a dashed line) on a section of the fold, with the trend-and-plunge values of the calculated fold-axis printed above.

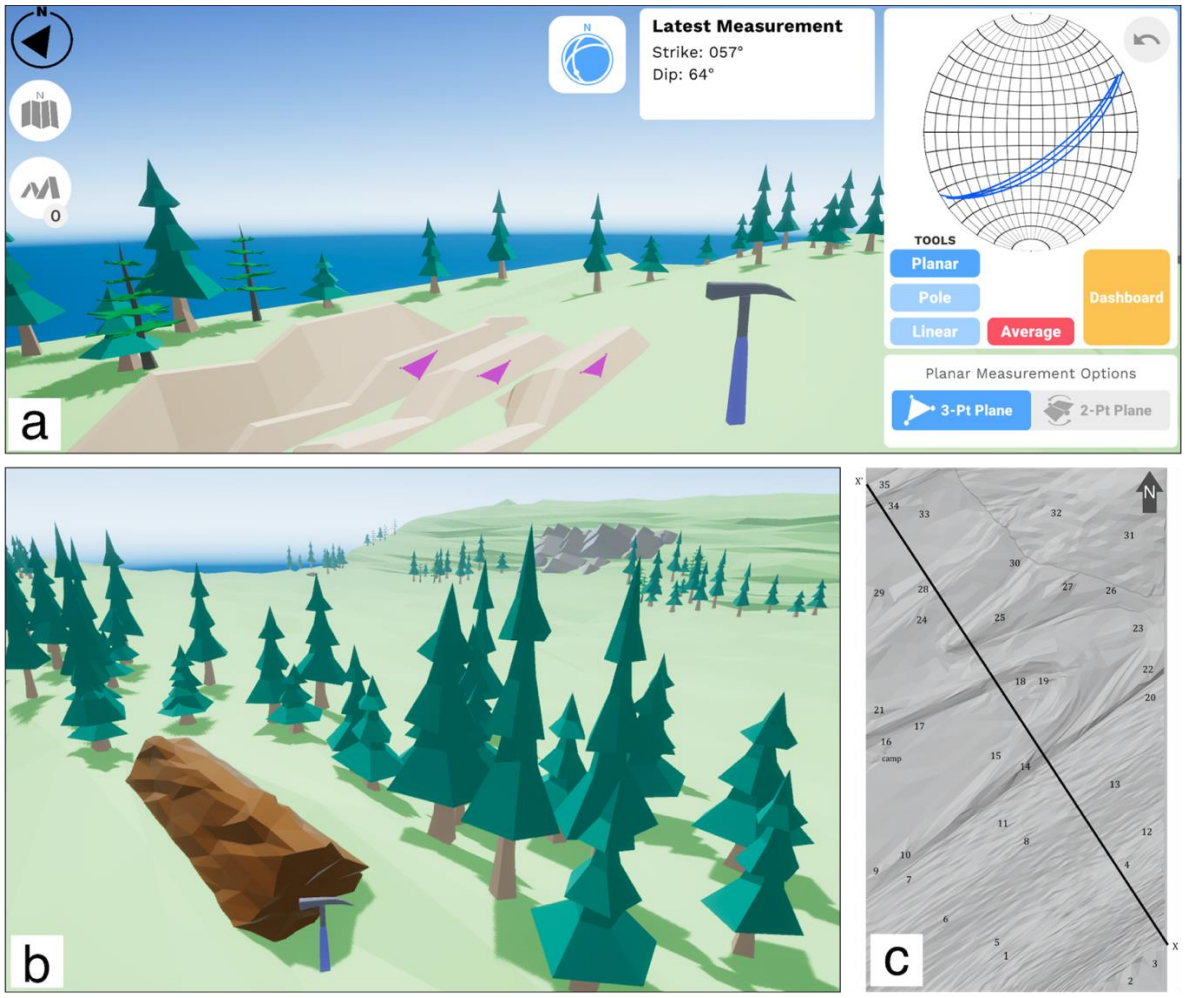

Fig. 3-3: Fictional virtual field experience.
(a) Planar measurements (magenta triangles) are taken on the bedding surfaces of a sandy-colored outcrop the with orientation data projected into a stereonet and printed onscreen. When the user clicks on the rock hammer, an informational canvas (not included in figure) opens to display photographs and other information about the outcrop. (b) A screenshot from a different part of the terrain shows two outcrops: a brown outcrop without bedding (foreground), and a blocky gray outcrop in the background. (c) The hillshade-style basemap provided to students includes the approximate locations (and numbers for organization) of outcrops and the position of X-X' cross section line for interpreting the subsurface during/after map construction.

Table 3-1: Learning outcomes.
From the National Association of Geoscience Teachers and the International Association for Geoscience Diversity (Atchison et al. 2020) and the assignments associated with our two virtual field experiences.

Learning Objectives (Atchison et al., 2020)	**Whaleback Anticline** Examples of student tasks and sample assignment questions	**Simplified fictional geology** Examples of student tasks and sample assignment questions
1. Design a field strategy to collect or select data in order to answer a geologic question.	Strategized with the freedom of where to make observations and what data to collect.	Strategized how to most efficiently collect their data from a base map with numbered outcrop locations.
2. Collect accurate and sufficient data on field relationships and record these using disciplinary conventions.	Measured the orientation of bedding, plotted map symbols and other data on orthophotos.	Made objective descriptions from photographs. Measured the orientation of bedding at outcrops. Plotted map symbols and contacts on maps.
3. Synthesize geologic data and integrate with core concepts and skills into a cohesive spatial and temporal scientific interpretation.	Used stereonets to analyze variation in fold axis. Constructed a profile of fold from elevation data.	Constructed a geologic map. Constructed structural cross-section from the map.
4. Interpret earth systems and past/current/future processes using multiple lines of spatially distributed evidence.	Searched for evidence to qualify whether the Whaleback's observable strain distribution is consistent with end-member kinematic fold models.	Wrote a step-by-step geologic history of the region from the stratigraphy, structures, and geochronological information.
5. Develop an argument that is consistent with available evidence and uncertainty.	Q: Is the Whaleback a cylindrical fold? Q: Based on conceptual models of fold mechanics, infer the rock type at the core of the anticline	Q: Based on rock type and structure, are there potential sites for geologic carbon sequestration?
6. Communicate clearly using written, verbal, and/or visual media with discipline-specific terminology appropriate to your audience.	Used graphics and text tools in shared, on-line documents to produce a project report	Submitted vector-designed geologic maps and cross-sections, and a written report of regional geologic history.
7. Work effectively independently and collaboratively.	Worked independently with support from an online instructor and a community discussion board.	Collaborated on navigated, rock identification, and mapping through screen sharing.

References in Chapter 3

Allmendinger, R. W., Cardozo, N., & Fisher, D. M. (2011). *Structural geology algorithms: Vectors and tensors*. *Structural Geology Algorithms: Vectors and Tensors*. Cambridge University Press. https://doi.org/10.1017/CBO9780511920202

Bond, C. E., & Cawood, A. J. (2021). A role for virtual outcrop models in blended learning-improved 3D thinking and positive perceptions of learning. *Geosci. Commun*, *4*, 233–244. https://doi.org/10.5194/gc-4-233-2021

Callahan, C. N., Libarkin, J. C., McCallum, C. M., & Atchison, C. L. (2015). Using the lens of social capital to understand diversity in the earth system sciences workforce. *Journal of Geoscience Education*, *63*(2), 98–104. https://doi.org/10.5408/15-083.1

Carabajal, I. G., Marshall, A. M., & Atchison, C. L. (2017). A Synthesis of Instructional Strategies in Geoscience Education Literature That Address Barriers to Inclusion for Students With Disabilities. *Journal of Geoscience Education*, *65*(4), 531–541. https://doi.org/10.5408/16-211.1

Cardozo, N., & Allmendinger, R. W. (2013). Spherical projections with OSXStereonet. *Computers and Geosciences*, *51*. https://doi.org/10.1016/j.cageo.2012.07.021

Cruz-Neira, C., Sandin, D. J., & DeFanti, T. A. (1993). Surround-screen projection-based virtual reality: The design and implementation of the CAVE. *Proceedings of the 20th Annual Conference on Computer Graphics and Interactive Techniques, SIGGRAPH 1993*, 135–142. https://doi.org/10.1145/166117.166134

Huntoon, J. E., & Lane, M. J. (2007). Diversity in the geosciences and successful strategies for increasing diversity. *Journal of Geoscience Education*, *55*(6), 447–457. https://doi.org/10.5408/1089-9995-55.6.447

Johnson, A., Leigh, J., Morin, P., & Van Keken, P. (2006). GeoWall: Stereoscopic visualization for geoscience research and education. *IEEE Computer Graphics and Applications*, *26*(6), 10–14. https://doi.org/10.1109/MCG.2006.127

Jones, C. (2008). History of Geoparks. *Geological Society, London, Special Publications*, *300*(1), 273–277. https://doi.org/10.1144/SP300.21

Marshak, S., & Mitra, G. (1988). *Basic methods of structural geology*. New Jersey: Prentice Hall.

NASA 3D Resources. (2021). Retrieved December 2, 2021, from https://nasa3d.arc.nasa.gov/

National Academies of Sciences Medicine and Engineering. (2021). *America's Geoheritage II: Identifying, Developing, and Preserving America's Natural Legacy: Proceedings of a Workshop*. (E. Sztein & P. Whitacre, Eds.). Washington, DC: The National Academies Press. https://doi.org/10.17226/26316

Needle, M. D. (2021). Virtual Field Geology: Field Experiences. Retrieved from https://www.virtualfieldgeology.com/field-experiences.html

Needle, M. D., Mooc, J., Akers, J. F., & Crider, J. G. (2021). Virtual field experiences in a web-based video game environment: open-ended examples of existing and fictional field sites. *Geosci. Commun*, *4*, 1–10. https://doi.org/https://doi.org/10.5194/gc-4-1-2021

Nesbit, P. R., Boulding, A. D., Hugenholtz, C. H., Durkin, P. R., & Hubbard, S. M. (2020). Visualization and Sharing of 3D Digital Outcrop Models to Promote Open Science. *GSA Today*, *30*(6), 25–28. https://doi.org/10.1130/GSATG425A.1

Orr, T. J., Macdonald, B. D., Iverson, S. R., & Hammond, W. R. (2015). Development of a generic mine visualization tool using unity. In *Proceedings of the Thirty-Seventh International Symposium on the Application of Computers and Operations Research in the Mineral Industry*.

Pavlis, T. L., & Mason, K. A. (2017). The New World of 3D Geologic Mapping. *GSA Today*, *271*(10). https://doi.org/10.1130/GSATG313A.1

Reynard, E., & Brilha, J. (Eds.). (2018). *Geoheritage: Assessment, Protection, and Management*. *Geoheritage*. Elsevier. https://doi.org/10.1016/C2015-0-04543-9

Robinson, A., Gordon, C. E., Houghton, J., Lloyd, G. E., & Morgan, D. J. (2015). ArcGIS to Unity: a design pipeline for creation of 3D terrain in serious egames for geology. *Geology Today*, *31*(6), 237–240. https://doi.org/10.1111/gto.12121

Schütz, M. (2015). *Potree: Rendering large point clouds in web browsers*. Univeristy of Wien.

Tony-Cristian, D., & Iulian-Vasile, B. (2017). 3-D minerals. Auxiliary material for the Physical Geology classes. *Analele Stiintifice de Universitatii AI Cuza Din Iasi. Sect. 2*, *Geologie 6*(1/2), 25–35. Retrieved from http://geology.uaic.ro/auig/AnaleleStiintificealeUniversitatii%22

Unity Technologies. (2021). Physics.Raycast. Retrieved August 11, 2021, from https://docs.unity3d.com/ScriptReference/Physics.Raycast.html

Wolfe, B. A., & Riggs, E. M. (2017, November 1). Macrosystem analysis of programs and strategies to increase underrepresented populations in the geosciences. *Journal of Geoscience Education*. National Association of Geoscience Teachers Inc. https://doi.org/10.5408/17-256.1

Chapter 4 The Structural Geology Query Toolkit for digital 3D models: Design custom immersive virtual field experiences

Abstract

We introduce the Structural Geology Query Toolkit to enable geoscientists to produce bespoke video-game-style field experiences from their own 3D digital outcrop models. Beyond simple visualization, these tools permit users to query the digital model and extract structural data. The set of original pre-coded modules and detailed instructions includes visualization and tools that reproduce the experience of being at an outcrop with a measuring tape and a geodetic compass, with the added ability to fly over the outcrop, annotate the rock face, and instantly visualize topographic profiles and measured orientations on a stereonet. Data can be exported for further analysis with other software. The features of a virtual field experience are customizable and can be based on digital models of any scale. We selected the free, industry-standard Unity game engine so that the virtual field experience can be built to share on the internet or as free-standing applications for desktop computers, mobile devices, or virtual reality headsets. Our Toolkit is free and open source; we encourage collaboration and additional contributions to the tool library. The resulting virtual field experiences can enhance scientific collaboration, geoscience education and educational equity, and geoheritage preservation efforts.

4.1 Introduction

Recent advances in surveying (laser scanning) and photogrammetry ("structure-from-motion") have made it relatively easy for individual researchers to generate highly detailed, photo-realistic, three-dimensional digital representations of research targets (e.g., Pavlis and Mason 2017). These digital models are typically in the form of point clouds (millions of points

representing positions and color of the surface of scanned or photographed objects) or they may be meshed surfaces derived from point clouds. Such models have become essential tools for visualization and analysis in structural geology to gather attributes of form and geometry as fundamental data (e.g., Bond and Cawood 2021).

With these new data comes a need for tools to examine and share 3D representations. In geology, there is a long history of using 3D visualization for landscapes and subsurface geologic data, from static analog stereophotography and red-blue anaglyph images to digital tools for organizing and visualizing spatial data, such as geographic information systems (GIS) and GoogleEarth (https://earth.google.com). In recent decades, 3D visualization rooms and systems ("CAVEs,") (Cruz-Neira et al. 1993) (e.g., KeckCAVES, http://www.keckcaves.org), dual-projector stereoscopic projection (e.g. GeoWall; Johnson et al. 2006), and 3D televisions have provided opportunities for immersive interaction with digital spatial data. These immersive visualization environments facilitate collaborative research and teaching but may require expensive and specialized hardware along with software systems that suffer from steep learning curves, rapid obsolescence, and the requirement that users visit the visualization facility. Consequently, these tools do not meet the general need.

The ideal visualization system works on widely available computing platforms (laptops, tablets, smartphones), can run on a variety of operating systems, and is inexpensive, simple to learn, intuitive to operate, and adaptable to specific research needs of the discipline or the project. Web-based viewers, such as Sketchfab (www.sketchfab.com) or potree (Schütz, 2015), offer straightforward platforms to visualize and share point clouds, but neither provide a simulation of a field environment. Sketchfab does not permit the integration of additional datasets with the 3D model, and while potree is customizable, coding is necessary (Nesbit et al.

2020). Video-game environments offer many of the same advantages as the web-based viewers, without the same constraints. Recent advances in game-development platforms (or "game engines"), including Unity, a popular game engine (www.unity.com), facilitate rapid creation of immersive 3D visualization, permit customized analysis tools, and can incorporate annotation, guidance, or supplemental data. Furthermore, because Unity is a free, game-industry standard, we anticipate it has longevity as a visualization platform.

Unity has already been used for designing 3D educational experiences in geology. Robinson et al. (2015) described a workflow for generating a terrain from ArcGIS for use in Unity. Tony-Cristian and Iulian-Vasile (2017) describe using structure-from-motion photogrammetry to generate a Unity-based atlas containing 70 models of minerals, and Orr et al. (2015) explored Unity's utility as a mine visualization tool using 3D models. Needle et al. (2021) designed a structural-geology-focused virtual field trip with a structure-from-motion derived model for online-field education during the COVID-19 pandemic. However, these works do not share the detailed process of building an application within Unity nor are the codes that govern interactions between game elements shared. Nesbit et al. (2020) identified game engines as tools for constructing modules that aid in the visualization and sharing virtual outcrops but notes that a significant amount of coding is required to construct such an experience. Despite the analysis and customization advantages relative to simple online viewers, the Unity environment has a high barrier to entry for geoscience visualization, analysis and collaboration.

To address this problem, we introduce our Structural Geology Query Toolkit and associated detailed instructions to provide geoscientists with a simple workflow to generate customized, open-ended, virtual field experiences from any 3D model at any scale. The Toolkit

enables researchers examine virtual outcrops with tools analogous to a standard geological field kit and to share observations with the public or a target end-user group (Fig. 4-1).

4.1.1 Terminology overview

For clarification, we define several frequently used terms: "Develop" here describes any coding by the authors that will not have to be recompleted by the end user, as it refers to prefabricated tools, objects, scripts, or code that are available within the Structural Geology Query Toolkit project files. "Designer," "design," and "build" are words that describe a person and the actions they take to generate their own virtual field experience with the Structural Geology Query Toolkit workflow. "User" describes someone who has access to the final product of a virtual field experience, in other words, the target audience for the virtual field experience. "Terrain" and "outcrop" are used interchangeably both refer to a 3D polygonal model and its associated texture. "Virtual field experience" is what the designer builds for the user: an opportunity to remotely visit and interact with a geologically interesting terrain with an open-ended ability to collect data using the tools within the Structural Geology Query Toolkit.

4.2 Toolkit Overview

4.2.1 Basic Mechanics

The ability to query the data from polygonal mesh terrains and/or outcrops serves as the basis for generating virtual field experiences using the Structural Geology Query Toolkit. Point-cloud data can be converted to polygonal meshes (e.g., Wavefront .obj files) and associated textures (.jpeg, .png, and .tiff files). Mesh files have data consisting of (but not limited to) vertices, vertex normals, and face normals (Fig. 4-2). Within the Unity game environment, a user

may “cast a ray” from a point of origin with a directional component (Unity Technologies, 2021). When this ray intersects a 3D object that has collisional properties enabled, an interaction between the user and the object will occur, if specified by a script. For the Structural Geology Query Toolkit, we developed scripts that allow a user to interact with geological terrain models by casting rays onto the model, which reads the 3-coordinate face normals and returns the data to the user in conventional geology representations for orientations: printing strike and dip and plotting within stereonets. Meshes can be generated with real-world elevation data (e.g., meters relative to sea level) and this elevation component can be sampled by the user with raycasts, as well.

Building within Unity permits the simulation of a first-person-perspective field experience by leveraging Unity’s first-person controller. The user translates a first-person character in 3D space with computer keys and a mouse or touchpad while viewing the terrain from the perspective of a camera affixed to this first-person character. Simulated gravity is initially applied to the first-person character so that the user may walk (or run or jump) on the terrain, but we also include the ability for the first-person character to move freely in three-dimensions, unconfined by gravity, in what we call “jetpack mode.” In this mode, the user can fly over the terrain and collect data from the geologic model at locations (e.g., cliff faces) that may be unsafe or impossible to reach in an actual field campaign.

4.2.2 Query Tools

The interface included with the Structural Geology Query Toolkit is composed of onscreen buttons that are fixed to the user’s first-person view. Each of these buttons permit the user to collect data from the mesh in different ways or add location-based annotations (“field

notes") to the model. At the time of writing, the onscreen buttons include: a map tool (Fig. 4-3a), which provides an orthorectified overview of the model showing the position of the character and its look-direction, as well as opportunity add simple annotations; a drawing tool (Fig. 4-3b), which allows the user to place lines on the outcrop; a text annotation tool; and three tools we describe further below: a profile tool (Fig. 4-3c), a linear-distance tool (Fig. 4-3d), and a stereonet tool (Fig. 4-4). Because we have made the Structural Geology Query Toolkit open source (https://github.com/UWRealityLab/StructuralQueryToolkit), a designer can add more tools if they are interested in scripting them. To facilitate the implementation of new tools, we designed the Toolkit such that a designer can simply drag-and-drop the new script into the game-element hierarchy to include a new game tool in the on-screen interface.

The profile tool collects x-z position along a 2D transect at points specified by mouse-clicks and sketches the form of the profile in real time. Users may export the profile data as a .txt file or the profile itself as an .svg for further analysis. Unlike with some standard terrain analysis software, we allow a profile to include more than one value for elevation in the same horizontal position, permitting profiles that include geomorphic or structural overhangs (e.g. caves, overturned fold limbs, wavecut notches) (Fig. 4-3c). Accurate representation of such features requires the model terrain to be constructed from 3D point-cloud data, rather than simple height-field data.

The linear distance tool calculates the distance between any two points on the model surface and is not constrained to solely horizontal distance. The tool will give the cumulative distance as if the user defines a path on the model surface with several points, displaying the total length and the length of the last increment. This tool can "pierce" through the terrain and renders a slightly faded version of the line where the measurement passes below the surface. In Fig. 4-

3d, the straight shorter line pierces through the terrain to measure the half wavelength of an exposed anticline, where the longer arc (made of several segments on the bedding surface) measures the arc-length of the fold at the same location.

4.2.3 Stereonet Tool

The stereonet tools extract orientation data from the model surface and display them on screen. We have created a series of tools that reproduce the style of measurements made at the outcrop (Table 4-1). Because the Structural Geology Query Toolkit is open source, the scripts describing how the stereonet tools work are visible to any designer, but we recognize that not everyone is fluent in game-engine scripting. Here, we describe how this set of tools serve the user, and what is happening with the game elements.

When the stereonet tool is activated, the user can measure the orientations of planar and linear features (Fig. 4-4). These measurements print data onscreen and plot the data as great circles or poles within the stereonet image (Figs. 4-4a-e). The visual and numerical representations of the data are stored in the "Dashboard," where new stereonets also may be initiated to better organize the data (Fig. 4-4f). The strike-and-dip and trend-and-plunge values printed next to the stereonet and stored within the dashboard are calculated from the face-normal vectors of objects, whether these objects are constructed by the user (see below) or sampled directly from the mesh. Values for strike-and-dip use the right-hand-rule convention (the down-dip direction is 90° clockwise from the strike; e.g., Marshak & Mitra, 1988). From the Dashboard, the user can export the data as a simple list in .txt format or as a .txt-file formatted specifically for the widely-used analysis software Stereonet 11 (Allmendinger et al. 2011; Cardozo and Allmendinger, 2013) for further analysis.

The onscreen stereonet is a live camera-feed of a 3D mesh bowl (hemisphere) within the game environment. Even though this bowl exists in the game environment, its 3D nature is not visible to users: a camera renders the contents of the bowl from the zenith (directly above the center) and the bowl appears as a 2D circle. When a user constructs a plane on the mesh to query an orientation, a second plane of the same orientation is generated within the 3D bowl, and the intersection of the plane with the bowl is rendered onscreen to the user, appearing as a great-circle arc within the stereonet. When a pole to a plane or linear feature is measured, a ray with the same orientation as the measured line is cast from the center of the openside of the bowl (the center of the equatorial circle on the diametral plane) into the bowl. At the intersection of the raycast and the bowl, a small sphere is generated that appears to the user as a dot within the stereonet.

The user can measure the orientation of surfaces by constructing planes in the model. Planes constructed by the user display on the geologic mesh and are accompanied by the strike-and-dip printed onscreen and represented as great circles within the stereonet. There are two ways to construct planes. The 3-point-plane option enables the user to click on a surface at three points to generate a triangular plane of any size (Fig. 4-4a). The face normal of this plane is read and converted to strike and dip. The 2-point-plane option was developed as a simulation of the field practice of using a hard surface (e.g., clipboard or notebook) to extend a planar feature with limited extent to measure with a geodetic compass. The 2-point-plane option enables the user to define an axis (approximating the strike) on a surface by clicking two points (Fig. 4-4b). Subsequently, the user moves a slider to rotate a square plane around the axis to align the plane with the feature of interest to estimate the dip. As the slider is adjusted, a great circle within the

stereonet moves in real time with the slider. This visualization may assist students with the 3D connections between planar features on the outcrop and their stereographic projections.

The pole tool has several functions. When activated, clicking once on the surface places a flagpole that is normal to the polygon at the position of the cursor (Figs. 4-4c-d). Compared to the plane tools, the pole tool enables the user to take multiple measurements rapidly. The pole tool prints the strike and dip of the sampled surface in the "latest measurement" window but plots the data as poles to planes within the stereonet. If the mesh has elevation data associated with it, the designer can enable the elevation to be displayed along with the strike-and-dip, when a surface is sampled (e.g., Fig. 4-4c).

After three pole measurements are made, the pi-plot function is available. This was developed with the intention of rapidly collecting bedding orientations of folded surfaces and calculating the trend and plunge of a fold axis. Once the pi-plot button is clicked, a plane is fit to the poles. The pi-plot trend-and-plunge is calculated from the normal to the best-fit-plane and is printed within the listed data in the enlarged view of the associated stereonet. Where the normal to this best-fit-plane intersects with the stereonet bowl, another sphere is generated and rendered as a dot that a point that represents the trend and plunge of the fold axis (Fig. 4-4d). As the user adds more pole-to-plane data when the pi-plot function is enabled, the best-fit-plane will continue to accommodate new measurements and update the calculated trend-and-plunge of the fold axis in real time.

The orientations of linear features can be measured by simply clicking two separate points to define a line that traces the feature (Fig. 4-4e). The trend and plunge the line are printed onscreen, and the feature's orientation is plotted within the stereonet as a pole.

4.3 Process of Building a Virtual Field Experience

On the GitHub repository for the software, we have a wiki (https://github.com/UWRealityLab/StructuralQueryToolkit/wiki) with detailed step-by-step instructions on how to design a virtual field experience using the Structural Geology Query Toolkit. Here, we provide an overview of some key steps of the process.

Downloading the project: First, the designer downloads UnityHub and makes a free account to have access to the Unity software. Then, the designer has two choices: A) download the Structural Geology Query Toolkit project file directly from GitHub and open it in Unity, or B) (recommended) download GitHub Desktop and import the project file through GitHub Desktop to Unity. The advantage of the latter is that the designer can receive bug fixes and new tools to their projects pushed by the software developers through GitHub Desktop.

Importing a 3D polygonal model to the scene: A "scene" in Unity is where a designer works with content ("assets"). With common video games, a scene is where a designer would build one level of a multi-level game. The Structural Geology Query Toolkit contains a pre-built scene with an original 3D model (Fig. 4-5a). This model contains objects such as a campfire, trees, tent, jet pack, geodetic compass, and some low-resolution representations of rocks. These assets were designed specifically for this project and are free to use for geology-related applications. More importantly, this 3D model contains a meter scale and a north arrow to assist in the orientation and, optionally, scaling of a 3D terrain model.

The designer imports their own 3D geology-related outcrop or terrain into this initial scene. Because Unity uses a y-up 3D coordinate system and other software builds 3D models from point clouds with z-up coordinate systems, one or more 90° rotations may be required to orient the terrain model to the scene so that the north-direction of the imported model and the

prefabricated scene are aligned. If the terrain model has associated elevation, it has been our experience that even when the designer must rotate the model, elevation data will be recognized in the Unity scene. Once the model is oriented with the scene's north, the designer imports the model's associated texture and applies it to polygonal mesh (Fig. 4-5b). Workflows for applying a single texture and multiple textures are described in the wiki.

Applying colliders for query and physics: When a user queries the surface of a model, they send a raycast from a mouse click that collides with the surface. For this interaction to occur, the designer must apply a "mesh collider" to their terrain. The mesh collider defines the terrain as solid, allowing the first-person character to walk on the terrain (rather than falling through) and permitting the measurement functions described above. Invisible, vertical mesh colliders may also be added to the furthest extents of the terrain model to prevent the end-user from "falling off" the terrain into digital oblivion. If there are holes due to missing or incomplete data in the terrain mesh, it is also possible for the designer to patch these holes with mesh colliders.

Parameter adjustments: The designer can place the first-person character at any initial location on the terrain to provide a specific starting location and view when users enter the virtual field experience (for example, repositioning the pink capsule in Fig. 4-5a on the imported terrain). The designer can adjust the default player walking and flying speeds. The default size of the first-person character is 1.8 m in height, but that size can be rescaled to account for the ideal locomotion through the 3D terrain (Fig. 4-5c). For example, if the imported 3D model is 1 m^2, (e.g., a scan of an analog model), the designer could scale the first-person player to simulate a life-sized field campaign of the deformation within the analog model. Alternatively, the same

effect could be achieved by changing the scale of the imported model while holding the player size constant.

4.3.1 Optional custom features for virtual field experiences

Elevation data: If there is real-world elevation data associated with the 3D model, there are two ways for the designer to enable access to this data. If the model imports with the associated elevation data, then the designer can simply enable access to this data by clicking "Show Elevation Data" within the designer settings in Unity. Alternatively, we've developed a prefabricated tool that permits the designer to place an altitude marker on a point of known elevation (e.g., GPS-referenced ground-control point) and manually enter the elevation at that point. This tool will then reference the rest of the model elevation relative to that point.

Sampling radius of the pole tool: If a mesh has very fine resolution and includes rough surfaces, sampling the normal of a single polygon may not provide an accurate measure of the attitude of the geologic feature. For this reason, we have designed two ways to increase the radius of sampling by the pole tool: 1) the radius of sampling can be increased by the designer when building the virtual field experience; or, 2) it may be adjusted by the end-user during gameplay within the pause-menu settings. Increasing the radius takes an average of the face-normal unit vectors of mesh polygons within a defined distance of the single polygon on which a pole was placed (Fig. 4-5d).

"Floor" models for outcrops with limited horizontal extent: Outcrop models may be vertical road cuts or quarry walls, with little horizontal ground surface. For these cases, we provide several simple horizontal terrains that can be placed into a scene to provide a "floor" on which the user can walk and stand while examining the vertically oriented outcrop. The floor

modules also provide a visual base which is more realistic than the default blue-sky background. These floors may also be useful with models that have irregularly shaped boundaries.

Pop-up user interfaces: Outcrops contain more information than is held in a 3D point cloud. A designer may want to embed additional information in the virtual field experience for their end-users, such as photographs, hyperlinks, text, or additional data (Fig. 4-6). To embed this data, the designer can drag and drop one of our prefabricated 3D rock hammers into a particular location in the terrain model. Each hammer has an associated user interface (UI) canvas (Fig. 4-6a-b) that may be edited to include images and text. When an end-user clicks on the rock hammer, the UI canvas appears on screen with the information embedded by the designer (Fig. 4-6c).

4.3.2 Sharing the virtual field experience

Because Unity allows designers to build to different platforms, the project can be shared in many ways. The Structural Geology Query Toolkit was designed primarily for three target platforms: WebGL, Microsoft Windows, and MacOS. These build versions have the same user controls and are meant to be accessed through a desktop computer, ideally with a mouse and keyboard. The wiki describes how to download support for building to these platforms when the designer initially downloads Unity; however, platform-build support can be downloaded later. Also in development are versions of the Toolkit that would allow designers to build virtual field trips for use on mobile devices and virtual-reality headsets.

WebGL enables a user to access the virtual field experience through common web browsers without the need to download plugins. Currently, Safari does not support WebGL, so we recommend Google Chrome and Firefox for accessing virtual field experiences. Publishing a

WebGL version of the virtual field experience is straightforward and involves uploading an archive file, such as .zip, of the Unity project folder and an .html file that Unity automatically generates upon building the project for sharing. Itch.io is a website where a designer can host their virtual field experience for free. Needle et al. 2021 describe hosting virtual field experiences designed with the Structural Geology Query Toolkit for remote education during the COVID-19 pandemic and report no access issues amongst college students; however, some elementary- and secondary-school security restrictions may impede access to virtual field experiences on this game platform. Alternatively, WebGL builds may be hosted on department websites.

Building to MacOS or Windows will generate an application in a designated directory on the host computer (e.g., the desktop). These applications are larger in size (take more disk space) than the WebGL versions but run more smoothly with more frames-per-second as they do not run through a web browser. Sharing these files with users is like sharing any computer file; however, the user will have to download the file that is specific to their own operating system: MacOS or Windows.

We have an alternate project file of the Structural Geology Query Toolkit formatted for use with virtual reality platforms, such as the Oculus Rift headset. If a designer intends to build to this platform, they must download the Structural Geology Query Toolkit project file for virtual reality and go through the workflow described in the wiki. Because the game controls within virtual reality are quite different from a desktop computer, we developed this second project file to take the burden of coding to virtual reality off the designers. Currently, the virtual reality version has only a subset of tool features (primarily, the stereonet tool) compared to all of the tools in the desktop version; however, we are sharing the virtual reality version as a proof-of-

concept for designing a truly immersive 3D experience using our toolkit. Unity also supports building to mobile platforms (e.g., tablets and smart phones). We have added support in our toolkit for designers to build to mobile devices. However, the user experience may be hindered by the smaller screens, and we recommend larger tablets rather than phones for mobile platforms.

4.4 Applications for video-game style virtual field experiences

We envision several applications for virtual field experiences designed with the Structural Geology Query Toolkit:

Facilitating scientific collaboration: In a game environment, it is possible for geoscientists to examine outcrops that they cannot otherwise visit, whether because of individual physical limitations, dangerous field locations, or travel restrictions. Other outcrops may be possible to image, but impossible for anyone to visit: on cliff faces, underwater, or on other planets. Our Structural Geology Query Toolkit provides an intuitive game interface to enable scientific examination in modes similar to traditional field study. The virtual field sites can be annotated, with notes and additional images or data embedded, and shared with a simple URL. Once a 3D model is created, a virtual site can be visited repeatedly by any number of research-team members to measure and interpret features or plan sampling or additional physical and chemical analyses.

Replicating the scientific process for students: During the 2020 COVID crisis, pandemic-related restrictions on field work motivated a group of North American geoscience educators to articulate key learning outcomes for geological field courses (Atchison et al. 2020). Important among the goals were: defining a field strategy for data collection, use and interpretation of

spatially distributed evidence, and data collection using disciplinary conventions. Other workers have recognized the importance of 3D spatial reasoning in geological interpretations, and the challenge that many students have with this skill (e.g., Callahan et al. 2015). In an initial application of the Structural Geology Query Toolkit, Needle et al. 2021 created an educational experience to address these goals in a virtual environment. In "The Whaleback Anticline Adventure", students could construct their own knowledge of the rock structure, because they could explore the site, view the features from different perspectives, and choose what to measure, using tools similar to equipment they would have in the field. The game environment also provided essential practice for 3D spatial reasoning for students engaged in an online "field" course.

Increasing access to geoscience: Geosciences are among the least diverse of all STEM disciplines (e.g., Huntoon and Lane 2007). Some scholars report that field course requirements may deter otherwise interested students from enrolling in a geoscience major (e.g., Wolfe and Riggs 2017, Carabajal et al. 2017), because requirements can be expensive, physically demanding, intimidating, unfamiliar, or simply incompatible with obligations to family and work. Our toolkit also enables the inclusion of people with locomotive disabilities without singling out individuals for their differences. Students can build skills in data collection and analysis via virtual environments as an alternative, supplement or precursor to traditional field activities.

Recording outcrops for future study and enhance reproducibility of geoscience findings: The video-game-based approach enables explicit recording of observations in the form of an annotated virtual outcrop. This record may be especially important for outcrops that are ephemeral: a tsunami deposit that can be eroded or buried, debris-flow deposits that are

remobilized, or an excavation across a fault scarp that is subsequently refilled. Other outcrops may be vulnerable to urban development, access restrictions, or over-visiting. Geoheritage efforts (e.g., Jones, 2008; Reynard & Brilha 2018; National Academies of Sciences Medicine and Engineering 2021) seek to preserve iconic sites of geologic discovery. Immersive, guided, virtual field trips can preserve a record of the geoheritage features for reproduction of findings, future study, and public education.

4.5 Concluding remarks and vision for the near future

Unity is a powerful game engine that can support the creation of virtual field experiences that leverage 3D polygonal meshes of geologic terrains and outcrops; however, defining the interactions of the end-users with the mesh data requires computer coding experience. Our Structural Geology Query Toolkit and associated workflow facilitates the creation of open-ended virtual field experiences without requiring the designer to code.

The toolkit is not limited to terrestrial 3D models of outcrops and terrains. Three-dimensional datasets of the ocean floor and extraterrestrial terrains are becoming available (e.g., "NASA 3D Resources," 2021), and the Structural Geology Query Toolkit provides a novel opportunity for students to explore these data as field geologists (Fig. 4-7a). Because the first-person character can be scaled to suit the terrain, designers can scale the character down to the size of an ant to explore a 3D scan of hand sample or an analog model made of wet clay or sand (Fig. 4-7b). With some 3D modeling skills, a designer may also create a virtual field trip with customized geologic features with a mapping module (e.g., Needle et al., 2021) or learn about variations of a geologic structure, for example, folds in the "Fold Islands" virtual field

experience at https://www.virtualfieldgeology.com/field-experiences.html (Needle, 2021) (Fig. 4-7c-d).

For geoscientists interested in exploring the development of new tools that can be used to explore terrains and outcrops in the video-game environment, we hope to foster a community of developers by making our code open source on GitHub. We welcome future collaborations. As the geoscience community continues to populate repositories with 3D models for public exploration, and personal computing power coevally grows to accommodate larger high-definition 3D datasets, we encourage the structural geology community to consider video-game-style platforms and interfaces to interact with this data.

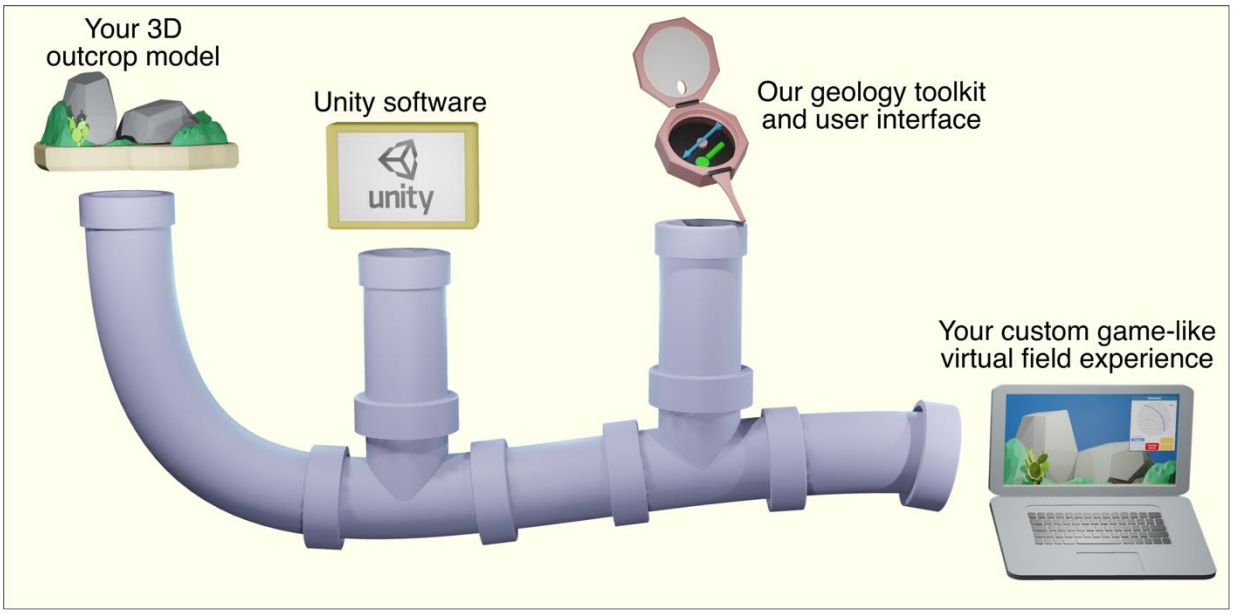

Fig. 4-1: A conceptual pipeline of the Structural Geology Query Toolkit workflow for creating bespoke virtual field experiences.

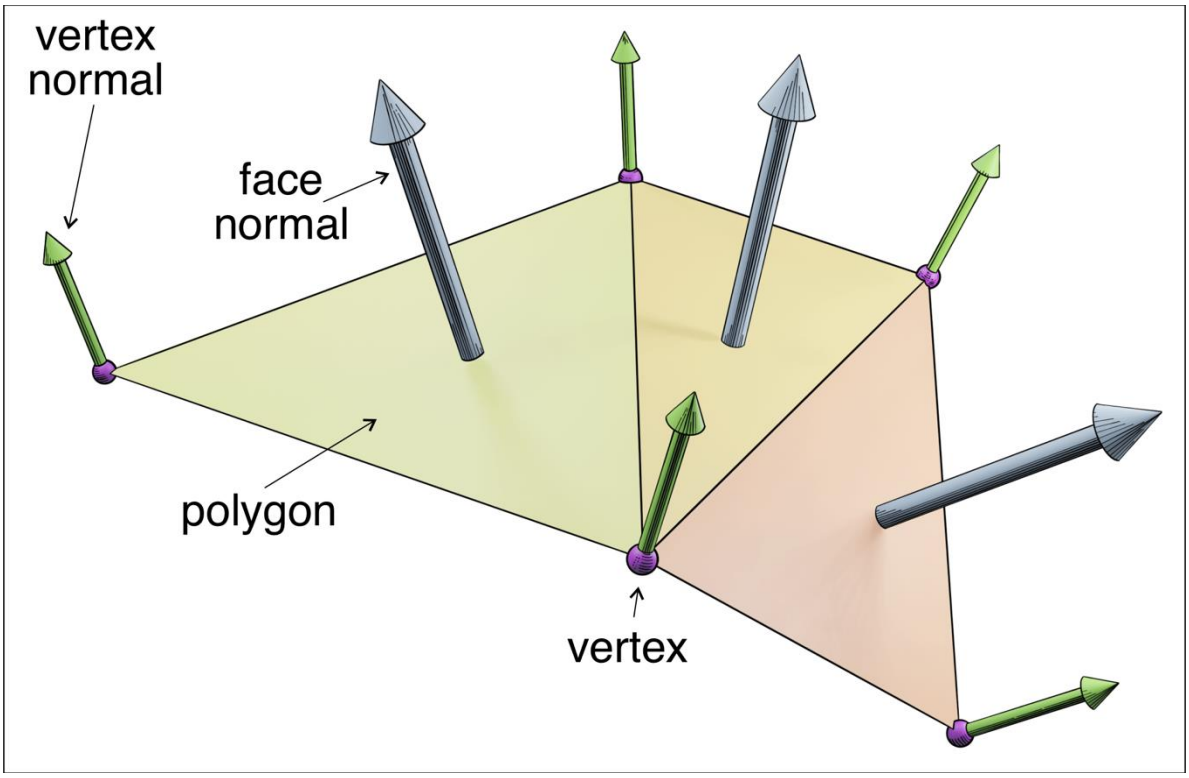

Fig. 4-2: Several components of a polygonal mesh.
Dark purple spheres are mesh vertices that terminate or join polygons. Each vertex has an associated vertex normal, represented by green arrows. The large blue arrows are face normals which are normal to each polygon.

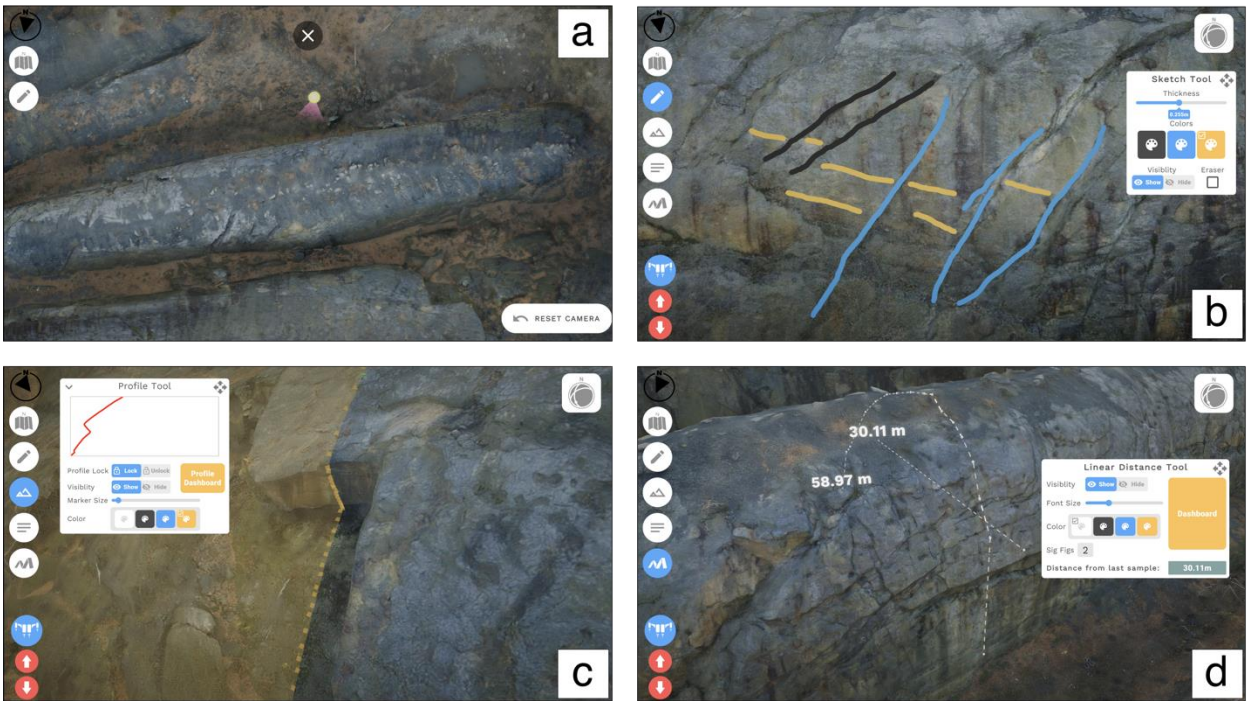

Fig. 4-3: Onscreen tools for visualization, annotation, and measurement.
A) The map button switches the user to an orthorectified map view of the terrain showing their position on the terrain (yellow dot). B) With the drawing tool, the user may draw in 3D on the terrain surface. C) With the profile tool, the user can construct a 2D profile across the terrain model, including overhanging features. D) The linear distance tool measures the distance between two points on the terrain surface or the cumulative distance along a path made of several segments. Here, two paths show the half-wavelength through a fold and the arc-length on the bedding surface.
(Images are screen shots from the "Whaleback Anticline Field Adventure," available at www.virtualfieldgeology.com (Needle et al. 2021).)

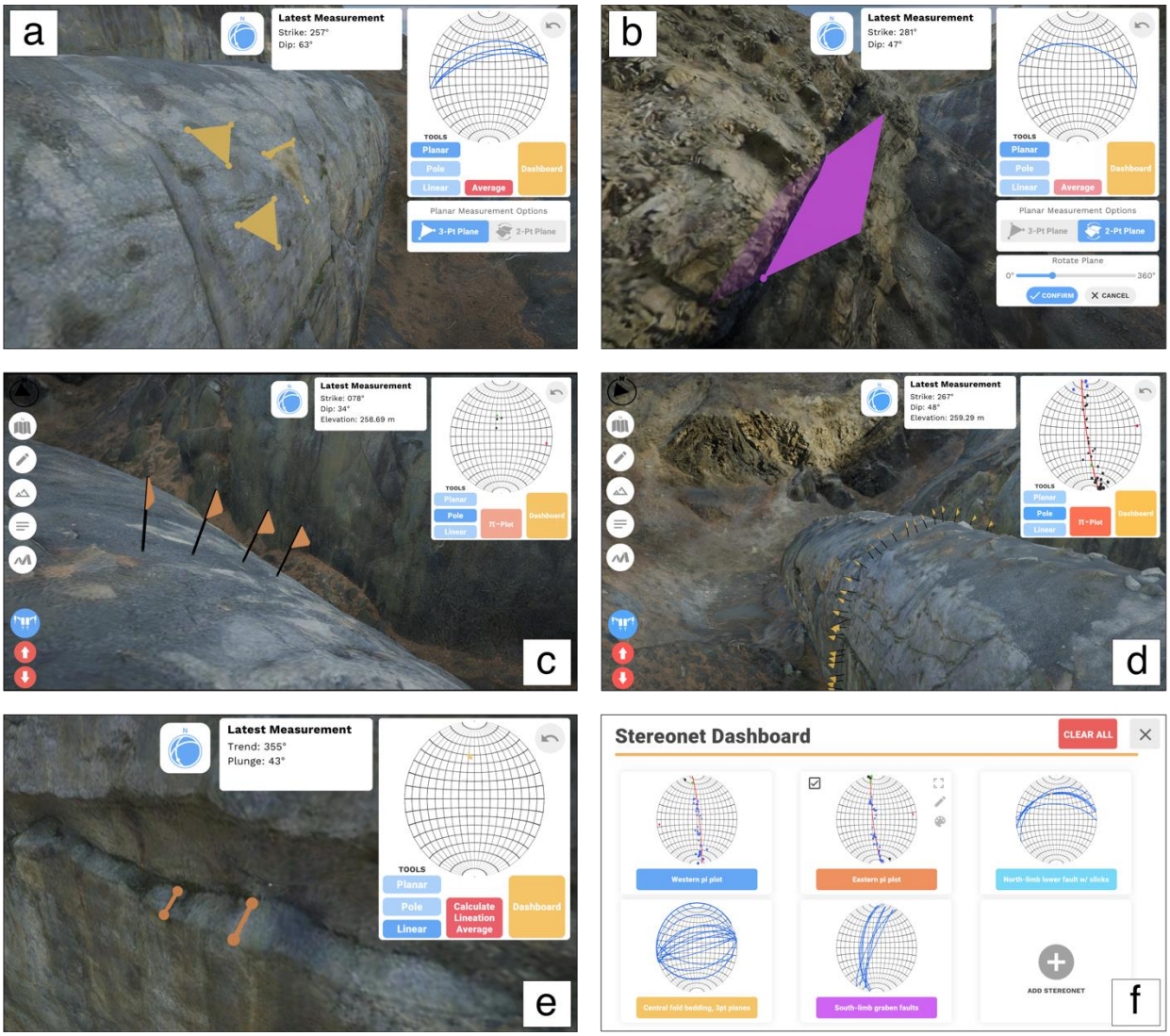

Fig. 4-4: Measurements and management with the Stereonet tool.
A) The three-point plane tool constructs triangular planes (orange) and prints the orientation in the "Latest Measurement" panel. B) The two-point plane tool collects planar attitudes when the user generates an axis and uses the "Rotate Plane" slider to fit the observed plane. C) The pole tool records strike, dip, and (optionally) elevation at the points marked by flags and plots the measurements as poles to planes within the stereonet. D) The pi-plot function is used to calculate the trend and plunge of a fold axis with orientation data taken from locations marked by flags. E) The orientation of linear features is measured by clicking on two points to generate a line. F) The Stereonet Dashboard is a way to organize sets of measurements and color-code the symbols representing the measurements in the field scene. Upon clicking on a stereonet in the Dashboard, a larger view of the stereonet is shown along with a list of all the measurements. (Images are screen shots from the "Whaleback Anticline Field Adventure," available at www.virtualfieldgeology.com (Needle et al. 2021).)

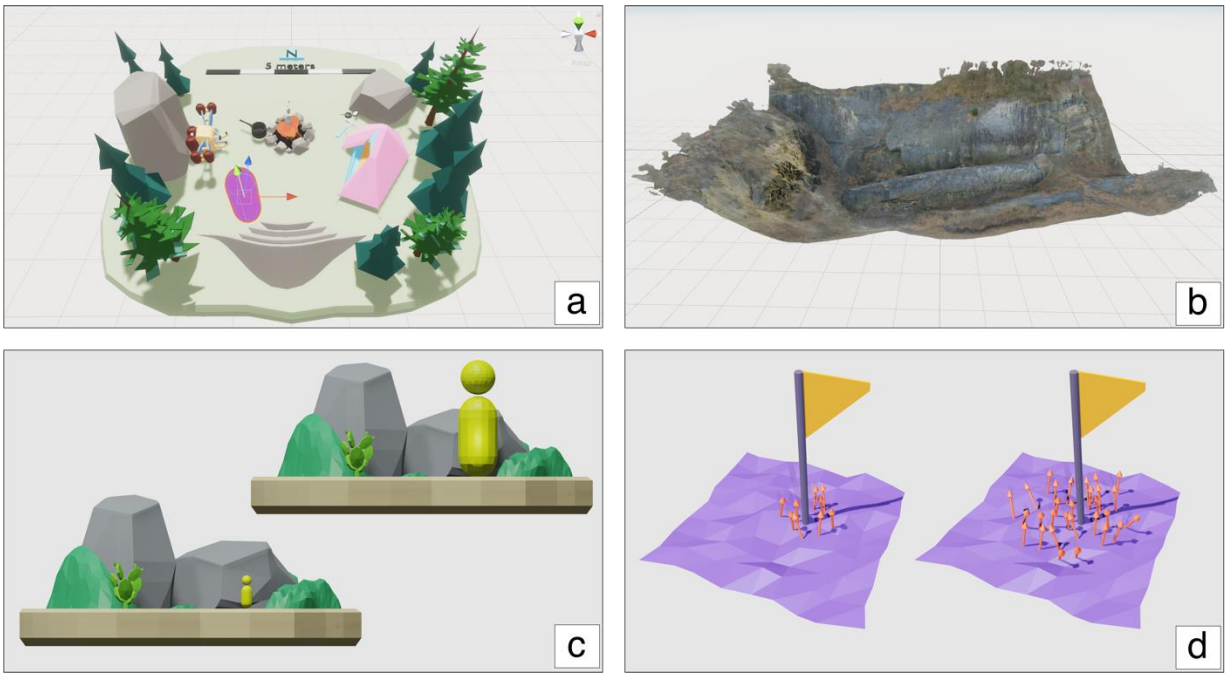

Fig. 4-5: Some steps in designing a virtual field experience.
A) View in Unity 3D-space of the model provided within the Structural Geology Query Toolkit. This model helps designers orient and/or scale their own 3D model. The pink capsule-shaped object represents the player scale and starting view. When playing the virtual field experience, the user does not see this capsule, rather, the user sees the terrain from the capsule's perspective. B) Example of Structure-from-Motion-generated 3D polygonal mesh after rotating the model to Unity space and applying the texture. C) The designer can change the scale of the first-person character or terrain. D) The designer can adjust the sampling radius for the pole tool. The small vectors represent face-normals to polygons of the model surface that are averaged to give the orientation at the position of the flag. Increasing the sampling radius includes more face-normals in the average orientation.

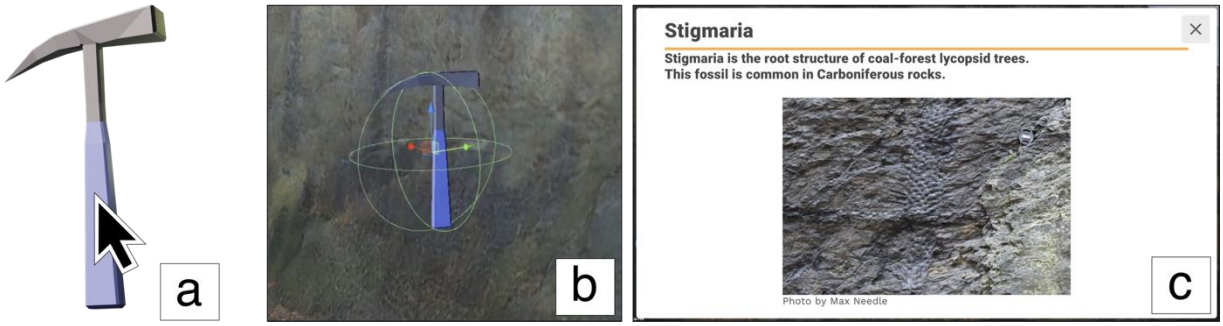

Fig. 4-6: Pop-up user interfaces (UIs).
A) The Structural Geology Query Toolkit contains prefabricated pop-up UIs that are activated when a user clicks on a 3D rock hammer within the game environment. B) A view from the Unity editor shows a designer placing a pop-up UI rock hammer near a place of interest. C) This is an example of information that the designer can arrange on a pop-up UI. The designer may also embed hyperlinks within the text.

Fig. 4-7: Beyond terrestrial outcrop/terrain models, there are applications of the Structural Geology Query Toolkit.
A) A remote field trip generated with the toolkit featuring Apollo 15 imagery and topography of Earth's Moon ("NASA 3D Resources," 2021). B) Conceptual rendering of a geologist exploring an analog model on-foot in virtual reality (photo of model by Kathleen Warrell, photo of person by Natalie Zielinski). C) A cartoon-style excursion, based on the geology of northwestern Washington State, was designed for university-level remote instruction during the Covid-19 pandemic (Needle et al., 2022). D) The "Fold Island" excursion introduces a variety of fold geometries and how folded bedding plots to a stereonet (Needle, 2022).

Table 4-1: A list of the measurements within the stereonet tool that simulate a geodetic compass.

Measurement		How the user measures	Data printed onscreen	Representation of data in stereonet	Additional functions
Plane	3-pt plane	Click 3x on a surface to generate a plane	Strike and dip	Great circle	Average: Generates a great circle that represents the most recent measurements and stores the average orientation in the dashboard
	2-pt plane	Click 2x on a surface to generate an axis. Then move a slider to rotate a plane to approximate the attitude of the feature	Strike and dip	Great circle	
Pole		Click 1x on a surface to generate a flagpole that is normal to the surface	Strike and dip, Elevation of sampled point (optional)	Pole to plane	Pi plot: Generates a best-fit great circle and associated normal to calculate the trend and plunge of a fold axis
Linear		Click 2x on a surface to generate a line	Trend and plunge	Pole	Average: Generates a pole that represents the most recent measurements and stores the average orientation in the dashboard

References in Chapter 4

Allmendinger, R. W., Cardozo, N., & Fisher, D. M. (2011). *Structural geology algorithms: Vectors and tensors*. *Structural Geology Algorithms: Vectors and Tensors*. Cambridge University Press. https://doi.org/10.1017/CBO9780511920202

Bond, C. E., & Cawood, A. J. (2021). A role for virtual outcrop models in blended learning-improved 3D thinking and positive perceptions of learning. *Geosci. Commun*, *4*, 233–244. https://doi.org/10.5194/gc-4-233-2021

Callahan, C. N., Libarkin, J. C., McCallum, C. M., & Atchison, C. L. (2015). Using the lens of social capital to understand diversity in the earth system sciences workforce. *Journal of Geoscience Education*, *63*(2), 98–104. https://doi.org/10.5408/15-083.1

Carabajal, I. G., Marshall, A. M., & Atchison, C. L. (2017). A Synthesis of Instructional Strategies in Geoscience Education Literature That Address Barriers to Inclusion for Students With Disabilities. *Journal of Geoscience Education*, *65*(4), 531–541. https://doi.org/10.5408/16-211.1

Cardozo, N., & Allmendinger, R. W. (2013). Spherical projections with OSXStereonet. *Computers and Geosciences*, *51*. https://doi.org/10.1016/j.cageo.2012.07.021

Cruz-Neira, C., Sandin, D. J., & DeFanti, T. A. (1993). Surround-screen projection-based virtual reality: The design and implementation of the CAVE. *Proceedings of the 20th Annual Conference on Computer Graphics and Interactive Techniques, SIGGRAPH 1993*, 135–142. https://doi.org/10.1145/166117.166134

Huntoon, J. E., & Lane, M. J. (2007). Diversity in the geosciences and successful strategies for increasing diversity. *Journal of Geoscience Education*, *55*(6), 447–457. https://doi.org/10.5408/1089-9995-55.6.447

Johnson, A., Leigh, J., Morin, P., & Van Keken, P. (2006). GeoWall: Stereoscopic visualization for geoscience research and education. *IEEE Computer Graphics and Applications*, *26*(6), 10–14. https://doi.org/10.1109/MCG.2006.127

Jones, C. (2008). History of Geoparks. *Geological Society, London, Special Publications*, *300*(1), 273–277. https://doi.org/10.1144/SP300.21

Marshak, S., & Mitra, G. (1988). *Basic methods of structural geology*. New Jersey: Prentice Hall.

NASA 3D Resources. (2021). Retrieved December 2, 2021, from https://nasa3d.arc.nasa.gov/

National Academies of Sciences Medicine and Engineering. (2021). *America's Geoheritage II: Identifying, Developing, and Preserving America's Natural Legacy: Proceedings of a Workshop*. (E. Sztein & P. Whitacre, Eds.). Washington, DC: The National Academies Press. https://doi.org/10.17226/26316

Needle, M. D. (2021). Virtual Field Geology: Field Experiences. Retrieved from https://www.virtualfieldgeology.com/field-experiences.html

Needle, M. D., Mooc, J., Akers, J. F., & Crider, J. G. (2021). Virtual field experiences in a web-based video game environment: open-ended examples of existing and fictional field sites. *Geosci. Commun*, *4*, 1–10. https://doi.org/https://doi.org/10.5194/gc-4-1-2021

Nesbit, P. R., Boulding, A. D., Hugenholtz, C. H., Durkin, P. R., & Hubbard, S. M. (2020). Visualization and Sharing of 3D Digital Outcrop Models to Promote Open Science. *GSA Today*, *30*(6), 25–28. https://doi.org/10.1130/GSATG425A.1

Orr, T. J., Macdonald, B. D., Iverson, S. R., & Hammond, W. R. (2015). Development of a generic mine visualization tool using unity. In *Proceedings of the Thirty-Seventh International Symposium on the Application of Computers and Operations Research in the Mineral Industry*.

Pavlis, T. L., & Mason, K. A. (2017). The New World of 3D Geologic Mapping. *GSA Today*, *271*(10). https://doi.org/10.1130/GSATG313A.1

Reynard, E., & Brilha, J. (Eds.). (2018). *Geoheritage: Assessment, Protection, and Management*. *Geoheritage*. Elsevier. https://doi.org/10.1016/C2015-0-04543-9

Robinson, A., Gordon, C. E., Houghton, J., Lloyd, G. E., & Morgan, D. J. (2015). ArcGIS to Unity: a design pipeline for creation of 3D terrain in serious egames for geology. *Geology Today*, *31*(6), 237–240. https://doi.org/10.1111/gto.12121

Schütz, M. (2015). *Potree: Rendering large point clouds in web browsers*. Univeristy of Wien.

Tony-Cristian, D., & Iulian-Vasile, B. (2017). 3-D minerals. Auxiliary material for the Physical Geology classes. *Analele Stiintifice de Universitatii AI Cuza Din Iasi. Sect. 2*, *Geologie 6*(1/2), 25–35. Retrieved from http://geology.uaic.ro/auig/AnaleleStiintificealeUniversitatii%22

Unity Technologies. (2021). Physics.Raycast. Retrieved August 11, 2021, from https://docs.unity3d.com/ScriptReference/Physics.Raycast.html

Wolfe, B. A., & Riggs, E. M. (2017, November 1). Macrosystem analysis of programs and strategies to increase underrepresented populations in the geosciences. *Journal of Geoscience Education*. National Association of Geoscience Teachers Inc. https://doi.org/10.5408/17-256.1

Chapter 5 Mesoscale faults accommodating extension at the Whaleback Anticline: A novel method of data collection provides insights to fold development

Abstract

Buckle-fold evolution, namely nucleation, amplification, and kinematic-growth, is categorized based on how strain is accommodated during each stage. Despite 60 years of research on folds, natural examples of folds are needed to confirm theories of buckle folding. The research presented here leverages the accessibility of a well-documented fold exposed in three dimensions, the Whaleback Anticline (Shamokin, Pennsylvania, USA), and aims to understand how meso-scale faults accommodate strain within the folded layer during folding. By utilizing 3D outcrop models and innovative digital field simulation tools, fault orientations and displacements are measured to calculate extensional strain values. Extension is uniformly distributed across the limb of the fold and is less than 6%. This distribution, and previous work at the Whaleback, indicate that the observed faults are accommodating extensional strain during the final stage of buckle folding and that late-stage flattening strain is evenly distributed both parallel and perpendicular to the fold axis. These findings inform future estimations of bedding thickness and length changes during folding, and thus advance buckle-fold theory models that require bedding dimensions to explore the role of rheology in folding. The values of extension on mesoscale faults in this study are similar to field-collected data at the Whaleback, which demonstrates the utility of this novel digital data-collection approach described in this work.

5.1 Introduction

Folds are common and important structures recognized in many geologic settings. One style of folding is buckle folding, in which layer-parallel shortening causes a more competent viscous layer to bend in a less-competent/more-ductile matrix. Starting with Biot (1961), more than 60 years of research on buckle folds has aimed to understand the connection between fold geometry to strain and the rheologic properties that permit buckling. Buckle folds accompanied by brittle structures, like faults, show a combination of ductile and brittle behavior. Not only can these structures provide information on orogenic events, but they encourage us to think about rocks behaving ductilely and brittlely on timescales not accessible to direct observation.

Folds are measured by their amplitude and wavelength (Fig. 5-1). Buckle fold evolution involves an increase in fold amplitude and horizontal shortening that reduces fold wavelength. Early theoretical and analog models demonstrated that when a Newtonian viscous layer and matrix experience layer-parallel shortening, a dominant wavelength will amplify from a small perturbation at a greater rate than other wavelengths (Biot, 1961; Biot et al., 1961). This work points out that the buckling process is largely dependent on the viscosity contrast between the viscous layer and its matrix. Sherwin and Chapple (1968) built upon this theory with hand-sample-sized natural examples of folds to show that there is uniform thickening and shortening of the layer that accompanies folding at the earliest stages, and that the wavelengths of the folds with the greatest cumulative amplification is a function of layer-parallel shortening.

Three stages of development have been theorized for buckle folding by multiple researchers. I use Schmalholz's (2006) to name these stages while also borrowing from descriptions of these stages by others (Fig. 5-2). In the first stage, nucleation, the fold initiates from a perturbation in the stiff layer. As the limb dips remain low, the shortening of the layer is

by layer-parallel homogenous strain (Ghosh, 1993). For single-layer buckle folds in viscous media, the transition from nucleation to the second stage, amplification, occurs when the folding becomes insensitive to viscosity contrasts (Schmalholz, 2006). In the amplification stage, the amplitude increases with layer-parallel shortening, decreasing the fold wavelength and increasing limb dips. During this stage, a change in arclength from inflexion point to hinges of the fold is expected (Hudleston and Treagus, 2010).

Finally, the kinematic-growth (late) stage involves tightening the fold, as the limbs rotate around the fold hinge and fold amplification is a result of pure-shear shortening. The kinematic-growth stage, referred to as "flattening" in the 20th century, may result in initially parallel folds deforming to having thinner limbs, and inner arcs becoming more strongly curved than outer arcs (e.g., Class 1C folds evolving from Class 1B folds (Fig. 5-3), by Ramsay and Huber, 1987). Estimating strain from flattening helps in estimating the strain in earlier stages, which can, in turn, provide the original length and thickness of undistorted beds (Srivastava and Shah, 2008); this division of stages constrains the rheological component of folding. Flattening produces differential thinning of the fold (Lisle, 1992). Theoretically, the arc length of the fold remains constant (Schmalholz, 2006), but if the limbs are being thinned during this stage, it is possible that they are elongating. Ghosh (1993) notes that in this stage, extension can be 1) parallel to the fold axis in the limbs, 2) perpendicular to the fold axis, or 3) a combination that can form "chocolate-tablet" boudins. Treagus (1997) using mathematical models stated that during all stages of fold evolution there is a partitioning of strain in both the competent and incompetent units, but for late-stage flattening, layer stretch is the main component of deformation in the most competent layer.

While strain can be provided by wavelength and amplitude (Fig. 5-1), the internal strain that accommodates folding is also of interest. Internal deformation can provide insight to how rocks behave rheologically. The tangential-longitudinal strain (TLS) model represents a mechanism for internal deformation during the amplification stage of a parallel fold without changing the orthogonal thickness (Ramsay, 1967). The TLS model shows strain concentrated in the hinges where curvature is highest, with extension of the outer arc and shortening of the inner arc (Fig. 5-4). In between these two surfaces is a neutral surface on which there is no extension or shortening. The expression of TLS may be in the form of tensional cracks, veins, or normal faults on the outer surface of the fold and thrust faults or pressure solution on the inner surface (e.g., Ghosh, 1993). The absolute value of tangential-longitudinal strain decreases from the hinge, where the fold curvature is at its maximum, to the limbs where curvature is zero. Roberts and Stromberg (1972) demonstrated TLS (which they called "arcuate hinge cleavage") in experimental physical models of rubber, putty, plasticene, and gelatin.

5.1.1 Motivation

Natural examples are needed to corroborate previous work on the stages of fold growth and internal deformation. Few studies document how the theorized pure-shear strain is accommodated in the shortening direction during the late stage of folding. It is still unclear if the TLS model applies to most buckle folds. Lastly, we assume that folds are not continuous cylinders, but the expression of strain in the third dimension during folding is not commonly reported.

Despite decades of interest, there are surprisingly few natural examples described. Most are on a hand-sample scale (e.g., quartz veins in Sherwin and Chapple,1968), regional scale (e.g.,

greater than 4000 m in Mynatt et al., 2007), and even fewer are exposed in 3D that would allow for strain to be investigated in the longitudinal axis of the fold. Hudleston and Holst (1984) recognized TLS in a folded competent limestone within a slate matrix at a centi- to decimeter scale. TLS was expressed through hinge-perpendicular extensional veining on the outer arc of the fold, with inner arc shortening being accommodated by pressure solution. Ormand and Hudleston (2003) observed TLS expressed as bed-normal veins in a hand-sample-sized limestone fold, but also noted bed-normal veins in the limbs that were interpreted as a being the products of late-stage flattening.

Due to its accessible scale and 3D exposure, at the Whaleback anticline, we have the opportunity to examine meso-scale structures that may accommodate strain in the late-stage of buckle folding, compare these structures to what current conceptual models predict particularly with regards to layer-parallel extension, and add insights to strain in the third dimension in the late-stage of buckle-fold evolution.

5.1.2 Natural example for investigation

The Whaleback Anticline is the central fold of an exposed fold train in the Bear Valley Strip Mine (Shamokin, PA). It is part of the Western Middle Synclinorium of the Pennsylvania anthracite region and is exposed in 3D as a result of strip mining. The folds are in between the regional scale and hand-sample scale: the wavelength of the folds is ~100 m, the Whaleback is exposed for 215 m on its longitudinal axis, and there is a 30-m elevation difference from its trough to crest, which is in between the regional scale and hand-sample scale of observed folds. The 4.3-5.2-m-thick “Whaleback” sandstone is underlain by ductile coal (known as the Mammoth bottom split leader) and overlain by 4.9 m of coal (Nickelsen 1979, 1987). The

Whaleback can be described as a single-layer fold to which we can apply buckle-fold theory for two reasons: 1) the stratigraphy is such that a competent unit of sandstone is encompassed by a less competent matrix of coal; and, 2) a 12-m-thick synformally-folded layer of sandstone overlies the coal stratigraphically above the Whaleback. This "disharmonic" juxtaposition of the syncline to the Whaleback Anticline demonstrates that these competent layers are decoupled and therefore we can treat the Whaleback as part of a single-layer fold train in buckle-fold theory.

Observed meso- and microscale structures at the Whaleback include cleavage, joints, and faults. It is possible to hike in troughs adjacent to the fold limbs to observe these structures., It is possible to walk along the crest of the Whaleback as well. Nickelsen (1979) correlated observable mesoscale structures at the Whaleback to six stages of deformation in the Appalachian orogeny that are regionally observable. Cross-cutting relationships of the faults that connect mesoscale structures of the Whaleback to regional deformation also enable a spatio-temporal investigation of the mesoscale structures that may accompany the second and third stages of buckle folding.

5.1.3 Previous work on faults accommodating extension at the Whaleback

To explore how faulting accommodates strain during buckle folding, Weil et al. (in prep) collected data from faults that were accessible on-foot and by 15-ft (5-m) ladder. They measured faults along 12 scanlines: four scanlines on the Whaleback's north limb (Fig. 5-5), two scanlines on the crest, and six scanlines on the south limb. These scanlines primarily run parallel to the fold axis, encountering fault orientations that are both parallel and transverse to the fold axis (Fig. 5-6). To calculate strain, data collected were bedding and fault attitudes, fault-slip vectors, and displacement along fault surfaces. Layer-parallel extensional linear strain accommodated by

faults during folding was observed to be relatively constant among the scanlines measured, averaging 2.67% for scanlines that recorded axis-parallel extension on the north limb and 3.43% for scanlines that recorded transverse extension on the crest and south limb of the Whaleback. The steeply-dipping geometry of the north limb created logistical difficulties that prevented Weil et al. (in prep) from collecting data from faults that record transverse extension.

The majority of the exposed folded surface is too dangerous from which to collect data, so this measured extensional strain may not represent how faults accommodate extension during folding, as only faults on the crest and the lowest-exposed-extent of the limbs were measured. Thus, to get a true distribution of strain accommodated by the faults, the distribution of faults needs to be measured at a greater spatial extent. The kinematic-growth stage of folding predicts extension within the limbs as they flatten, and the north limb of the Whaleback in particular has a large fault population that is inaccessible by foot or ladder. A more spatially extensive data collection may further our understanding of late-stage flattening.

5.2 Methods

Three-dimensional outcrop/terrain models provide opportunities to collect data from otherwise inaccessible areas. Point-cloud datasets, the initial outputs of 3D scanning, have become ubiquitous in geoscience in the past decade due to increases in collection and availability of lidar data and Structure-from-Motion photogrammetry. I use this approach to augment the field data at the Whaleback.

5.2.1 Generating digital outcrop models for research

A drone-based campaign of the Bear Valley Strip Mine produced a comprehensive point cloud with Structure-from-Motion photogrammetry (see Chapter 2), but this was primarily beneficial at capturing the bulk geometry of the fold train and many of the mesoscale faults, while visible, have noise on their surfaces (Fig. 5-7a). To generate more accurate models of the mesoscale faults on the fold's limbs, I used high resolution photos from a handheld, digital single-lens reflex (DSLR) camera, taken from the ground. The images were processed with Agisoft Photoscan, a Structure-from-Motion photogrammetry software. The resulting point cloud for the north limb of the Whaleback contains 9.8 x 10^7 points, representing 215 m horizontally and 30 m vertically (Fig. 5-7b). The fault surfaces are visibly more distinct when compared to the bulk-fold model produced by the drone photos. This photo set does not resolve faults near the crest. Fortunately, this area was accessible on foot and field data exist there.

The Bear Valley Strip Mine point cloud is georeferenced with >25 high-resolution ground-control points georeferenced 3D model of the fold limbs. The 3D model of the Whaleback's north limb used for this study was aligned to the model of the strip mine. To estimate uncertainty in positioning, I used CloudCompare to "difference" the two models. They are closely aligned: with a mean distance of 0.015 m based on 3 million values, with a standard deviation of 0.341.

In order to directly compare this new digital dataset, with the in situ field measurements, I simulate the process of the field work performed by Weil et al. (in prep). To do this, I use the open-source Structural Geology Query Toolkit software (Needle et al. 2022a) to generate a video-game-style virtual field simulation of the Whaleback's limbs. The Toolkit has tools that easily measure planar and linear orientations like a geodetic compass. While use of this software

package has been reported on for educational purposes (Needle et al., 2022b), using this software to enhance a dataset for scientific for research is novel. Below, I report on how this software can enhance research and the limitations of this approach, with the goal to improve usage of this software in future remote field campaigns for other researchers with 3D models.

5.2.2 Simulating field methods to measure strain from faults

Linear strain can be represented by the extension $e = (L_f - L_i) / L_i$,where L_i is the original length of the material and L_f is the observed final length. At the Whaleback, L_f is the measured length of a section-of-interest (a scanline) and L_i is L_f - *fault heaves* measured along the scan line (Fig. 5-8). Here, I use 12 scanlines parallel to the fold axis (including 4 lines measured by Weil et al.) and 8 scanlines perpendicular to the fold axis. The lines average 17 m in length (ranging from 11 m to 33 m) are spaced about 6-7 m apart and are distributed in four sections of the north limb of the fold (Fig. 5-7c).

Scanline locations were plotted on the Whaleback model in Blender, a free 3D-modeling software (Fig. 5-7c). For every location where a fault intersects a scanline, a "station" is assigned. In Blender, generating lines and planes with orthogonal relationships is a built-in feature; I use this function to plot an assumed displacement vector on the fault surface, that is perpendicular to the edge where the fault and bedding surfaces intersect. This work assumes pure dip-slip displacement because slickenlines (if present) are not resolvable on the 3D model. Within Blender, displacement on the fault surface is measured at 90° to the fault scarp (Fig. 5-8). The Blender interface permitted toggling between a textured version of the model and its shaded untextured version (Fig. 5-9). Toggling between both versions enabled the ability to distinguish

between “perceived” 3D features created by color contrasts in the texture and the actual 3D polygonal data of the model.

The 3D outcrop model and Blender-constructed annotations were imported to Unity with the Structural Geology Query Toolkit. I generated a 3D field simulation with the Toolkit and built it to a stand-alone MacOS platform. Within this simulation, I measured bedding, fault, and fault-slip attitudes at each station for each scanline.

5.2.3 Scanline Procedures

The north limb of the Whaleback was sectioned into quarters (Fig. 5-7b). Each section contains three E-W-trending scanlines and two scanlines that trend perpendicular to the fold axis (vertically with a N-S component). All faults, from which orientation data could be acquired, were recorded on each scanline regardless of the fault’s orientation relative to the trend of the scanline (Fig. 5-10). There are two situations in which faults were not measured along scanlines: 1) if a fault had been previously identified as a thrust fault, e.g., mapped by Nickelsen (1979) and subsequent visitors; and, 2) if the fault appeared in the model texture (colored pixel information) on the model but had no three-dimensional expression in the polygonal-mesh component of the model.

The E-W-trending scanlines (presented with indices of “a,” “b”, and “c,”) were intended for observing the extensional strain that is parallel to the long-axis of the fold, as the Whaleback’s axis trends ~80° (see Chapter 2). Although this strain may most likely be accommodated by faults striking transverse to the fold axis (Fig. 5-6), axis parallel faults were also measured along these scanlines as they may bear some component of E-W extension. When the heave of an individual fault was calculated, we solved for the E-W component (specifically

80/260°) of the fault-slip vector (Fig. 5-11). For all faults on a single scanline, these values were added and were used to determine the total strain accommodated by E-W extension.

Scanlines running perpendicular to the fold axis (presented with indices of "x" and "y") were intended for observing extensional strain that is parallel to the fold limb as seen in cross section (the plane that also contains the greatest component of shortening strain). The faults that would likely record this strain are axis-parallel extensional faults with dip-slip vectors; however, all faults along each of these scanlines were measured. Similar to the case of the E-W trending scanlines, the heaves of the faults on these scanlines were decomposed to a vector that is perpendicular to the fold axis and these values were added to calculate the strain accommodated by extension perpendicular to the fold axis (Fig. 5-11).

5.3 Data

Fifty-nine faults were identified on the horizontal (axis-parallel) scanlines. The orientation and sliplines of these faults are shown in Fig. 5-12a. I measured 36 faults on vertical (axis-perpendicular) scanlines. These are shown in Fig. 12b. The orientation and sliplines are similar to faults measured in the field (Figs. 5-12c, d).

I determined the extension due to faulting along the 20 scanlines. Extension values are shown on scanlines (Fig. 5-13). The average extension for scanlines oriented parallel to the fold axis is 1.84% extension (range: 0.43% to 3.72%). The average extension for scanlines perpendicular to the fold axis is 3.22% (range: 0.92% to 5.96%).

5.3.1 Strain distribution in data from digital models

There is no clear pattern of strain distribution from the fold hinge to limb, though in 3 of 4 sections, the smallest extension is furthest from the hinge. Axis-parallel extension is greater at the western end of the fold. Axis-perpendicular extension is greater at the eastern end of the fold.

5.3.2 Uncertainty in Data

The smallest displacement vector I measured on the 3D model is 0.03 m. The texture of the 3D model contains features that may have smaller displacements, but the mesh component of the model did not contain measurable geometries below this threshold (Fig. 5-9). The extension values do not include contributions from faults with slip smaller than 3 cm, even though I can recognize these features on the imagery. Thus, the values I present are minimum estimates of the true extension.

To estimate the uncertainty in extension measured from the digital model, I compare scanlines directly to those measured by Weil et al. (in prep) in the field. Scanline "Test" (Fig. 5-5) was made a meter above and parallel to Scanline 2 of Weil et al. (in prep). Scanline 2 includes seven fault measurements on faults identified as exclusively transverse to the fold axis. The total heave recorded by these faults is 0.50 m, and over a scanline that is 12.5 m in length, produced an extension of 4.17% (Weil et al., in prep). My "Test" scanline includes six fault measurements, one of which is on a fault that strikes parallel to the fold axis. The total heave recorded was 0.57 m, and over a scanline that is 13.5 m in length, produced an extension of 4.43%.

Although the positions of these scanlines are not identical, they record similar amounts of extension. The extension value measured by Weil et al. (in prep) does not include an axis-

parallel fault, whereas my "Test" scanline does. Weil et al. (in prep) are able to measure to the scale of a millimeter, whereas my work could not resolve fault displacements less than 3 cm. Thus, there is at least an order of magnitude difference in the resolution of the two datasets. Out of 30 faults measured on the north limb by Weil et al. (in prep), 14 faults had less than 0.03 m of displacement, and because the resolution limit of my study was 0.03 m, I may be measuring only 50% of the faults on the north limb.

This comparison of data suggests that Weil et al. can observe smaller scale faults and thus my study will produce an underestimation of measured strain. Furthermore, with the exception of the "Test" scanline, the extension values in this work are presented with respect to axis-parallel and axis-perpendicular decomposed components of the heave which are smaller than the heave.

5.4 Discussion

Weil et al. (in prep) estimated <5% layer-parallel extension accommodated by faults both parallel and transverse to the fold axis. No spatial pattern was discerned. By increasing access to more faults around the fold, we have produced data to complement those of Weil et al. (in prep). Similar observations can be made within these data: Every scanline, both perpendicular and parallel to the fold axis, demonstrated extensional strain of <6%.

5.4.1 Extension magnitudes relative to the fold axis

Extension parallel to the axis is consistent: the values do not exceed 5% and there is no observable progression from the central part of the Whaleback towards its ends. Of the four sections, the western-most section has the overall largest extension values (Fig. 5-13, scanlines 1a, 1b, and 1c). Here, the measured faults in this study strike primarily transverse to the fold axis

and thus have a larger component E-W extension. Extension perpendicular to the axis does not exceed 6%. Of the four sections, the western-most section has the lowest extension values (Fig. 5-13, scanlines 1x and 1y). Again, the measured faults here predominantly strike transversely to the fold's axis and thus include only a small component of axis-perpendicular extension; where E-W-striking faults are predominant (Fig. 5-13, scanlines 4x, 3y, 2x), the axis-perpendicular extension recorded is greatest.

Because dip-slip was assumed for all slip vectors on fault surfaces, rather than using slickenlines for the slip orientations, the dominant fault orientations at each scanline had a strong effect on strain recorded. Smaller faults (with displacements < 0.03 m) that were not represented in the 3D model could change the strain values and make these values more heterogenous or homogenous across the north limb. For example, where large transverse faults were primarily measured in the western section of the north limb, there may be small axis-parallel faults that accommodate similar amounts of extension but orthogonally to the transverse faults that are below the resolution of the images.

5.4.2 TLS and Late-stage flattening

Weil et. al (in prep) did not observe a meaningful spatial distribution of strain that correspond to TLS at the Whaleback. Monfort's (2016) finite-strain analysis on the grain-scale at the Whaleback with scanlines oriented perpendicularly to the fold axis and did not find a correlation between strain at the Whaleback and the expected strain pattern in TLS. The observed distribution of strain in this study, both axis-parallel and -perpendicular, does not add weight to the faults being representative of TLS at the Whaleback.

Nickelsen's (1979) observations of cross-cutting relationships at the Whaleback suggest that the faults on the north limb are the last faults to have formed, and because a spatial distribution of strain that represents TLS is not recorded, late-stage flattening is likely the process that these faults record. My work indicates that late-stage flattening involves well distributed <5% extension both parallel and perpendicular to the Whaleback's axis, and this is in line with Ghosh's (1993) model of late-stage flattening. If the Whaleback's presentation and magnitude of extension in late-stage flattening is observed at other folds, we can constrain the effect of late-stage flattening to arrive at more accurate pre-folded geometries of bedding (length and thickness) to enhance estimations of the role of rheological contrasts in buckle-fold-theory models.

5.4.3 Structural Geology Query Toolkit as a research tool

The process of measuring strain in this study demonstrates that the novel approach to using Blender and the Structural Geology Query Toolkit can answer geologic questions and are more than just visualization tools (e.g., Fig. 5-12). Most of the measurements could be done with the Structural Geology Query Toolkit software package.

Toggling between the untextured and textured mesh in Blender was useful in identifying where the 3D model represented 3D data and where only the color data from the texture represented 3D features. Measuring orthogonal relationships between lines to capture the orientations of dip-slip vectors was a feature only available in Blender. Because the Structural Geology Query toolkit is open source, a "toggle-mesh texture" and an "orthogonally-snap line" feature could be designed as custom tools for the Structural Geology Query Toolkit in the future.

The resolution of the model was a limitation of this study. Weil et al. (in prep) had access to faults with < 0.03 m of displacement, whereas these could not be resolved in the Structure-from-Motion-generated model. Consequently, the model's resolution produced lack of a direct comparison of data between in-situ field measurements and measurements made with the Structural Geology Query Toolkit. The field campaigns involving data collected by Weil et al. (in prep), as well as the photographs used for this study, were made prior to the release of the Structural Geology Query Toolkit.

There are advantages of using the Structural Geology Query Toolkit. I had the ability to comfortably measure faults in areas where the field conditions (e.g., steep fold limbs) produced logistical challenges for Weil et al. (in prep). Also, because these digital outcrops are now "packaged" as digital field simulations, I have the ability to share the "video-game" version of the outcrop with colleagues for the reproduction of measurements to increase data precision.

5.5 Final Remarks

The meso-scale faults accommodate <6% extension both parallel and perpendicular to the Whaleback's fold axis, documenting late-stage flattening. The values and distribution of extension are similar to the field data collected by Weil et al. (in prep). Using a photogrammetry-derived 3D model with the Structural Geology Query Toolkit permitted the investigation of strain accommodated by hard-to-reach faults that are logistically difficult to measure in-situ.

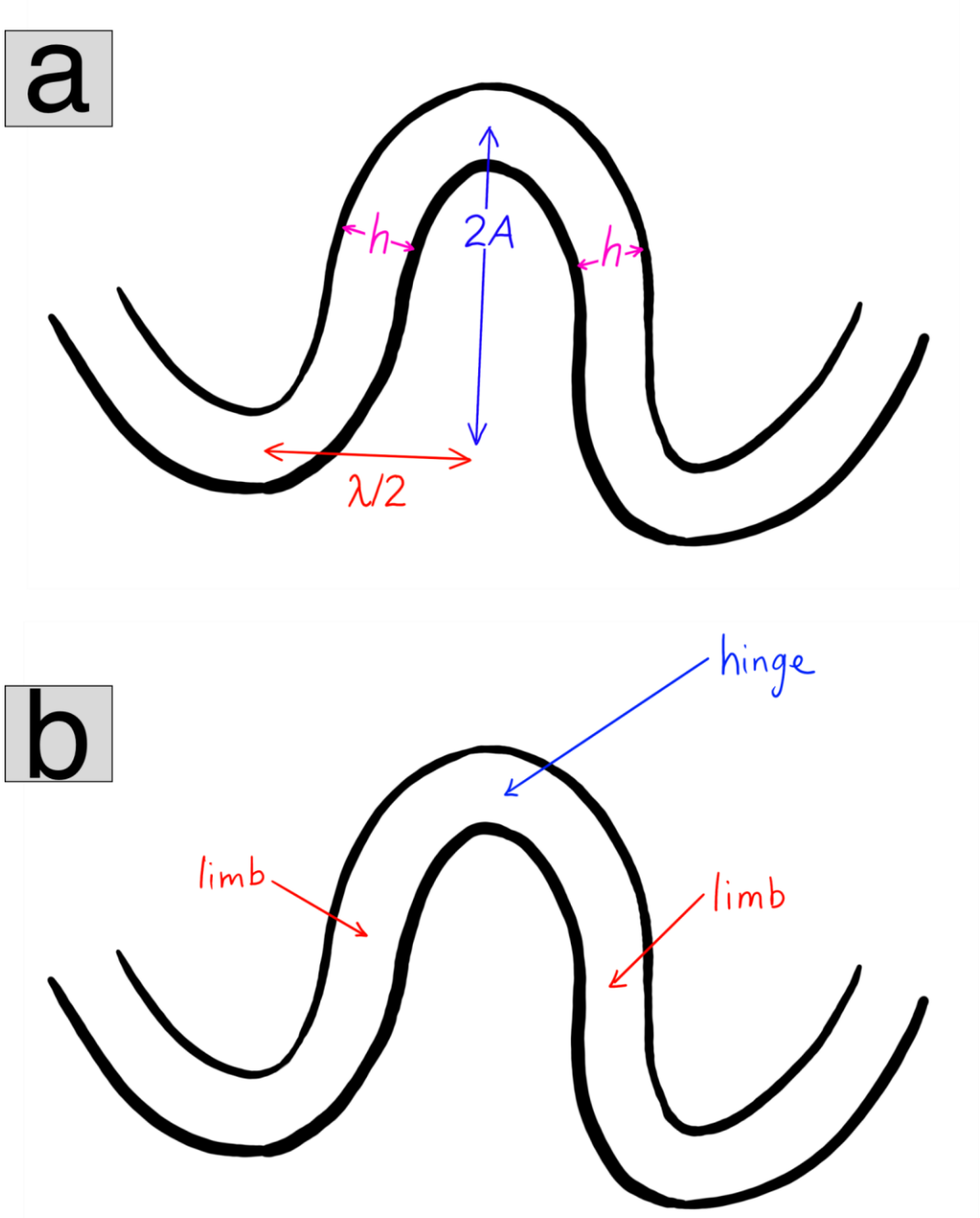

Fig. 5-1: Fold anatomy.
a) Amplitude (*A*) and wavelength (***λ***). Orthogonal thickness of the bedding (*h*) is the same throughout this fold, thus, this is termed a "parallel" fold. b) The hinge of the fold is the location of greatest curvature. The limbs are the flanks of the folds joined by the hinge. Arrows associated with the limbs are pointing to inflexion points where curvature is zero. Figure is redrawn from Hudleston and Treagus (2010).

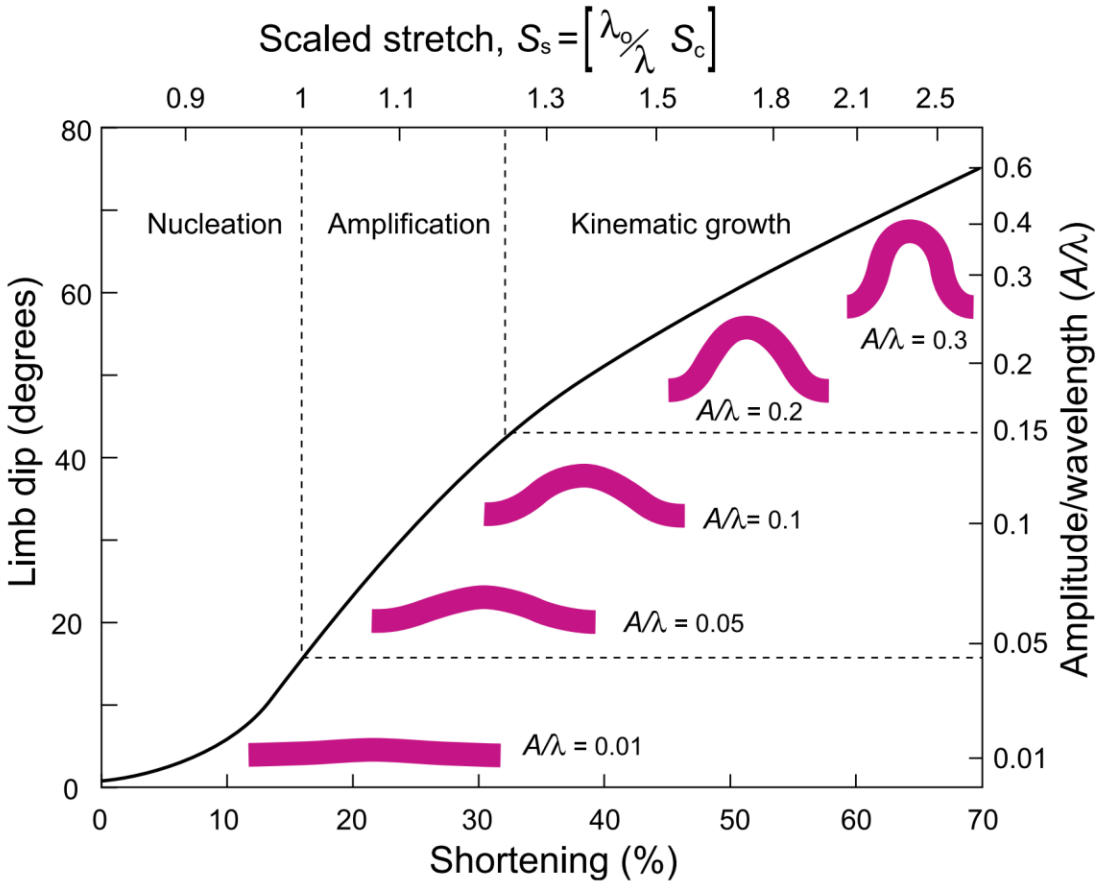

Fig. 5-2: Stages of development for buckle folds from Schmalholz (2006).

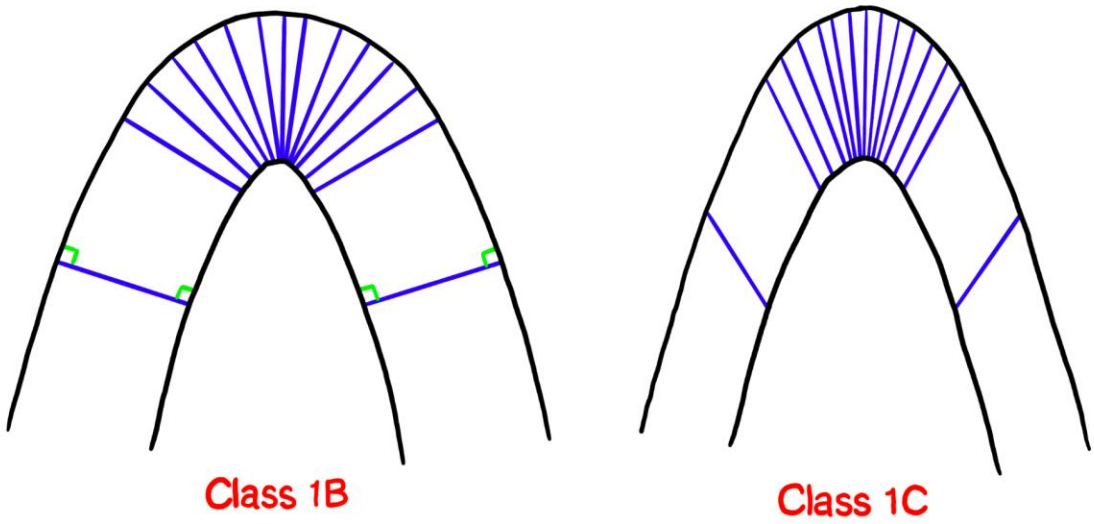

Fig. 5-3: Class 1 folds have curvature of the inner arc that is greater than that of the outer arc.
Blue lines are dip isogons that draw attention to differences in outer arc and inner arc curvature. (left) Class 1B are ideal concentric with uniform thickness across the fold profile. (right) Class 1C folds show some thickening in the hinge and thinning in the limbs. Figure is redrawn from Ramsay (1967).

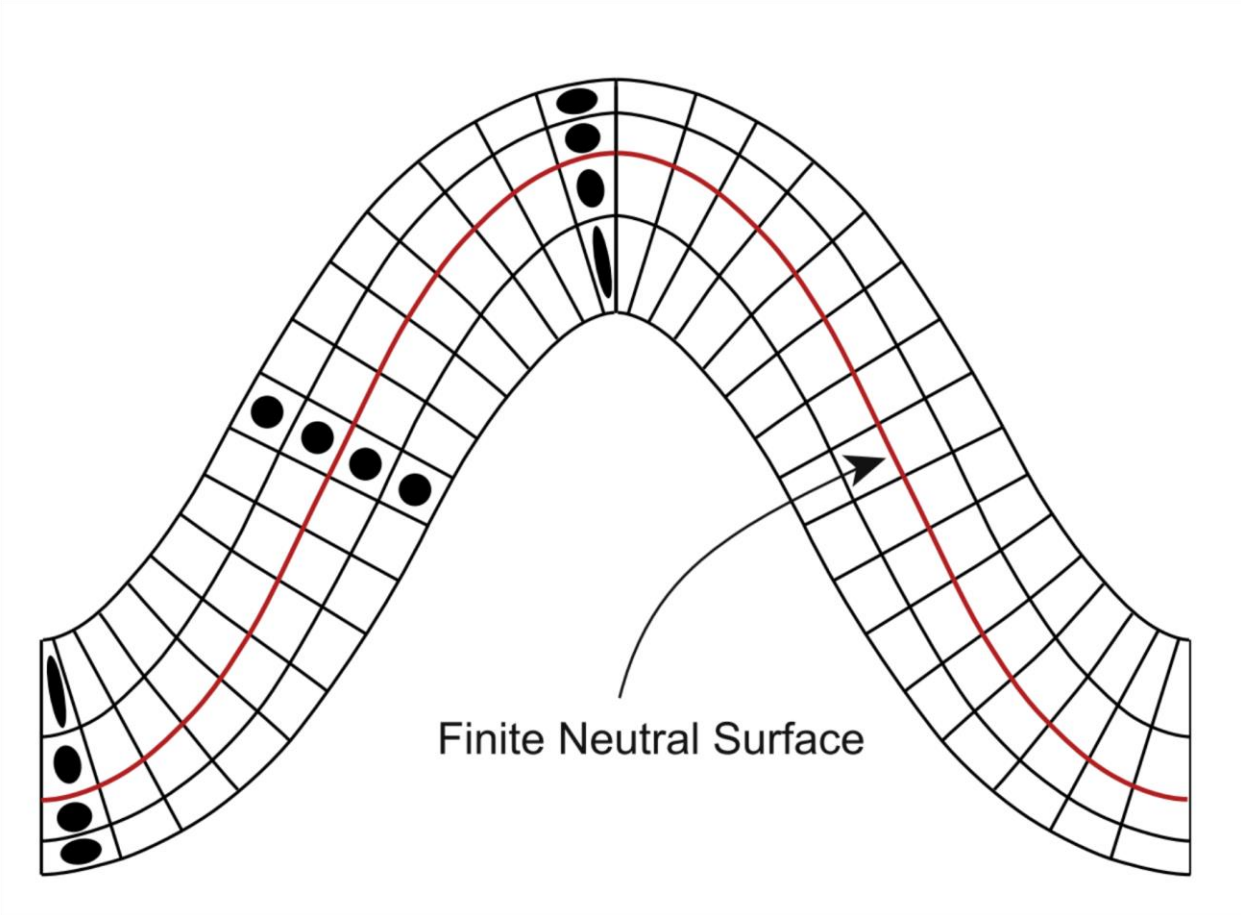

Fig. 5-4: Tangential-longitudinal-strain model.
Outer-arc extension is parallel to the bedding surface (and inner arc shortening) at the fold hinge (from Hudleston and Treagus, 2010).

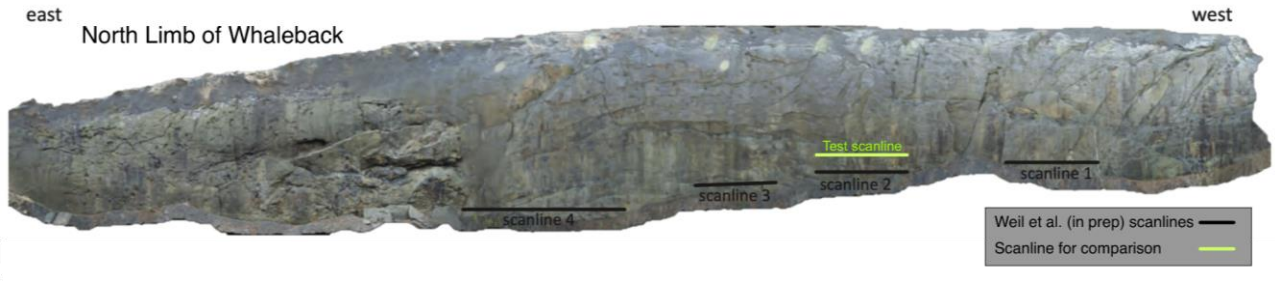

Fig. 5-5: Previous scanline positions.
The north limb of the Whaleback with scanline positions for measurements performed by Weil et al. (in prep). Note that East is to the left of the image and West is to the right.

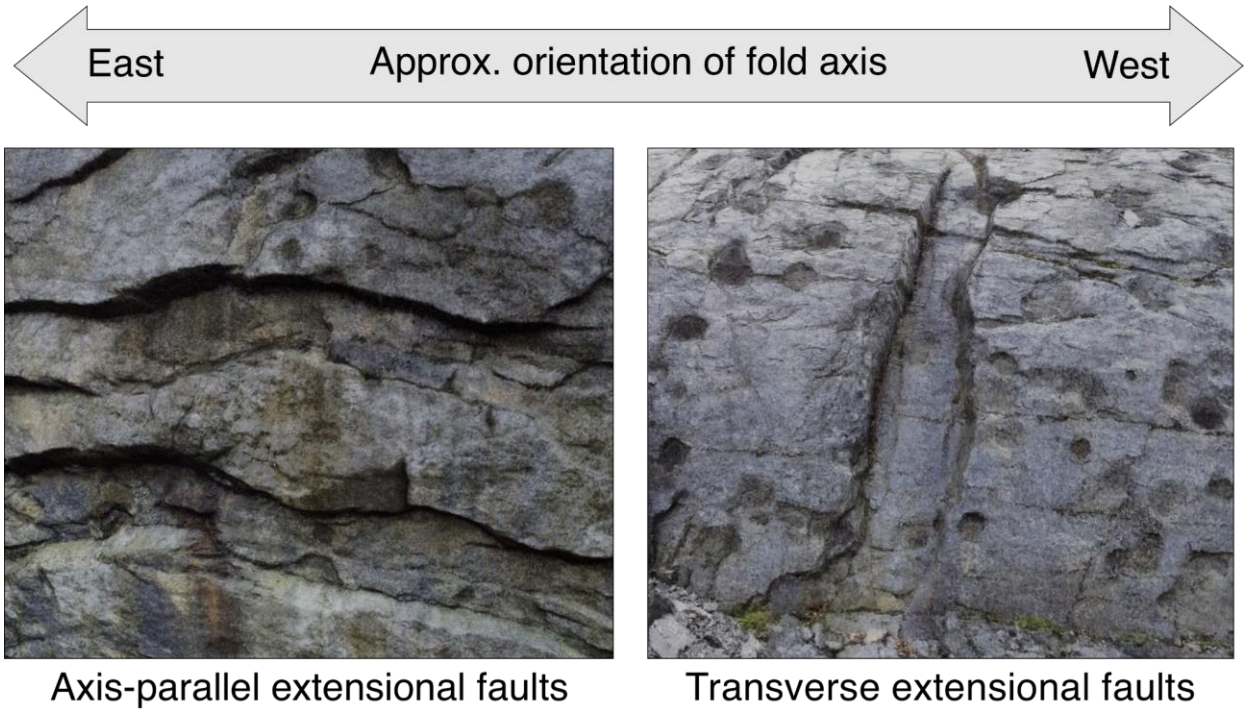

Fig. 5-6: Faults on the north limb of the Whaleback have different orientations.
These images are from a high-resolution structure-from-motion model. Field of view for both images is approximately 9 m across.

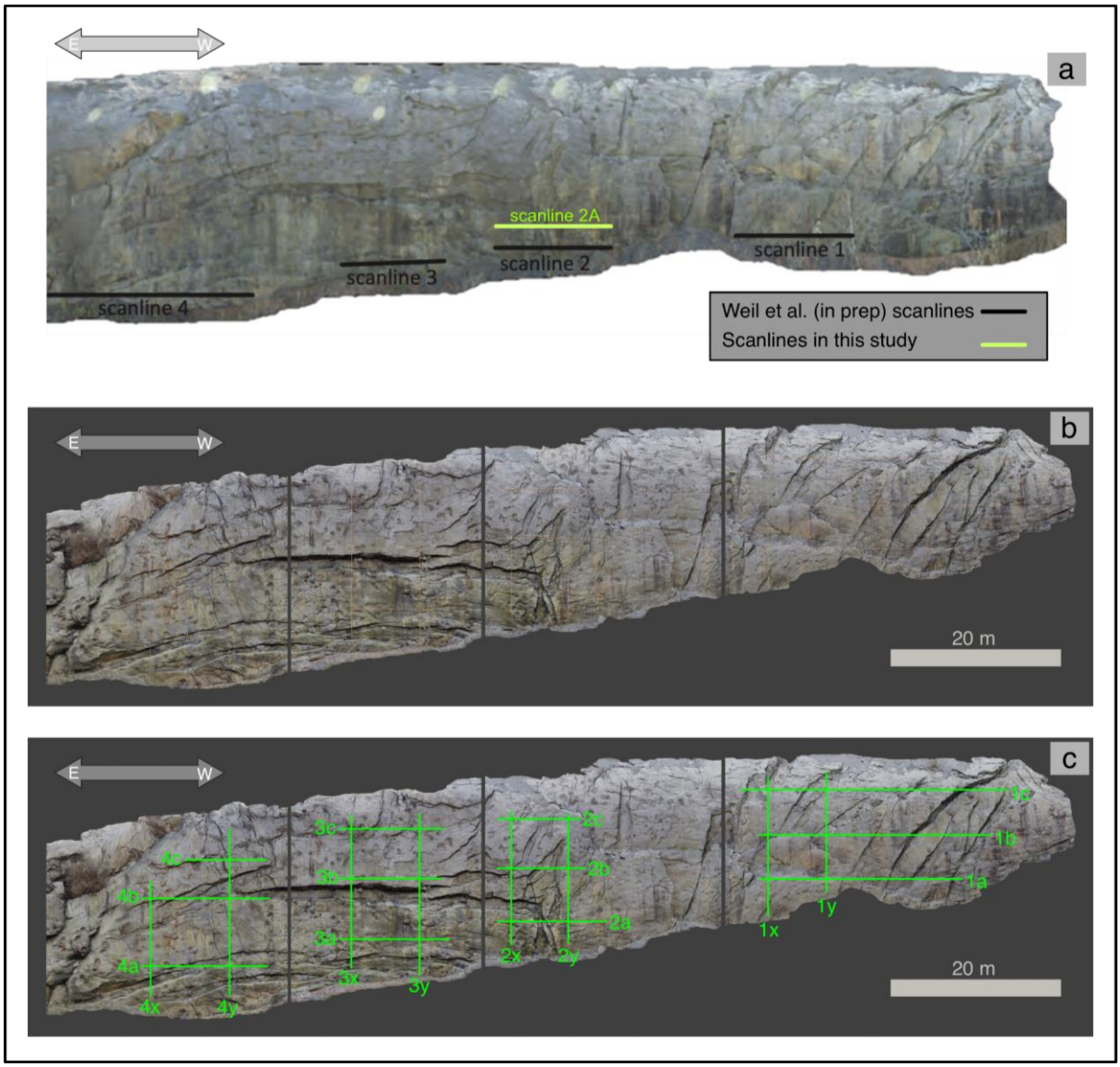

Fig. 5-7: Mesh models of the Whaleback's north limb from point-cloud data.
a) Scanline positions measured by Weil et al. (in prep) on an image from a model made of the whole strip mine using drone photos and Structure-from-Motion photogrammetry. b) High-resolution model from DSLR photos using Structure-from-Motion photogrammetry. In this image, the model has been sectioned for data management. c) Positions of scanlines for this study. Scanline 2a is in a similar position to the "Test" scanline used to compare Weil's field-measured scanline.

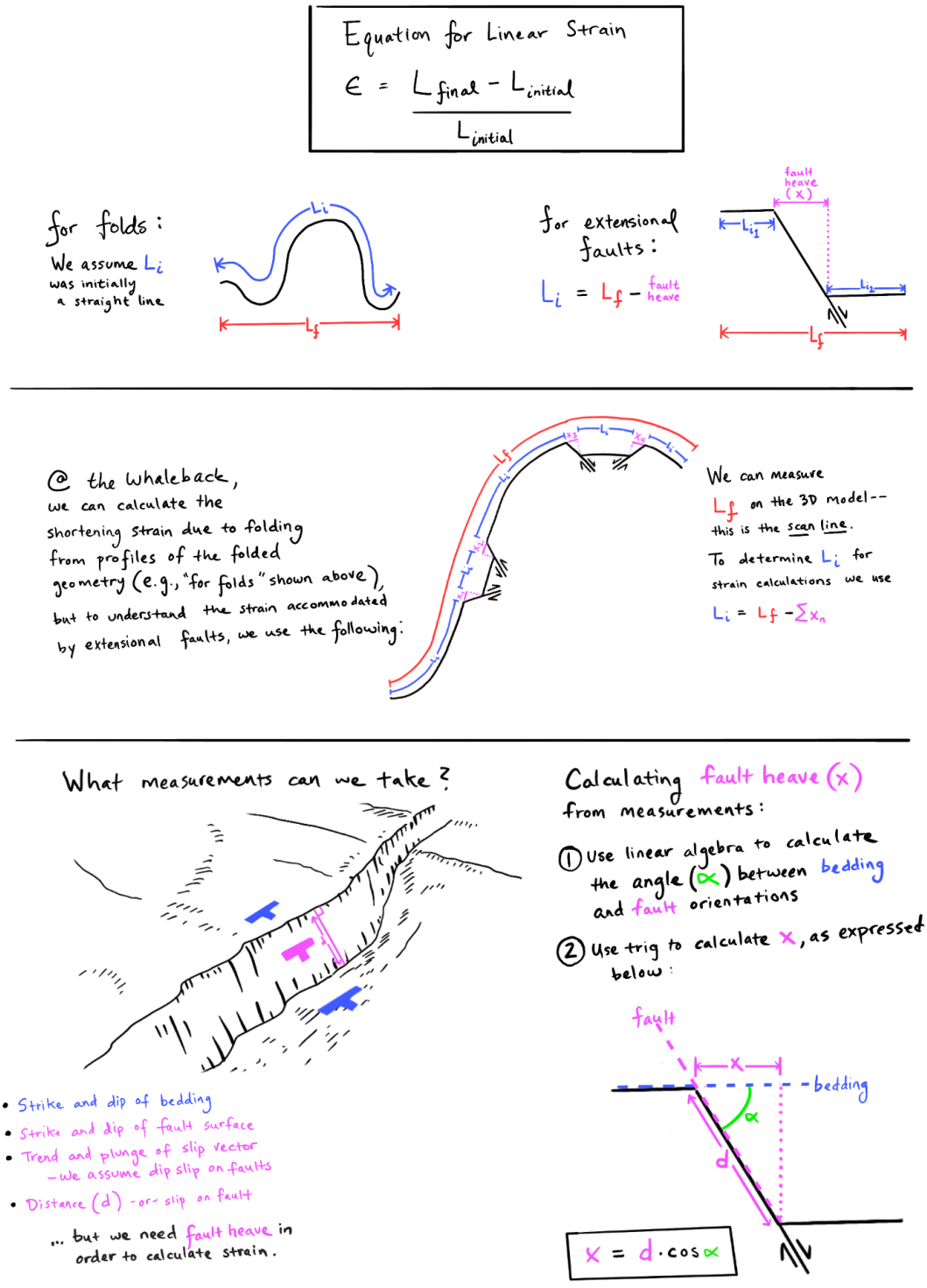

Fig. 5-8: Calculating extension.

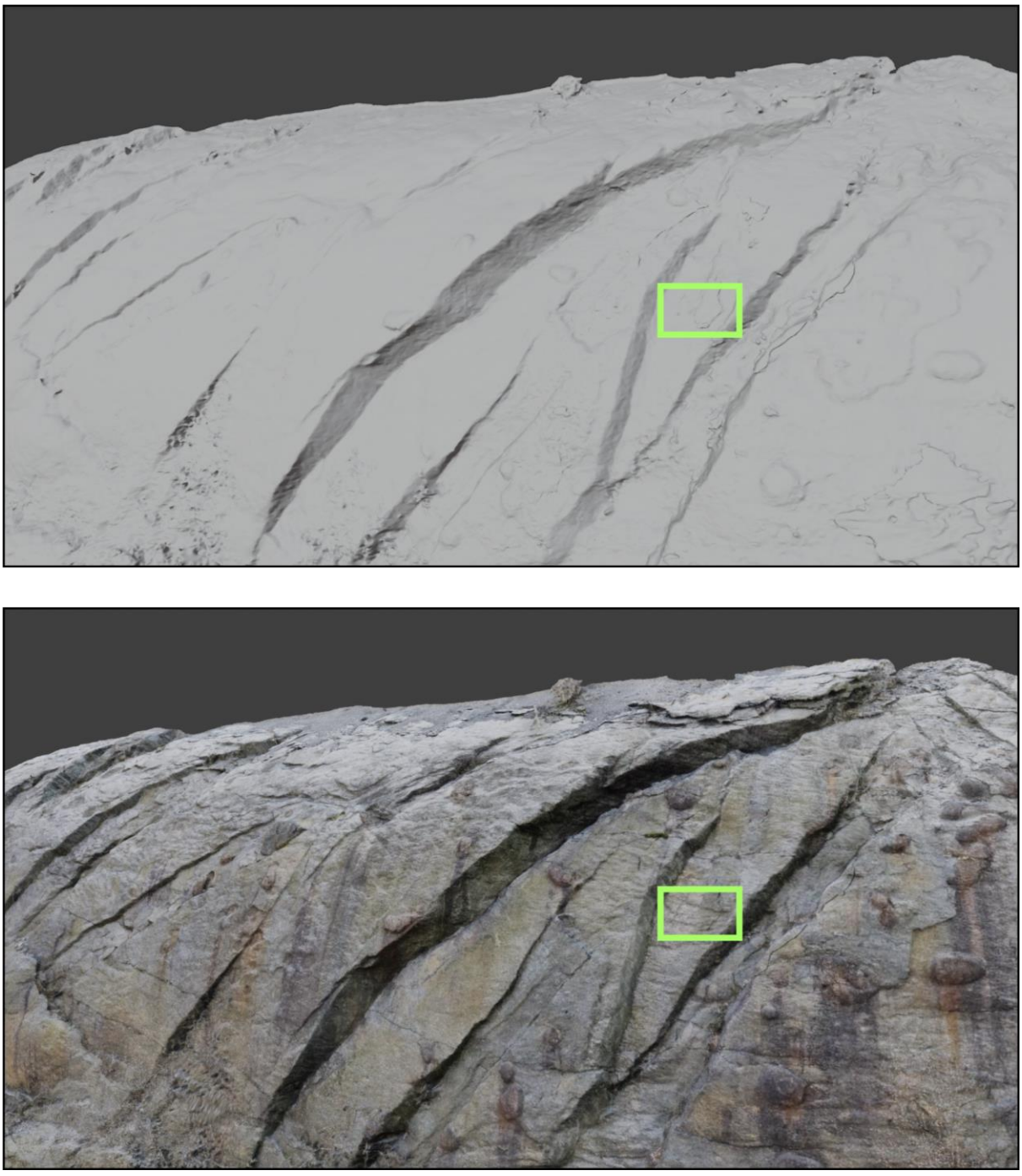

Fig. 5-9: Some features are only represented by the model's color data within the texture. Top) This shaded polygonal model was useful in determining contacts between fault surfaces and bedding. Yellow box does not include small horizontally oriented faults. Bottom) This is the same view of the model but textured. Yellow box includes small horizontally oriented faults. There are smaller faults represented in these color data that are not three-dimensionally represented by the polygons in the mesh data.

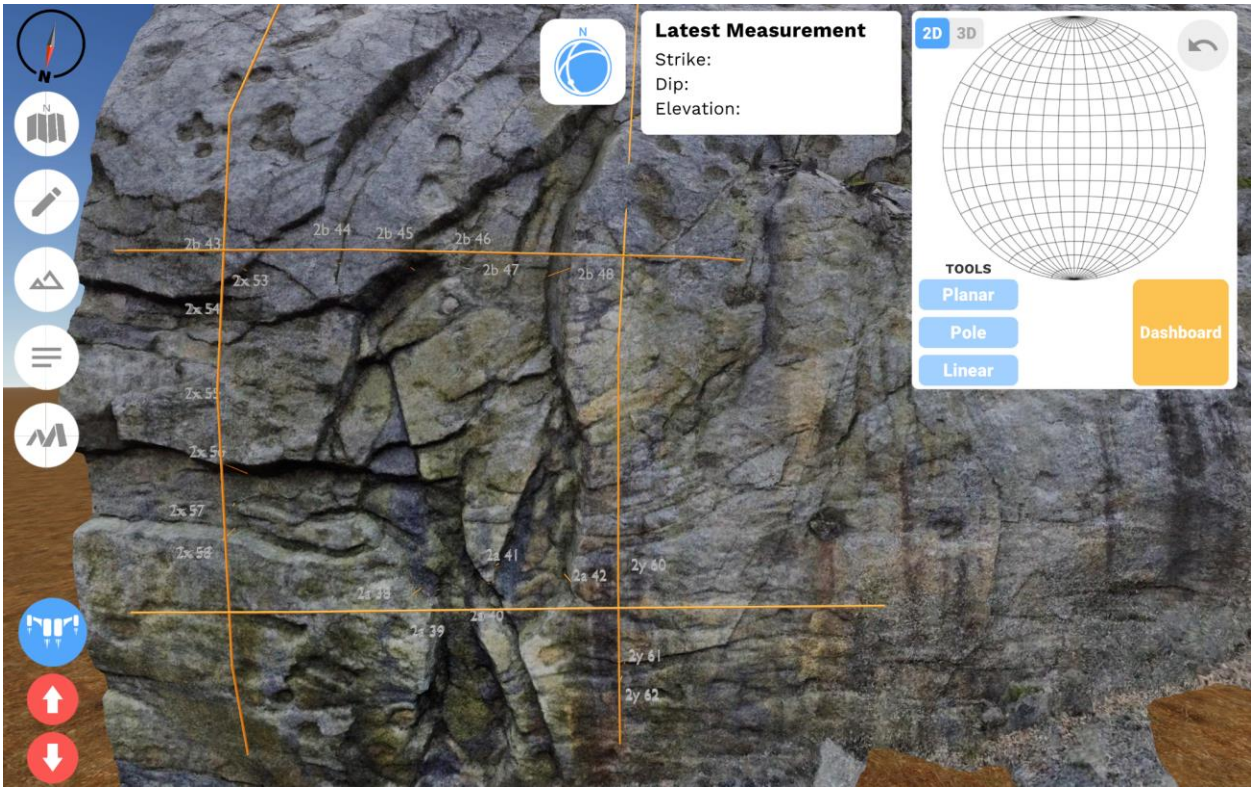

Fig. 5-10: Oblique perspective of the north limb within the video-game environment. The orange lines are scanlines and the small white labels represent individual "stations" where data were collected.

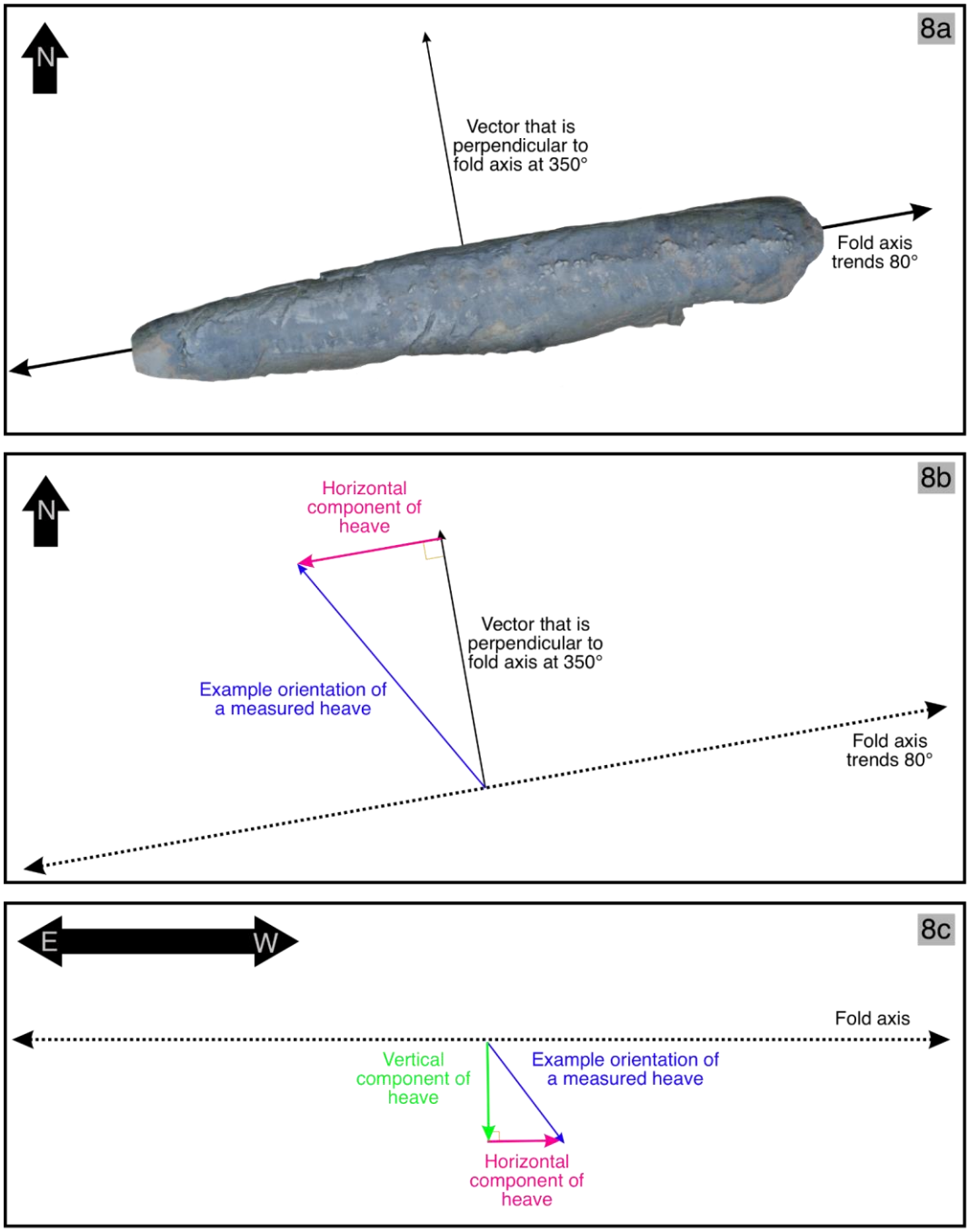

Fig. 5-11: Deriving the axis-parallel and axis-perpendicular components of fault heave. a) An aerial view of the Whaleback with the fold-axis trend labeled. b) In this map view, the horizontal component of the heave, relative to the trend of the fold axis, is decomposed. c) In this profile view, the vertical component of the heave is decomposed from the heave's orientation and the horizontal component.

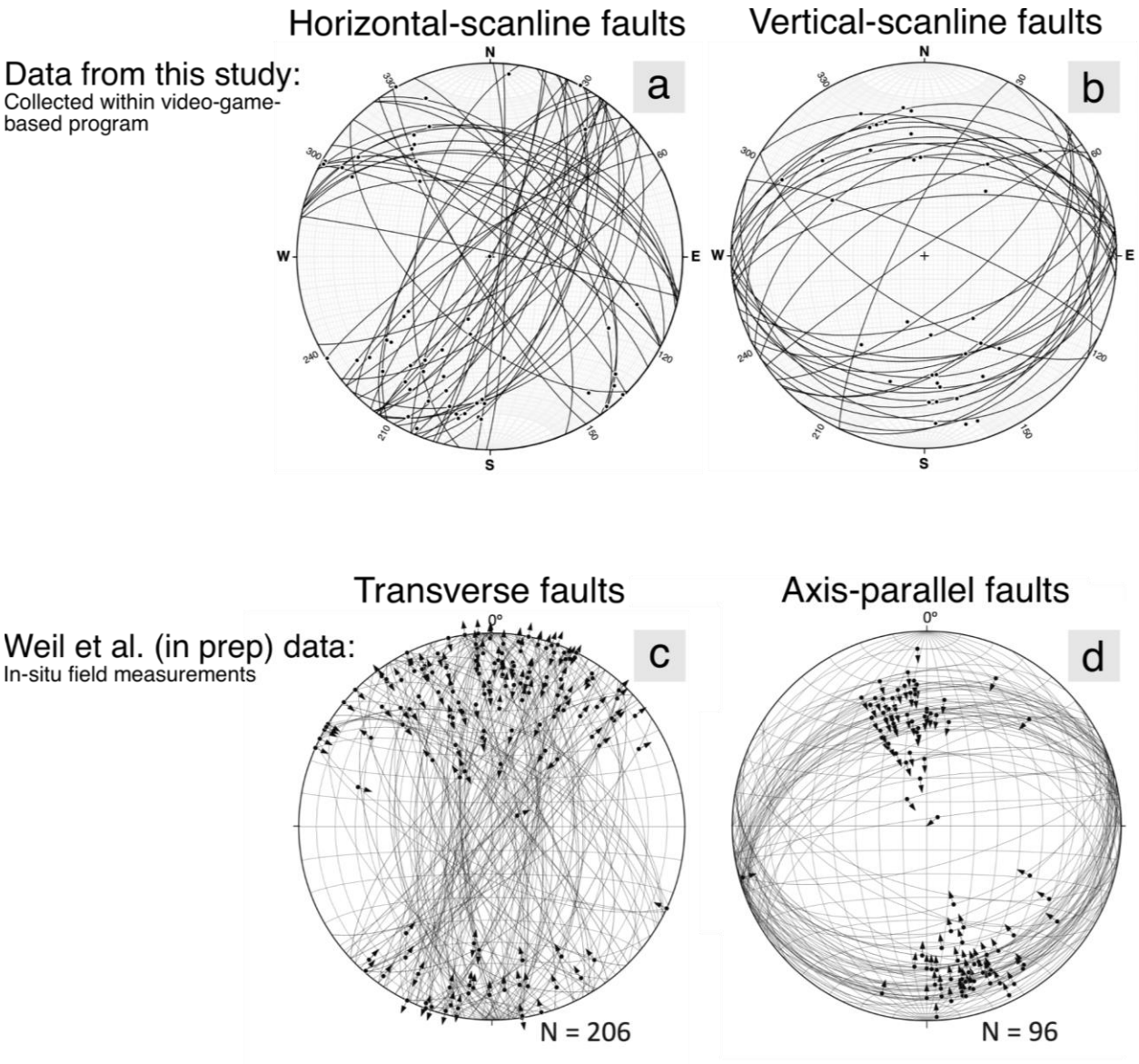

Fig. 5-12: The video-game-based measurements reproduce data similar to the in-situ field measurements.

Horizontal scanlines should principally intersect the transverse faults. Vertical scanlines principally intersect the axis-parallel faults. Orientations (great circles) and slip lines (small dots) are similar in the data collected from the model (upper stereonets, a and b) and in the field (lower sterenets, c and d). Although slip lines are visible in the digital models, the sense of slip (small arrows on lower plots) is not discernable.

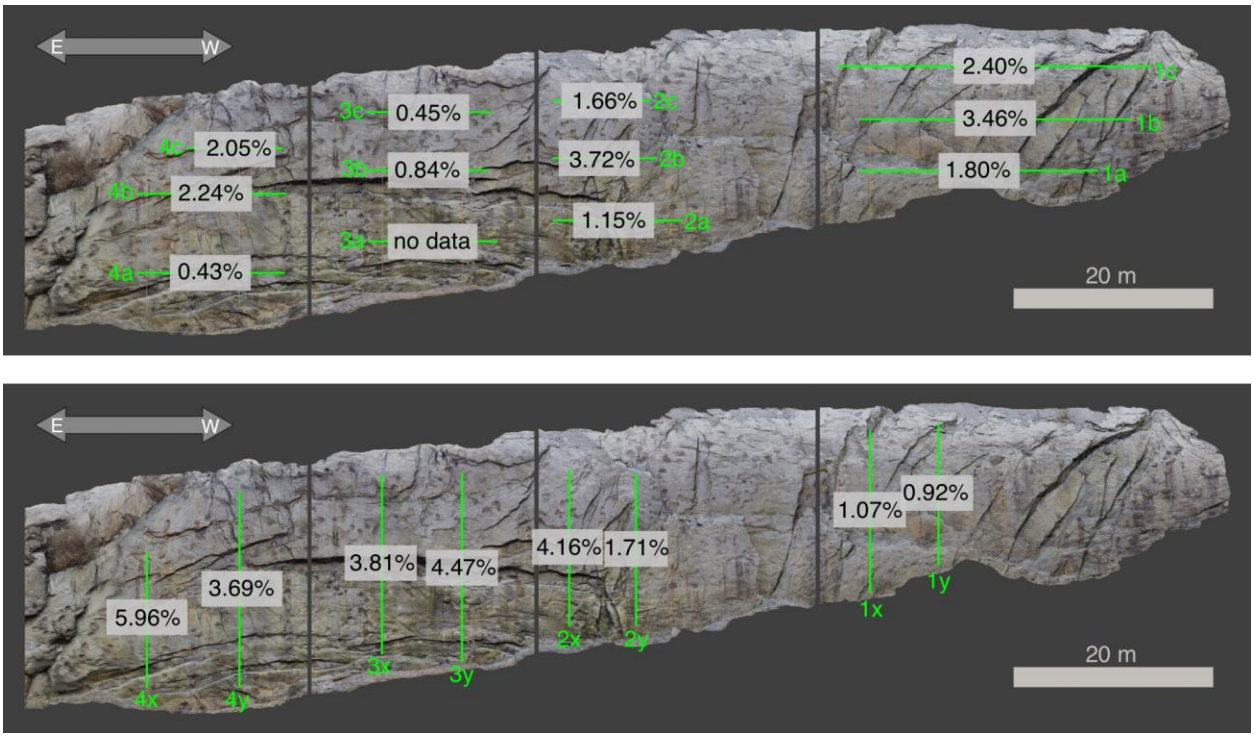

Fig. 5-13: Values of extension plotted by scanline on the north limb.
Top) Extension parallel to the fold axis. Bottom) Extension perpendicular to the fold axis.

References in Chapter 5

Biot, M. A., H. Ode, and W. L. Roever. 1961. "Experimental Verification of the Theory of Folding of Stratified Viscoelastic Media." *Geological Soc. of Am. Bulletin* 72 (November): 1621–32.

Biot, M.A. 1961. "Theory of Folding of Stratified Viscoelastic Media and Its Implications in Tectonics and Orogenesis." *GSA Bulletin* 72 (11): 1595–1620.

Ghosh, S. K. 1993. *Structural Geology: Fundamentals and Modern Developments*. Pergamon.

Hudleston, P J, and T B Holst. 1984. "Strain Analysis and Fold Shape in a Limestone Layer and Implications for Layer Rheology." *Tectonophysics* 106 (3–4): 321–47. https://doi.org/https://doi.org/10.1016/0040-1951(84)90183-5.

Hudleston, Peter J., and Susan H. Treagus. 2010. "Information from Folds: A Review." *Journal of Structural Geology* 32 (12): 2042–71. https://doi.org/10.1016/j.jsg.2010.08.011.

Lisle, Richard J. 1992. "Strain Estimation from Flattened Buckle Folds." *Journal of Structural Geology* 14 (3): 369–71.

Monfort, Eric Michael. 2016. "A Study of Three-Dimensional Grain-Scale Strain on the Bear Valley Strip Mine Whaleback Anticline Using Normalized Fry Analysis, Shamokin, PA." Bucknell University. https://digitalcommons.bucknell.edu/honors_theses.

Mynatt, Ian, Stephan Bergbauer, and David D Pollard. 2007. "Using Differential Geometry to Describe 3-D Folds." https://doi.org/10.1016/j.jsg.2007.02.006.

Needle, Mattathias D., Jacky Mooc, John F. Akers, and Juliet G. Crider. 2022a. "Virtual Field Experiences in a Web-Based Video Game Environment: Open-Ended Examples of Existing and Fictional Field Sites." *Geosci. Commun* 5 (3): 251–60. https://doi.org/https://doi.org/10.5194/gc-5-251-2022.

———. 2022b. "The Structural Geology Query Toolkit for Digital 3D Models: Design Custom Immersive Virtual Field Experiences." *Journal of Structural Geology* 163 (October). https://doi.org/10.1016/J.JSG.2022.104710.

Nickelsen, Richard P. 1979. "Sequence of Structural Stages of the Alleghany Orogeny, At the Bear Valley Strip Mine, Shamokin, Pennsylvania." *Am J Sci* 279 (3): 225–71. https://doi.org/10.2475/ajs.279.3.225.

———. 1987. "Sequence of Structural Stages of the Alleghany Orogeny at the Bear Valley Strip Mine, Shamokin, Pennsylvania." *North-Eastern Section of the Geological Society of America: Decade of North American Geology, Centennial Field Guides* 5 (5).

Ormand, CJ, and P. J. Hudleston. 2003. "Strain Paths of Three Small Folds from the Appalachian Valley and Ridge, Maryland." *Journal of Structural Geology* 25 (11): 1841–54.

Ramsay, J. G. 1967. *Folding and Fracturing of Rocks*. New York: McGraw-Hill.

Ramsay, John G., and Martin I. Huber. 1987. *The Techniques of Modern Structural Geology, Vol 2: Folds and Fractures. Academic Press (Elsevier)*. 4th printi. Academic Press.

Roberts, D, and KE Stromgard. 1972. "A Comparison of Natural and Experimental Strain

Patterns around Fold Hinge Zones." *Tectonophysics* 14 (2): 105–20.

Schmalholz, Stefan M. 2006. "Scaled Amplification Equation: A Key to the Folding History of Buckled Viscous Single-Layers." https://doi.org/10.1016/j.tecto.2006.03.008.

Sherwin, J.-A. A, and W M Chapple. 1968. "Wavelengths of Single Layer Folds: A Comparison between Theory and Observation." *Am. J. Sci.*

Srivastava, Deepak C, and Jyoti Shah. 2008. "The '"isogon Rosette"' Method for Rapid Estimation of Strain in Flattened Folds." *Journal of Structural Geology* 30 (4): 444–50. https://doi.org/10.1016/j.jsg.2008.01.010.

Treagus, Susan H. 1997. "Modelling Deformation Partitioning in Folds." In *Evolution of Geological Structures in Micro- to Macroscales,* edited by S. Sengupta, 341–72. London: Chapman & Hall.

Weil, Arlo B., Mary Beth Gray, Kylie G. Cush, Mattathias D. Needle, and Juliet G. Crider. n.d. "Fold-Related Faulting within the Classic Three-Dimensionally Exposed Appalachian Buckle Folds of the Bear Valley Mine, Shamokin, PA, USA." *In Prep*.